

รายงานวิจัยฉบับสมบูรณ์

โครงการผลิตสารประกอบไฮโดรคาร์บอน C2 และพลังงานไฟฟ้าจากมีเทนโดย ใช้เครื่องปฏิกรณ์ชนิดเซลเชื้อเพลิงแบบออกไซด์ของแข็ง

โดย รองศาสตราจารย์ ดร. สุทธิชัย อัสสะบำรุงรัตน์

รายงานวิจัยฉบับสมบูรณ์

โครงการผลิตสารประกอบไฮโดรคาร์บอน C2 และพลังงานไฟฟ้าจากมีเทนโดย ใช้เครื่องปฏิกรณ์ชนิดเซลเชื้อเพลิงแบบออกไซด์ของแข็ง

ผู้วิจัย รองศาสตราจารย์ ดร. สุทธิชัย อัสสะบำรุงรัตน์ สังกัด ภาควิชาวิศวกรรมเคมี คณะวิศวกรรมศาสตร์

จุฬาลงกรณ์มหาวิทยาลัย

สนับสนุนโดยสำนักงานกองทุนสนับสนุนการวิจัย (ความเห็นในรายงานนี้เป็นของผู้วิจัย สกว.ไม่จำเป็นต้องเห็นด้วยเสมอไป)

Abstract

Project Code: RSA4580028

Project Title: Production of C2 Hydrocarbon and Electricity from Methane in

a Solid Oxide Fuel Cell Reactor

Investigator: Associate Professor Suttichai Assabumrungrat,

Department of Chemical Engineering, Faculty of Engineering,

Chulalongkorn University

Email: Suttichai.A@chula.ac.th

Project Period: 15 August 2002 – 14 August 2005

The research studies the co-generation of C2 hydrocarbons and electric power from methane in a solid oxide fuel cell (SOFC) reactor using La_{0.8}Sr_{0.2}MnO₃ (LSM) as the cathode catalyst, 8 mol% yttria-stabilized zirconia (YSZ) as the electrolyte and La_{1.8}Al_{0.2}O₃ (LaAlO) as the anode catalyst. The study is divided into 5 parts: 1) investigation of the behaviors of oxygen species by fuel cell type temperatureprogrammed desorption (FC-TPD) measurement, 2) oxygen permeation through the LSM/YSZ/LaAlO cell, 3) oxidative coupling of methane (OCM) in SOFC reactor, 4) modeling of SOFC reactor and 5) performance comparison between different reactors. From the studies, it was found that oxygen species involved in SOFC is active for the OCM reaction. The increase of the applied potential during the pretreatment increases the amount of desorbed oxygen and decreases the activation energy of oxygen desorption. By applying an external potential to the cell, the oxygen permeation flux increases while the activation energy of oxygen permeation decreases. The studies of the OCM in SOFC reactor show the C2 selectivity and the methane conversion of 91.7% and 23.7 % at 1273 K, respectively. The effect of external load is investigated both by performing experiments and calculations. Methane conversion decreases with increasing the external load resistance while C2 selectivity is insignificantly affected. When operating at higher temperature and pressure, higher electric power and C2 production can be obtained. Comparison between different reactors revealed that SOFC required higher operating temperature (about 200 K) than a conventional fixed bed reactor and membrane reactors with porous and dense membranes.

Keywords: Solid oxide fuel cell, C2 hydrocarbons, Oxidative coupling of methane

บทคัดย่อ

รหัสโครงการ: RSA4580028

ชื่อโครงการ: การผลิตสารประกอบไฮโดรคาร์บอน C2 และพลังงานไฟฟ้าจากมีเทน

โดยใช้เครื่องปฏิกรณ์ชนิดเซลเชื้อเพลิงแบบออกไซด์ของแข็ง

ชื่อนักวิจัย: รองศาสตราจารย์ คร.สุทธิชัย อัสสะบำรุงรัตน์

Email: <u>Suttichai.A@chula.ac.th</u>

ระยะเวลาโครงการ: 15 สิงหาคม 2545 – 14 สิงหาคม 2548

งานวิจัยนี้ศึกษาการร่วมผลิตของสารประกอบไฮโครคาร์บอน C2 และกำลังไฟฟ้าจาก มีเทน โดยใช้เครื่องปฏิกรณ์ชนิดเซลล์เชื้อเพลิงแบบออกไซด์แข็งซึ่งเซลล์ที่ใช้ประกอบด้วยขั้วแค โธคคือ $La_{08}Sr_{02}MnO_3$ (LSM) อิเล็กโตรไลท์คือ 8% โมล yttria-stabilized zirconia (YSZ) และขั้ว แอโนคคือ $La_{1.8}Al_{0.2}O_3$ (LaAlO) โดยแบ่งการศึกษาเป็น 5 ส่วนคือ 1) การศึกษาพฤติกรรมของ ออกซิเจนสปีชี่ส์โดยเทคนิคการหลุดออกด้วยการโปรแกรมอุณหภูมิ 2) การศึกษาการเคลื่อนที่ของ ออกซิเจนผ่านเซลล์ LSM/YSZ/LaAlO 3) การศึกษาปฏิกิริยาคู่ควบของมีเทนในเครื่องปฏิกรณ์ชนิด เซลล์เชื้อเพลิงแบบออกไซค์แข็ง 4) การสร้างแบบจำลองทางคณิตศาสตร์ของเครื่องปฏิกรณ์ชนิค เซลล์เชื้อเพลิงแบบออกไซค์แข็ง และ 5) การศึกษาเปรียบเทียบสมรรถนะของเครื่องปฏิกรณ์ชนิค เซลล์เชื้อเพลิงแบบออกไซค์แข็งกับเครื่องปฏิกรณ์ชนิดอื่นๆ จากการศึกษาพบว่าออกซิเจนสปีชี่ส์ที่ ้ได้จากเครื่องปฏิกรณ์ชนิดเซลล์เชื้อเพลิงแบบออกไซค์แข็งนั้นให้ค่าการเลือกเกิดต่อปฏิกิริยาคู่ควบ ของมีเทน การจ่ายศักย์ใฟฟ้าระหว่างการเตรียมการดูดซับออกซิเจนเป็นการเพิ่มปริมาณออกซิเจนที่ หลุดออกและลดพลังงานกระตุ้นในการหลุดออกด้วย เมื่อง่ายศักย์ไฟฟ้าให้กับเซลล์พบว่าฟลักซ์ใน การเคลื่อนที่ของออกซิเจนมีค่าเพิ่มขึ้นขณะที่พลังงานกระตุ้นมีค่าลดลง สำหรับการศึกษาการเกิด ปฏิกิริยาคู่ควบของมีเทนในเครื่องปฏิกรณ์ชนิดเซลล์เชื้อเพลิงแบบออกไซค์แข็งนั้นได้ทำการศึกษา ทั้งการทำการทดลองและการสร้างแบบจำลองทางคณิตศาสตร์ พบว่าค่าการเลือกเกิดของสารผลิต ภัณฑ์ C2 มีค่า 91.7 % และค่าการเปลี่ยนของมีเทนเท่ากับ 23.7 % ที่ 1273 เคลวิน การเพิ่มภาระภาย นอกมีผลทำให้ค่าการเปลี่ยนของมีเทนลดลงแต่ไม่มีผลต่อค่าการเลือกเกิดของ C2 การคำเนินการที่ อุณหภูมิและความคันสูงทำให้ได้กำลังไฟฟ้าและไฮโดรคาร์บอน C2 เพิ่มขึ้นได้ เมื่อเปรียบเทียบ เครื่องปฏิกรณ์ชนิดเซลล์เชื้อเพลิงแบบออกไซด์แข็งกับเครื่องปฏิกรณ์ชนิดอื่นๆ ได้แก่ เครื่อง ปฏิกรณ์แบบเบคนิ่ง และเครื่องปฏิกรณ์แบบเมมเบรนที่ใช้เมมเบรนชนิคที่มีรูพรุนและเมมเบรนที่ ไม่มีรูพรุน พบว่าเครื่องปฏิกรณ์ชนิดเซลล์เชื้อเพลิงแบบออกไซด์แข็งต้องใช้อุณหภูมิการดำเนินงาน ที่สูงกว่าประมาณ 200 K

คำหลัก: เซลล์เชื้อเพลิงแบบออกไซค์แข็ง สารประกอบไฮโครคาร์บอน C2 ปฏิกิริยาคู่ควบของ มีเทน

Acknowledgement

This research project is financially supported by The Thailand Research Fund (TRF). The project is completed successfully by the supports of my hard working students, Dr. Worapon Kiatkittipong and Mr. Kampol Silpasup, and by the strong collaboration with Professor Shigeo Goto and Professor Tomohiko Tagawa from the Department of Chemical Engineering, Nagoya University, Japan. The supports from TJTTP-JBIC, Chulalongkorn University and a Grant-in-aid for Scientific Research, from the Ministry of Education, Culture, Sports, Science & Technology of Japan (MEXT) are also gratefully acknowledged.

Table of Content

Abstract	Page No.
Abstract (Thai)	4
Acknowledgement	5
Chapter 1 TPD study in LSM/YSZ/LaAlO system for the use of fuel cell type reactor	7
Chapter 2 Oxygen transport through LSM/YSZ/LaAlO system for the use of fuel cell type reactor	22
Chapter 3 Oxidative Coupling of Methane in LSM/YSZ/LaAlO SOFC Reactor	39
Chapter 4 Simulation of Oxidative Coupling of Methane in Solid Oxide Fuel Cell Type Reactor for C2 Hydrocarbon and Electricity Co-Generation	62
Chapter 5 Comparative Study of Oxidative Coupling of Methane Modeling in Various Types of Reactor	77
Summary of Research Outputs	88
Appendix	
Appendix A Manuscript "TPD study in LSM/YSZ/LaAlO system for the use of fuel cell type reactor"	91
Appendix B Manuscript "Oxygen transport through LSM/YSZ/LaAlO system for the use of fuel cell type reactor"	102
Appendix C Manuscript "Oxidative Coupling of Methane in LSM/YSZ/LaAlO SOFC Reactor"	111

Chapter 1
TPD study in LSM/YSZ/LaAlO system for the use of fuel cell type reactor

1.1 Introduction

Solid oxide fuel cell (SOFC) is a promising energy-conversion technology for future application [1,2]. In our previous papers, the SOFC system was applied as a selective oxidation reactor for chemical-energy co-generation [3-9]. In these studies, the oxidative coupling of methane to ethane and ethylene was studied. The solid electrolyte is used as an oxygen separator and an oxygen distributor to achieve high C2 selectivity. In this electro-catalytic system, combined effects of activation of oxygen on an anode and permeation of oxygen through the electrolyte control the performance of reactor. A number of reviews were published on this topic [10-12].

The use of external potential is also of recent interest. Special attention has been focused on the effect of non-Faradaic electrochemical modification of catalytic activity (NEMCA) [13-14] observed for a wide range of reactions in the presence of metals such as Pt, Pd, Rh, Au, Ag and Ni, and those of oxides such as IrO₂ and RuO₂. Conventional solid electrolytes used in most studies are O²⁻ conductors like YSZ [15-17] or CeO₂ [18].

Temperature-programmed desorption (TPD) technique is usually used to investigate behaviors of oxygen species on the selective oxidation catalyst by detecting gas phase oxygen desorbed from pretreated oxide surface with increasing the temperature of the sample oxide. Tsiplakides *et al.* investigated oxygen TPD on metal electrode (e.g. Pt and Ag) deposited on YSZ [16]. However, very limited studies on TPD in SOFC reactor are reported. Baker *et al.* [19] studied TPD in system of solid oxide fuel cell by using CaO-stabilized zircinia (CSZ) tube and Ag as the electrolyte and the cathode, respectively. The formation of new species under electrochemical oxygen pumping conditions and lowering of the desorption temperature of other oxygen species were observed from both researchers [16,19]

As a tool for designing an anode catalyst for the oxidative coupling of methane in the SOFC reactor, the conventional TPD technique has been successfully applied [5]. A novel fuel cell type temperature-programmed desorption (FC-TPD) was proposed and proved to be very useful tool for characterization of the SOFC type reactors [8]. In the same report [8], the effect of applied potential on reactivity was also investigated. The change in the selectivity with applied potential when the anode was employed as a selective oxidation catalyst with a pre-mixed feed of air and methane gave a new aspect to the NEMCA phenomena. In this study, unsteady state experiments with FC-TPD technique on open circuit, closed circuits with and without applied potential were conducted and the reactivity of oxygen species was correlated to surface active sites.

1.2 Experimental

1.2.1 Apparatus

Fuel cell type temperature-programmed desorption (FC-TPD) experiments were carried out using an apparatus illustrated in Fig. 1.1. A tube-type YSZ membrane (8 mol% Y_2O_3 , thickness = 1.5 mm, inside diameter = 18 mm, outside

diameter = 21 mm, length = 500 mm, effective surface area = 0.0148 m^2) was used as an electrolyte. La_{1.8}Al_{0.2}O₃ (abbreviated as LaAlO) prepared by a mist decomposition method was used as an anode catalyst on the inner surface of the tube while La_{0.85}Sr_{0.15}MnO₃ (abbreviated as LSM) prepared by a conventional paste method on the outer side was used as the cathode.

Details of the electrode preparation methods were described elsewhere [3, 6, 7]. Platinum wire was connected to platinum meshes placed on both electrode surfaces to serve as current collectors. The outlet gas from the anode side was directly connected to a thermal conductivity detector (TCD). A potentiostat was used to supply an external electrical potential to the system. Oxygen transport from the cathode side to the anode was promoted under the applied positive potential.

1.2.2 Fuel cell type temperature-programmed desorption (FC-TPD) measurement

Before the FC-TPD measurement, the cell was pretreated under the following condition: the air flow rate in the anode = 1.36×10^{-5} mol.s⁻¹, the oxygen flow rate in the cathode = 1.02×10^{-5} mol.s⁻¹ and T = 1273 K. Three modes of pretreatment; i.e. open circuit pretreatment, closed circuit pretreatment and closed circuit pretreatment with applied potential (V_P) , were considered in this study. After the pretreatment for 7 h, the system was cooled down to T = 600 K at a rate of 0.093 K.s⁻¹. Then, the anode gas was switched to helium carrier gas (1.36x10⁻⁵ mol.s⁻¹) while the cathode gas remained unchanged. The applied potential (V_P) was disconnected for the closed circuit pretreatment. The anode exit gas was analyzed using the TCD. After the baseline was stabilized, the FC-TPD measurement was started by increasing the temperature at a desired rate (= 0.05, 0.083, 0.117 and 0.133 K.s^{-1}). Oxygen spectra was recorded by the TCD. There were three modes of FC-TPD measurement; i.e. open circuit FC-TPD, closed circuit FC-TPD and closed circuit FC-TPD with applied potential. In the closed circuit mode, both electrodes were connected to allow oxygen permeation from the cathode to the anode. An external potential (V_T) can be supplied to the cell by the potentiostat during the closed circuit mode.

1.3 Results and Discussion

1.3.1 FC-TPD experiment and proposed schemes for oxygen adsorption and desorption

Desorption of oxygen from a fuel cell unit was continuously observed under the constant rate of temperature increase under helium flow at the anode side. Three kinds of TPD operation were conducted after three kinds of pretreatment. Proposed scheme for adsorption and desorption of oxygen on the anode of fuel cell system is summarized in Fig. 1.2. For open circuit pretreatment, since the circuit is not connected, there is no oxygen permeation from the cathode side to the anode side. However, the thermal migrations of oxygen ions through the solid electrolyte may be occurred due to the high temperature pretreatment condition. Oxygen adsorbed on the anode is from air feed stream at the anode side as shown in Fig. 1.2 (a). When the circuit is closed during the pretreatment, the permeation of oxygen species is also allowed. Therefore, the closed circuit pretreatment provides the combined effect of oxygen adsorption from the surface and the permeation through the electrolyte as shown in Fig. 1.2 (b). Especially, for the pretreatment under applied potential, it is expected that the amount and quality of the adsorption site should be altered as shown

in Fig. 1.2 (c). Fig. 1.2-(1) shows the open circuit FC-TPD where surface oxygen species on the anode desorb without permeation. The dotted line with arrow shows a possibility that a small amount of oxygen in YSZ desorbs at high temperature. When the circuit is closed, the permeation of oxygen is also possible in addition to desorption of surface oxygen as shown in Fig. 1.2-(2). For the closed circuit FC-TPD under applied potential, the rate of oxygen permeation should be promoted with the driving force of applied potential as shown in Fig. 1.2-(3).

Table 1.1 lists the FC-TPD experiments (case 1-8) at various operating modes of FC-TPD ((1)-(3) in Fig. 1.2) and pretreatment conditions ((a)-(c) in Fig. 1.2).

1.3.2 Temperature-programmed desorption results

Open circuit FC-TPD

Open circuit FC-TPD measurements were carried out to investigate the nature of adsorbed oxygen on the anode catalyst of the fuel cell system (LSM/YSZ/LaAlO). Since the circuit was not connected, there was no oxygen permeation from the cathode side to the anode side. Therefore, the observed spectra is arisen from oxygen desorbed from the anode and the electrolyte as shown in Fig. 1.2-(1). Figure 1.3 shows the effect of external applied potential during the pretreatment on the FC-TPD spectra. The pretreatment conditions included the open circuit pretreatment, Fig. 1.2 (a) (case 1), the closed circuit pretreatment, Fig. 1.2 (b) (case 2) and the closed circuit pretreatment with external applied potential, Fig. 1.2 (c), $V_P =$ 1 V (case 3) and 2 V (case 4). It is noted that for the open circuit and closed circuit pretreatment (case 1 and 2, respectively), an internal potential as high as that from a concentration cell condition at 1273 K are 197 and 189 mV, respectively, existed even if no external potential was applied ($V_P = 0 \text{ V}$). The internal potential at 1273 K before and after pretreatment is insignificantly observe in both cases. It was found that the increase of the applied potential during the pretreatment increased the amount of desorbed oxygen especially at temperature lower than 1250 K. This suggests that the applied potential can activate the ability of the anode material (LaAlO) on oxygen adsorption.

In our previous TPD study of the anode powder [5], it was proposed that the oxygen species desorbed at low temperature (below 1000 K) were active for CO and CO₂ formation (oxygenate site) while the oxygen species desorbed at higher temperature (above 1000 K) were active for oxidative coupling of methane to C2-hydrocarbon (coupling site). Two peaks similar to those observed in the previous TPD study of the anode powder are found in the open circuit FC-TPD measurements. By performing the FC-TPD experiment with different values of temperature increase, the behavior of these two oxygen species can be revealed.

Figure 1.4 shows the effect of rate of temperature increase () on oxygen desorption in the open circuit mode for case 1 (open circuit FC-TPD with open circuit pretreatment). It was found that the temperatures for maximum amount of desorbed oxygen ($T_{\rm m}$) of oxygenate site and coupling site are shifted to higher temperature with the increasing . According to Cvetanovic and Amenomiya [20], the activation energy of desorption ($E_{\rm d}$) from TPD data with different can be estimated by the following equation.

$$2\ln T_{\rm m} - \ln(\beta) = \frac{E_{\rm d}}{R_{\rm g}T_{\rm m}} + \ln\left(\frac{E_{\rm d}}{AR_{\rm g}}\right) \tag{1.1}$$

Figures 1.5 and 1.6 show the plot of Eq. (1.1) for the oxygenate site and the coupling site, respectively.

The values of the activation energy of desorption for both sites are summarized in Table 1.2. It was found that the activation energy of desorption decreases with increasing the applied potential during the pretreatment for both sites, suggesting the qualitative change of adsorption site with the electrostatic field. The activation energy of the steady state oxygen permeation from preliminary experiments is 170 kJ.mol^{-1} which is higher than the activation energy of desorption of adsorbed oxygen ($E_{\rm d}$) obtained from this study.

Closed circuit FC-TPD

When the circuit is closed during the FC-TPD experiment, the permeation of oxygen species is also allowed. Therefore, the closed circuit FC-TPD mode provides the combined effect of oxygen desorption from the surface and oxygen permeation through the electrolyte as shown in Fig. 1.2-(2). The rate of temperature increase () was varied to obtain the activation energy. Figure 1.7 shows the effect of rate of temperature increase () on total oxygen desorption in the closed circuit mode with the open circuit pretreatment (case 5). Two peaks similar to those observed in the open circuit mode are found in this case. Oxygen desorption increases with decrease of . This may be due to the effect of oxygen permeation through cell system. Figures 1.8 and 1.9 show plots of Eq. (1.1) for the oxygenate site and the coupling site, respectively.

The values of the activation energy for both sites are summarized in Table 1.3. Similar to the open circuit FC-TPD, the activation energy decreases with increasing the applied potential during pretreatment for both sites. This also suggests the qualitative change of adsorption site with the electrostatic field. The activation energy of the oxygenate site from the open circuit and closed circuit operation modes is almost the same. On the other hand, the activation energy of the coupling site from the closed circuit mode is much higher than that from the open circuit mode. The value is rather near that from the steady state permeation (170 kJ.mol⁻¹). As far as YSZ concerns, the oxygen permeation at temperature lower than 1000 K can be neglected. Therefore, the desorption from oxygenate site (T < 1000 K) is not affected by oxygen permeation. However, at higher temperature above 1000 K, the permeation through the YSZ cannot be neglected. Relationship between adsorbed oxygen and permeating oxygen should be studied in further details.

Closed circuit FC-TPD with external applied potential

In our previous work [8], the effects of applied potential on the rates of oxidative coupling of methane in the SOFC reactor were studied. As shown in Fig. 1.10, the external potential was applied when mixture of air and methane was fed on the anode (air + CH₄/LaAlO/YSZ/LSM/O₂). When the circuit was closed with no applied potential, the rate of CO₂ formation was significantly decreased and the CO formation rate was increased while C₂ formation was almost the same. The similar tendency was observed with applied potential. These effects of applied potential cannot be explained by "Faraday's Law". Therefore, we proposed these effects as the NEMCA phenomena [8].

These behaviors can be explained by considering the results from the closed circuit FC-TPD with and without external applied potential (case 5 and 8, respectively). As shown in Fig.1.2-(3), with external applied potential, the qualitative change in adsorption site may be induced as discussed in the previous section at low temperature. Permeation of oxygen is also enhanced at high temperature with applied potential as shown in Fig. 1.11. Oxygen starts to desorb below 700 K with open circuit mode (case 1), but the temperature shifts to 800 K when the circuit is closed (case 5). The amount of desorbed oxygen species at 1000 K from the closed circuit mode dominates the open circuit mode. Similar tendency is observed when the external potential ($V_T = 1 \text{ V}$) was applied (case 8). Assuming that loosely bound oxygen species (the one that desorbs at T = 700-800 K) is active for the combustion reaction (CO₂ formation), an increase of interaction between adsorbed oxygen species and the anode by applied potential (species desorbed at 800-1000 K) reduces the activity of oxygen species to form oxygenates and the combustion hardly occurs, resulting in the production of CO. The NEMCA effect shown in Fig. 1.10 can be correlated to the behavior of active site to interact with oxygen under the electrostatic field.

1.4 Conclusion

The effect of applied potential on the oxygen adsorption and oxygen desorption in the LSM/YSZ/LaAlO SOFC type reactor was studied. The fuel cell type temperature-programmed desorption (FC-TPD) measurements of oxygen were conducted. This technique enables to discuss the oxygen species for the combustion reaction and the coupling reaction separately. By applying external potential, the amount of adsorbed oxygen on the anode catalyst is altered and the activation energy of desorption is decreased. The FC-TPD analysis also correlates the behavior of adsorbed oxygen species to the change in the selectivity of oxidative coupling of methane in SOFC reactor regarded as the NEMCA phenomena.

Nomenclature

```
A pre-exponetial factor (s^{-1})
```

 $E_{\rm d}$ activation energy of desorption (kJ.mol⁻¹).

 $R_{\rm g}$ gas constant (J.mol⁻¹.K⁻¹)

T absolute temperature (K)

 $T_{\rm m}$ temperature for the maximum of amount of desorbed oxygen (K)

 $V_{\rm P}$ applied external potential during pretreatment (V).

 $V_{\rm T}$ applied external potential during TPD (V).

Greek Letter

rate of temperature increase (K.s⁻¹)

References

- [1] B.C.H. Steele, J.Material. Sci 36 (2001) 1053.
- [2] O. Yamamoto, Electrochim. Acta 45 (2000) 2423.
- [3] T. Tagawa, K.K. Moe, M. Ito, S. Goto, Chem. Eng. Sci. 54 (1999) 1553.
- [4] T. Tagawa, H. Imai, J. Chem. Soc., Faraday Trans 84 (1) (1988) 923.

- [5] T. Tagawa, K.K. Moe, T. Hiramatsu, S. Goto, Solid State Ionics 106 (1998) 227.
- [6] K.K. Moe, T. Tagawa, S. Goto, J. Ceram. Soc. Jpn. 106 (1998) 242.
- [7] K.K. Moe, T. Tagawa, S. Goto, J. Ceram. Soc. Jpn. 106 (1998) 754.
- [8] T. Tagawa, K. Kuroyanagi, S. Goto, S. Assabumrungrat, P. Praserthdam, Chem. Eng. J. 93 (2003) 3.
- [9] A.S. Carrillo, T. Tagawa, S. Goto, Mater. Res. Bull. 36 (2001) 1017.
- [10] D. Eng, M. Stoukides, Catal. Rev. Sci. Eng. 33 (1991) 375.
- [11] E.N. Voskresenskaya, V.G. Roguleva, A.G. Anshits, Catal. Rev. Sci.Eng. 37 (1995) 101.
- [12] M. Stoukides, Catal. Rev. Sci. Eng. 42 (2000) 1.
- [13] C.G. Vayenas, M.M. Jaksic, S. Bebelis, S.G. Neophytides, in: P. Horsman, B.E. Conway, R.E. White (Eds.), Mod. Aspects Electrochem., vol. 29, Plenum, New York, 1996, p. 57.
- [14] I.S. Metcalfe, Solid State Ionics 152-153 (2002) 669.
- [15] V.D. Belyaev, T.I. Politova, V.A. Sobyanin, Solid State Ionics 136-137 (2000) 721.
- [16] D. Tsiplakides, S. Neophytides, C.G. Vayenas, Solid State Ionics 136-137 (2000) 839.
- [17] P. Vernoux, F. Gaillard, L. Bultel, E. Siebert, M. Primet, J. Catal. 208 (2002) 412.
- [18] P.D. Petrolekas, S. Balomenou, C.G. Vayenas, J. Electrochem. Soc. 145 (1998) 1202.
- [19] R.T. Baker, I.S. Metcalfe, P.H. Middleton, J. Catal. 155 (1995) 21.
- [20] R.J. Cvetanovic, Y. Amenomiya, Application of a temperature-programmed desorption technique to catalyst studies, Advance in catalysis and related subjects, vol 17, Academic Press, New York, 1967.

Table 1.1 Summary of FC-TPD experiments.

Case No.	$egin{array}{c} ext{Pretreatment} \ ext{Condition, } V_{ ext{P}} \ \end{array}$	Operating type of FC-TPD, V_T	
1	(a) open circuit	(1) open circuit	See Sec.3.2.1
2	(b) closed circuit, 0 V	(1) open circuit	See Sec.3.2.1
3	(c) closed circuit, 1 V	(1) open circuit	See Sec.3.2.1
4	(c) closed circuit, 2 V	(1) open circuit	See Sec.3.2.1
5	(a) open circuit	(2) closed circuit, 0 V	See Sec.3.2.2
6	(b) closed circuit, 0 V	(2) closed circuit, 0 V	See Sec.3.2.2
7	(c) closed circuit, 2 V	(2) closed circuit, 0 V	See Sec.3.2.2
8	(a) open circuit	(3) closed circuit, 1 V	See Sec.3.2.3

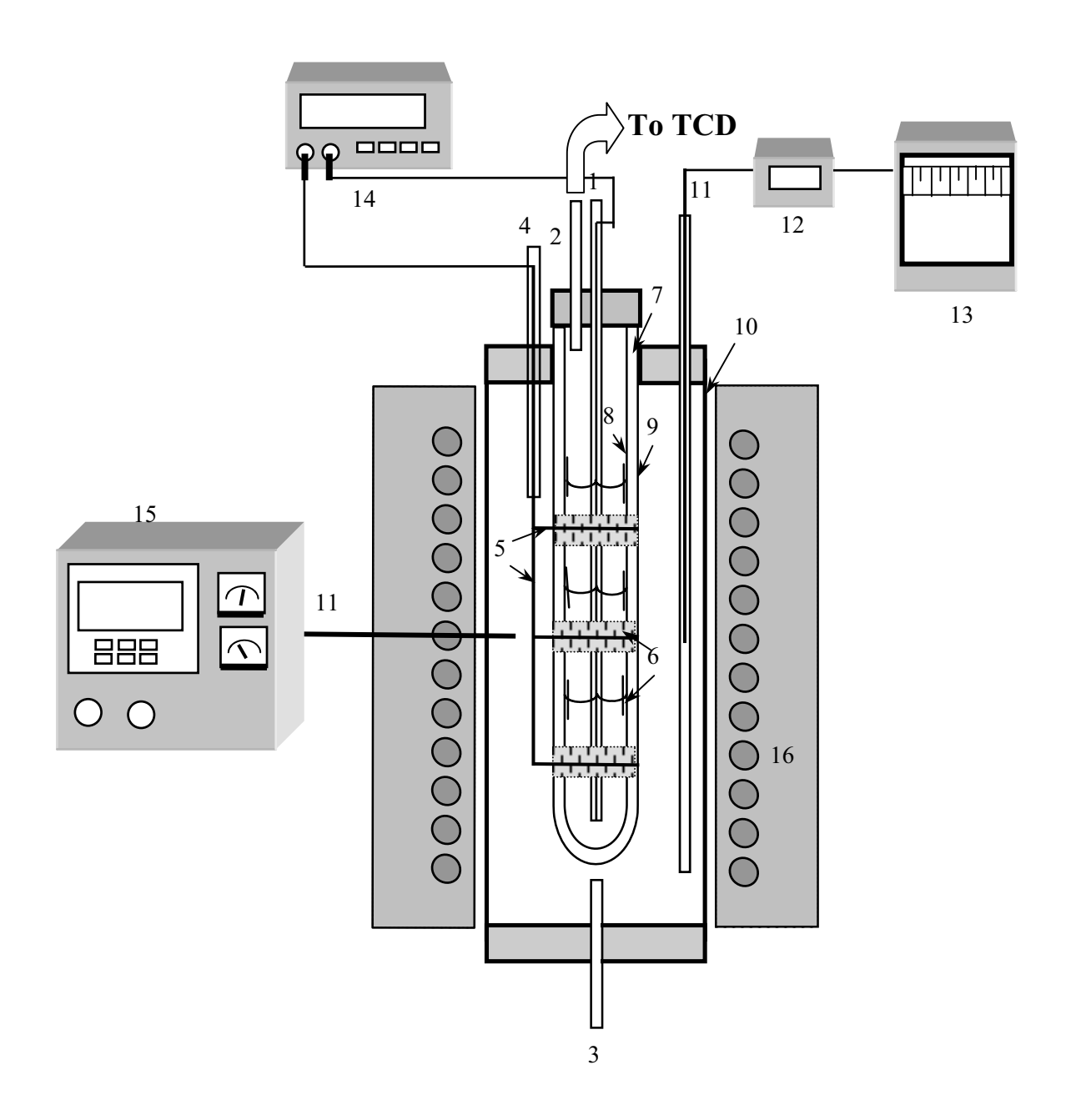
Table 1.2 Summary of activation energy of desorption at different levels of applied potential pretreatment condition from the open circuit FC-TPD measurements (Case 1-4).

Case No.	Oxygenate site		Coupling site	
	A (s ⁻¹)	$E_{\rm d}$ (kJ.mol ⁻¹)	$A(s^{-1})$	$E_{\rm d}$ (kJ.mol ⁻¹)
1	24.7	90	31.64	111
2	4.86	81	5.62	99
3	0.67	69	1.55	90
4	0.21	63	0.32	78

Table 1.3 Summary of activation energy at different levels of applied potential pretreatment condition from the closed circuit FC-TPD measurements (Case 5-7).

Case No.	Oxygenate site		se No. Oxygenate site Coupling site		ng site
	$A (s^{-1})$	$E_{\rm d}$ (kJ.mol ⁻¹)	$A (s^{-1})$	$E_{\rm d}$ (kJ.mol ⁻¹)	
5	0.46	92	14.49	140	
6	0.09	83	0.48	112	

 4.47×10^{-3} 65 0.03 93



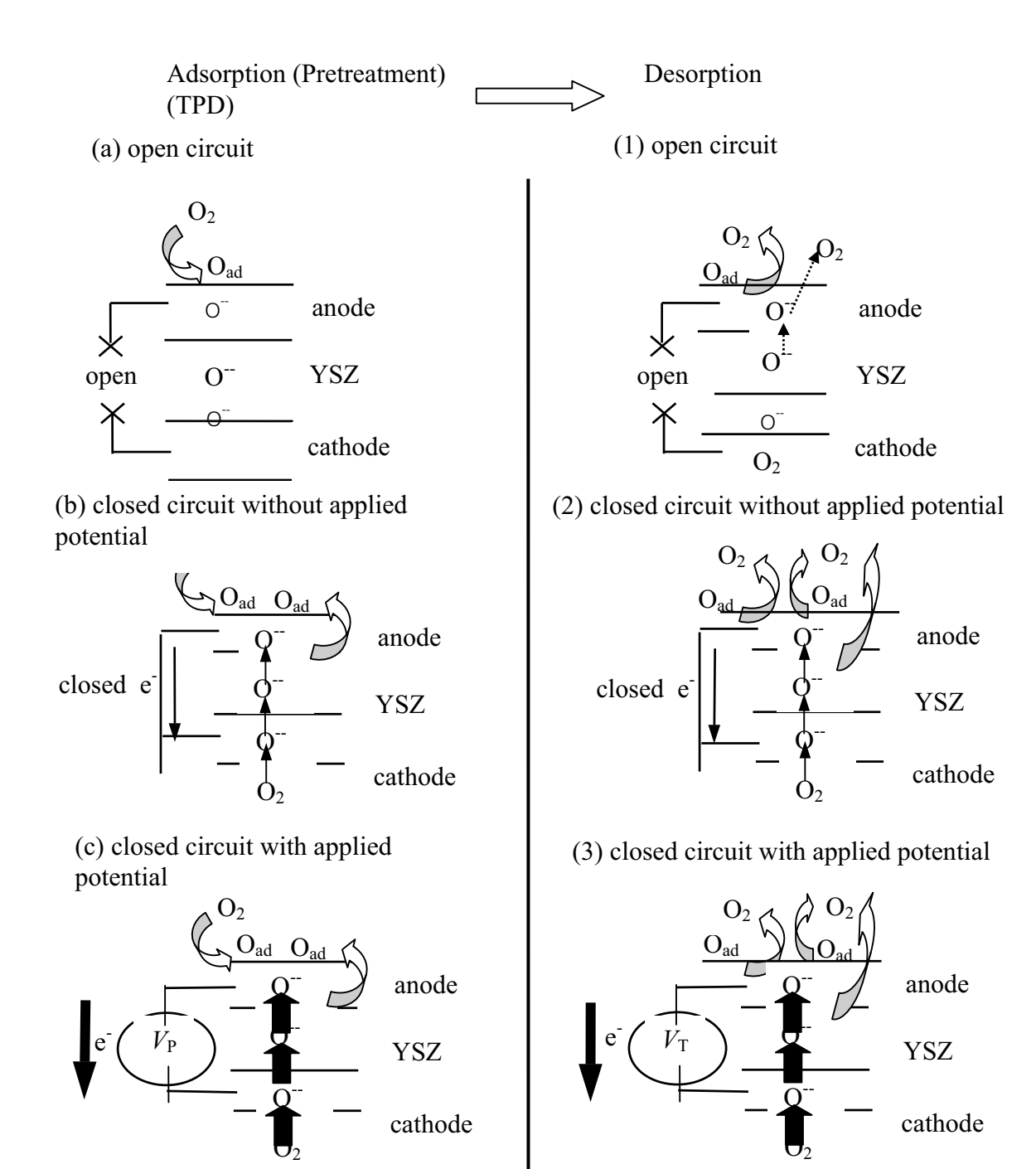


Fig. 1.2 Proposed scheme for adsorption and desorption of oxygen on the anode of fuel cell system.

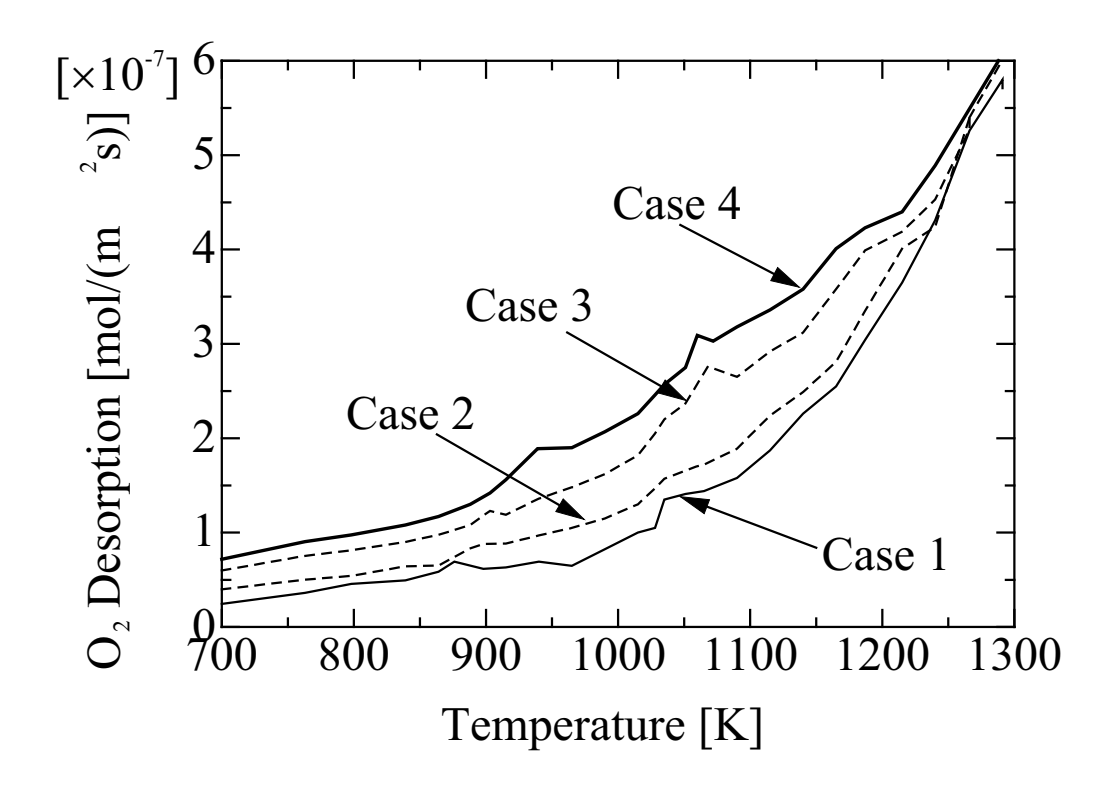


Fig. 1.3 Effect of pretreatment condition on the open-circuit FC-TPD results ($= 0.117 \text{ K.s}^{-1}$).

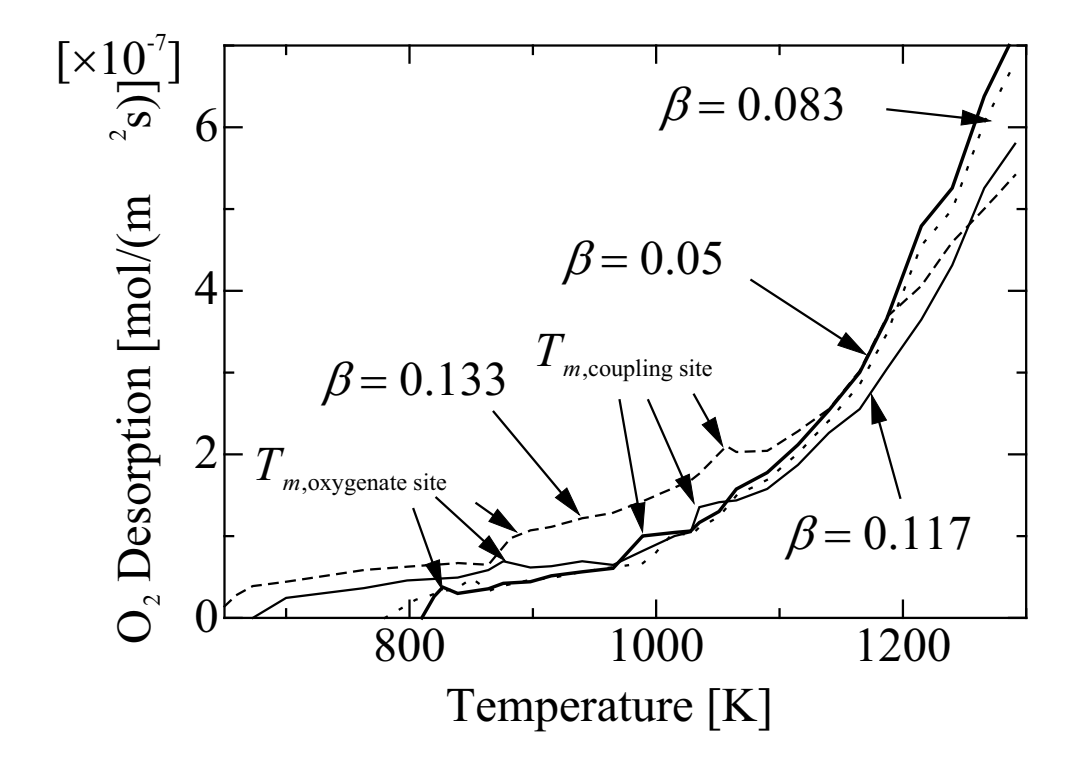


Fig. 1.4 Effect of rate of temperature increase () on the results of the open circuit FC-TPD with the open circuit pretreatment (Case 1).

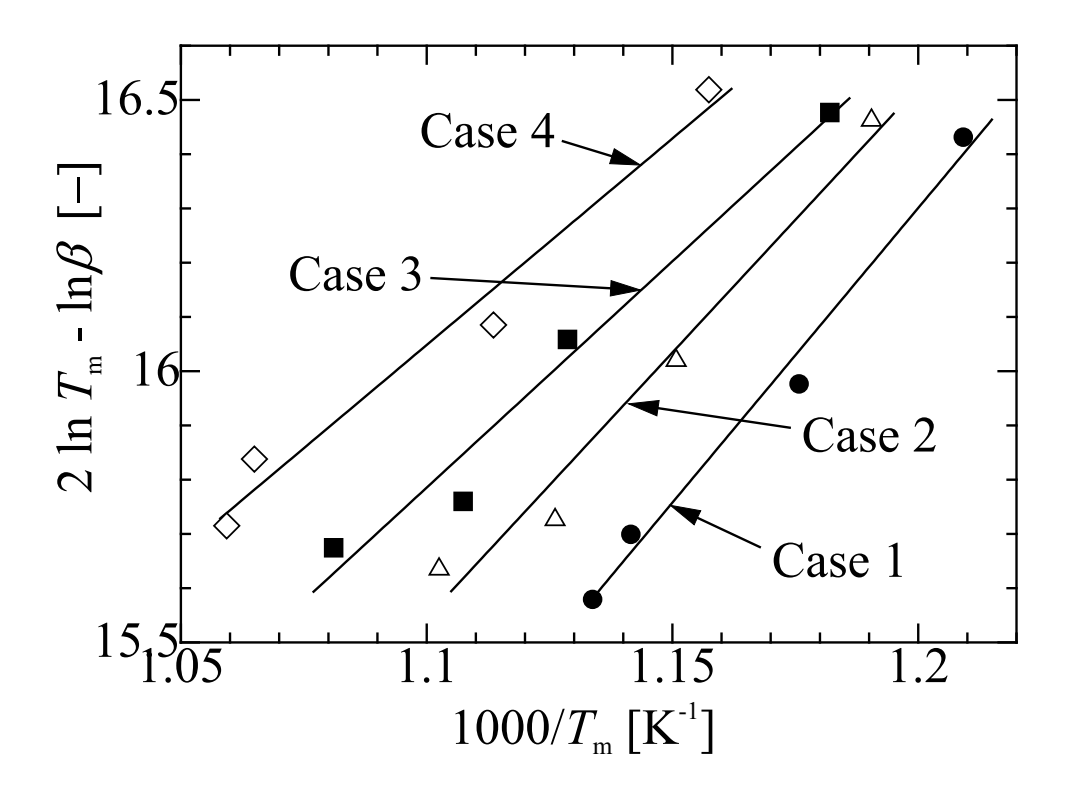
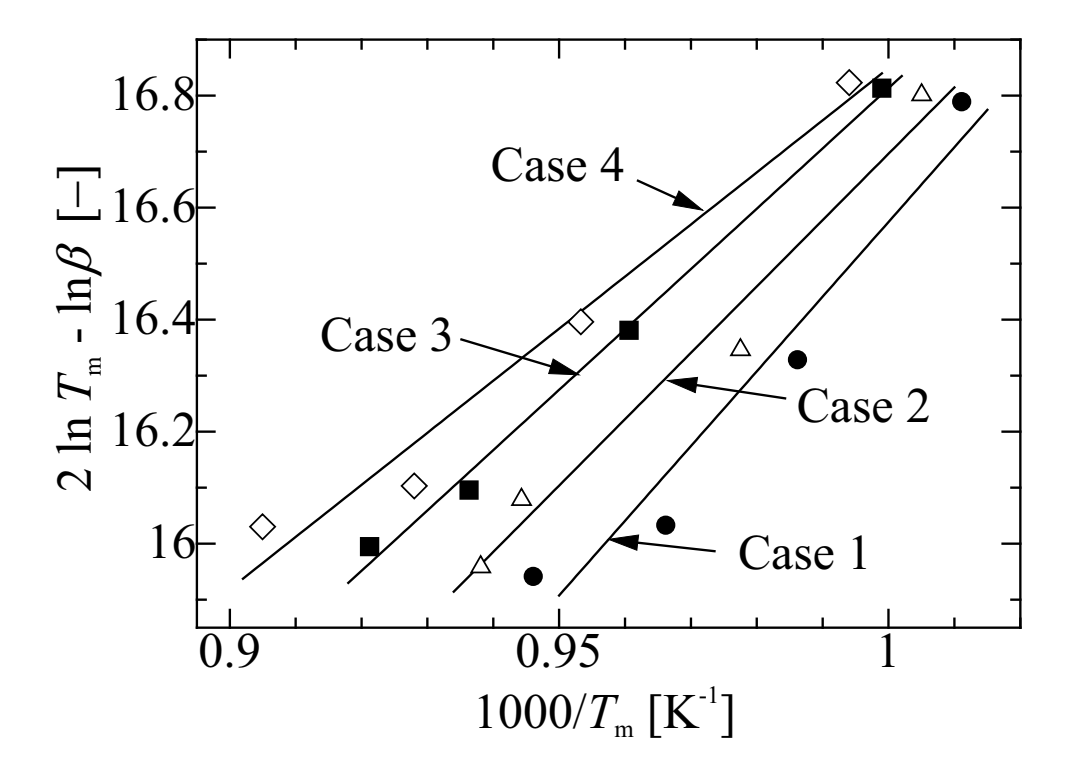


Fig. 1.5 Plots of $(2 \ln T_m - \ln)$ against $1/T_m$ for oxygenate site in the open circuit FC-



TPD mode.

Fig. 1.6 Plots of $(2 \ln T_m - \ln)$ against $1/T_m$ for coupling site in the open circuit FC-TPD mode.

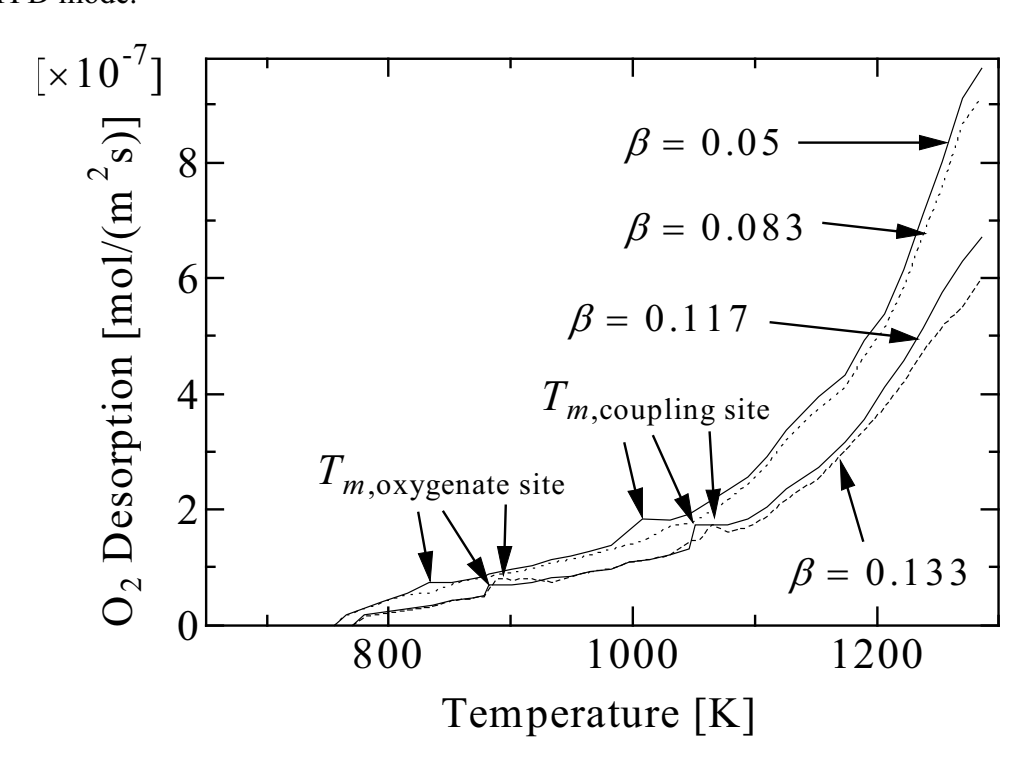
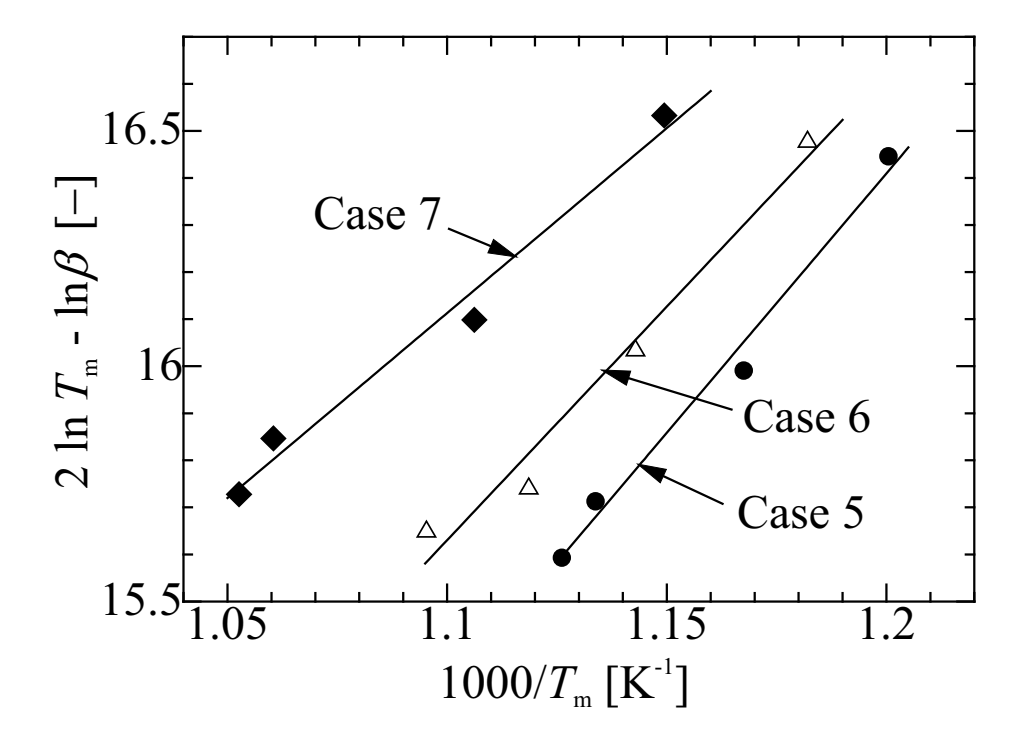


Fig. 1.7 Effect of rate of temperature increase () on the results of the closed circuit



FC-TPD with the open circuit pretreatment (Case 5).

Fig. 1.8 Plots of $(2 \ln T_m - \ln)$ against $1/T_m$ for oxygenate site in the closed circuit FC-TPD mode.

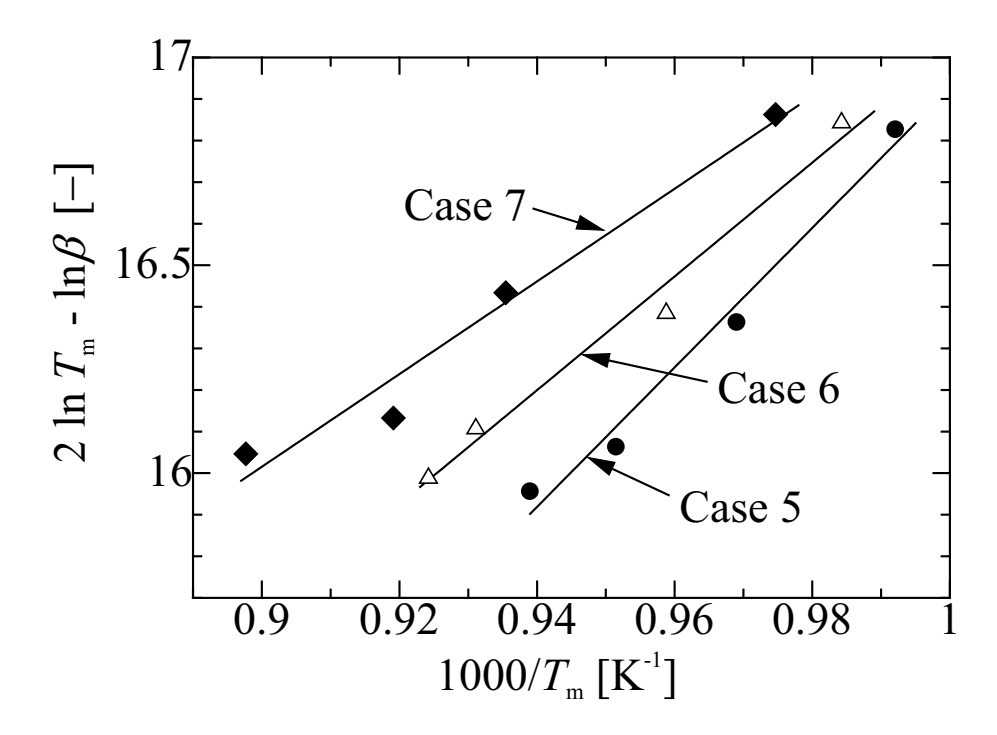


Fig. 1.9 Plots of $(2 \ln T_m - \ln)$ against $1/T_m$ for oxygenate site in the closed circuit FC-TPD mode.

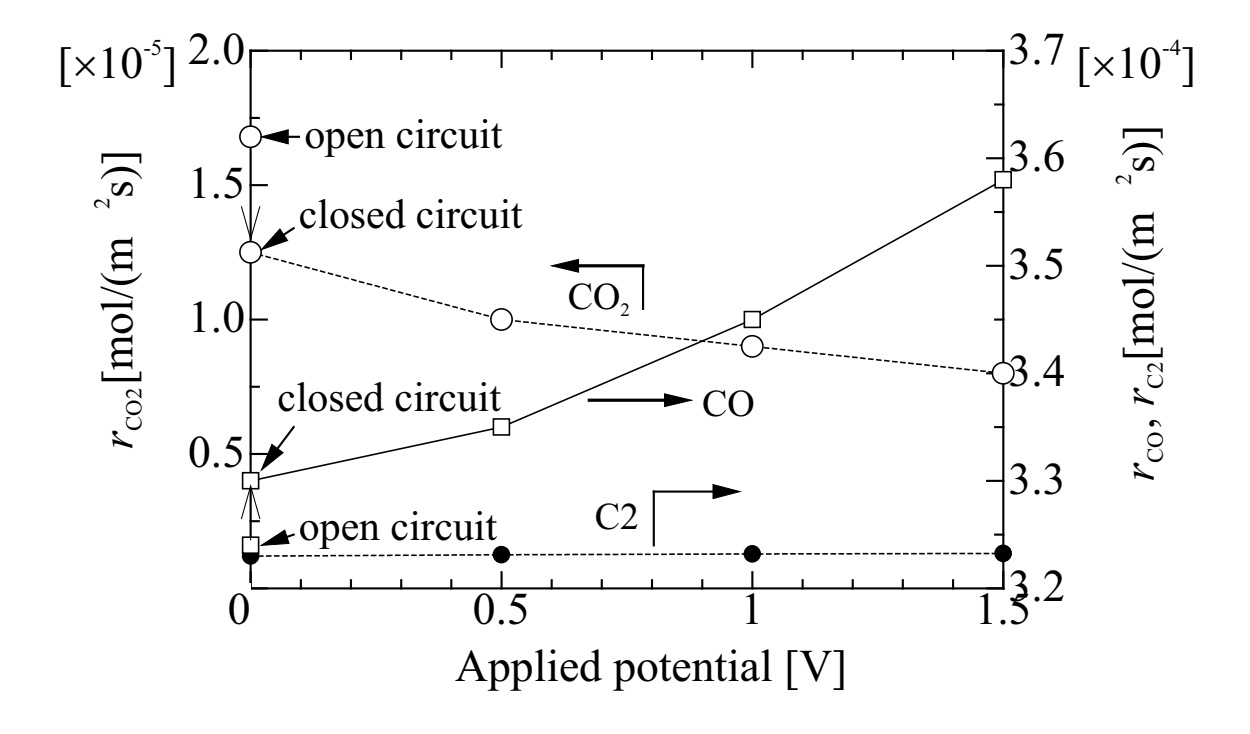


Fig. 1.10 Effect of applied potential on rates of formation of products (T = 1223 K) (pre-mixed feed of oxygen ($2.4 \times 10^{-6} \text{ mol.s}^{-1}$) and methane ($5.1 \times 10^{-5} \text{ mol.s}^{-1}$) in the anode side and oxygen feed ($6.8 \times 10^{-6} \text{ mol.s}^{-1}$) in the cathode side).

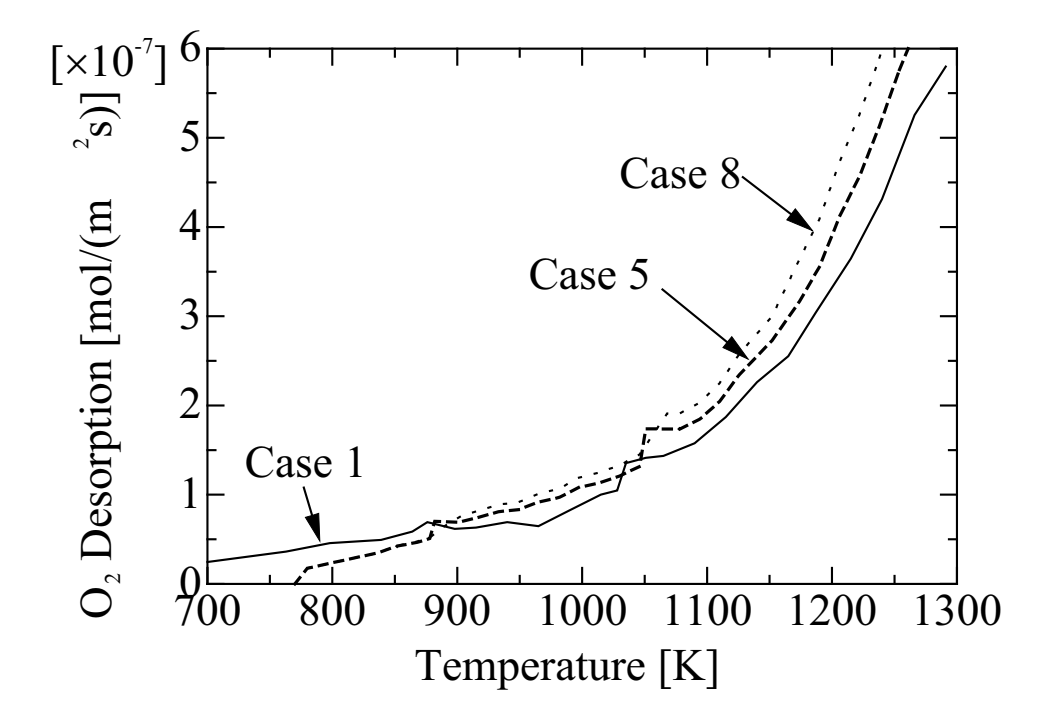


Fig. 1.11 Effect of applied potential on the FC-TPD results (open circuit pretreatment, = 0.117 K.s^{-1}).

Chapter 2
Oxygen transport through LSM/YSZ/LaAlO system for the use of fuel cell type reactor

2.1 Introduction

Solid oxide fuel cell (SOFC) is a promising energy-conversion technology for future applications [1,2]. In our previous papers, the SOFC system was applied as a selective oxidation reactor for chemicals energy co-generation. Particular focuses were on catalyst preparation method [3-5] and reactor performance test [6-8]. In these studies, the oxidative coupling of methane to ethane and ethylene (C2) was studied. The solid electrolyte was used as an oxygen separator and an oxygen distributor to achieve high C2 selectivity. In these electrocatalytic systems, combined effects of activation of oxygen on an anode and permeation of oxygen through a Yttria Stabilized Zirconia (YSZ) controlled the reactor performance.

Therefore, the oxygen transport through the electrochemical system should be studied. Several research groups have published their experimental results on the overall oxygen permeation through many oxygen permeable electrolyte membranes such as YSZ [9], Calcia Stabilized Zirconia (CSZ) [10], mixed ion-electronic conducting materials such as $La_{1-x}Sr_xCo_{1-y}Fe_yO_{3-\delta}$ (LSCF) [11,12] and other perovskite type ceramics, for example, $Bi_{1.5}Y_{0.3}Sm_{0.2}O_{3-\delta}$ (BYS) [13,14], $BaBi_xCo_{0.2}Fe_{0.8-x}O_{3-\delta}$ [15], $BaCo_{0.4}Fe_{0.6-x}Zr_xO_{3-\delta}$ [16].

Several studies focused on the steady state oxygen permeation in membrane reactors for oxidation reactions, for example, partial oxidation of methane [17] and oxidative coupling of methane [14,18]. However, very limited studies on oxygen permeation in the SOFC reactors have been reported. The conventional Yttria Stabilized Zirconia (YSZ) electrolyte has been widely used to provide the electrochemical permeation of oxygen for the oxidative coupling of methane [3-8]. The use of external potential as well as the effect of non-Faradaic electrochemical modification of catalytic activity (NEMCA) are of recent interest.

In the previous paper [8], the fuel cell type temperature-programmed desorption (FC-TPD) was studied on the LSM/YSZ/LaAlO system. Increasing the applied potential increased the amount of adsorbed oxygen. The change in the selectivity of active sites gave a new aspect to the NEMCA phenomena in the oxidative coupling of methane in the SOFC reactor. The applied potential also decreased the activation energy of desorption of oxygen at the anode catalyst [19]. In addition, the FC-TPD analysis could correlate the behavior of adsorbed oxygen species to the NEMCA effect.

In this study, the steady state oxygen permeation using helium or methane as an anode gas was investigated. The effect of applied potential on the oxygen permeation through the LSM/YSZ/LaAlO in the SOFC reactor was studied. In addition, a model of oxygen permeation was proposed.

2.2 Experimental

2.2.1 Apparatus

The schematic diagram of the solid oxide fuel cell type reactor is illustrated in Fig. 2.1. A tube-type YSZ membrane (8 mol% Y₂O₃, thickness = 1.5 mm, inside diameter = 18 mm, outside diameter = 21 mm, length = 500 mm, effective surface area = 0.0148 m^2) was used as an electrolyte. La_{1.8}Al_{0.2}O₃ (abbreviated as LaAlO) prepared by a mist decomposition method was used as an anode catalyst on the inner surface of the tube while La_{0.85}Sr_{0.15}MnO₃ (abbreviated as LSM) prepared by paste method was used as the cathode on the outer surface [7,8]. Details of the electrode preparation methods were described elsewhere [3,4,7].

Platinum wire was connected to platinum meshes placed on both electrode surfaces to serve as current collectors. The outlet gas from the anode side was directly connected to a gas chromatograph for analysis of gas composition. A potentiostat was used to supply an external electrical potential to the system. Oxygen transport from the cathode side to the anode side was promoted under the applied positive potential.

2.2.2 Steady state oxygen permeation

Steady state oxygen permeation measurements were performed at various temperature levels: i.e., T = 1073, 1123, 1173, 1223 and 1273 K. Helium (1.36×10^{-5}) mol s⁻¹) and oxygen (1.02x10⁻⁵ mol s⁻¹) were fed to the anode and the cathode, respectively. The oxygen permeation flux was calculated from the flow rate and composition of the anode exit gas. The flow rate and its composition was measured and analyzed by a bubble flow meter and a gas chromatograph with a TCD detector, respectively. Sampling was conducted every 5 min until reaching to a steady state condition (approximately 0.5 h). Another set of steady-state oxygen permeation was carried out by using methane (6.8x10⁻⁶ mol s⁻¹) as an anode reactant gas at various temperature levels: i.e. T = 1073, 1123, 1173, 1223 and 1273 K. In this case, permeated oxygen has reacted with methane to produce oxygen containing species such as CO, CO₂, H₂O. Thus, the oxygen permeation flux was estimated by analyzing these oxygen containing products. The steady state measurements for both sets of experiments were carried out at various levels of the applied potential.

2.3 Results and Discussion

2.3.1 Oxygen transport model

2.3.1.1 Oxygen permeation through thin YSZ membranes modeled by Han et al. [9]

In our previous study on the micro fuel cell system [20], we have referred an oxygen permeation model presented by Han et al. [9]. The proposed permeation process is summarized in Fig. 2.2. In their study, a thin YSZ membrane prepared by the electrochemical vapor deposition (EVD) method was employed. The oxygen permeation flux can be described by the following equations [9].

At gas-membrane interface of the cathode side:

$$J_{O_2} = \alpha \left(P_{\text{rich}}^{1/2} - P_{O_2(I)}^{1/2} \right)$$
 In bulk oxide of YSZ: (2.1)

$$J_{O_2} = \frac{\beta}{L} \left(P_{O_2(I)}^{1/4} - P_{O_2(II)}^{1/4} \right)$$
 (2.2)

At membrane-gas interface of the anode side:

$$J_{\rm O_2} = \alpha \left(P_{\rm O_2(II)}^{1/2} - P_{\rm lean}^{1/2} \right) \tag{2.3}$$

The rate parameters α and β at T=1173 K are 9.4×10^{-7} mol m⁻² s⁻¹ Pa^{-1/2} and 5.2×10^{-11} mol m⁻¹ s⁻¹ Pa^{-1/4}, respectively. The activation energy of α and β are 53.1 and 72.0 kJ mol⁻¹ K⁻¹, respectively. As shown in Fig. 2.2, this system was operated under open circuit without the anode and cathode electrodes. 1% of hydrogen in helium was used as a reacting sweep gas. These conditions were not the same as our present system, which was operated under closed circuit with or without applied potential with LSM as the cathode and LaAlO as the anode catalyst.

2.3.1.2 A model for the oxygen permeation through the LSM/YSZ/LaAlO

In this study, an oxygen permeation model through the LSM/YSZ/LaAlO fuel cell type reaction system with closed circuit and applied potential is proposed. Schematic models of oxygen permeation are shown in **Fig. 2.3**. The circuit was closed to allow the electron transfer. Two kinds of carrier gas were used: i.e. helium (Fig. 2.3 (a)) and methane (Fig. 2.3(b)).

In the case of helium feed without applied potential

Fig.2.3(a) shows general reaction paths as follows: 1) electrochemical reduction at the LSM surface to form oxygen ions, 2) incorporation of oxygen ions into the YSZ lattice, 3) recombination and desorption of oxygen ions to form oxygen molecules at the LaAlO anode.

The permeation of oxygen through a electrochemical media depends upon ionic conductivity (σ_i) and electronic conductivity (σ_e) of the media. Assuming surface concentration of oxygen ions is equilibrated with gas phase, they can be estimated from the following equations [21].

estimated from the following equations [21].
$$J_{O_2} = \frac{Per_{O_2}}{L} \ln \left(\frac{P_{\text{rich}}}{P_{\text{lean}}} \right)$$
(2.4)

$$Per_{,O_2} = \frac{R_g T}{16F^2} \frac{\sigma_i \sigma_e}{\sigma_i + \sigma_e}$$
 (2.5)

$$\sigma_{j} = \left(\frac{A_{j}}{T}\right) \exp\left(\frac{-E_{j}}{R_{o}T}\right); j = i, e$$
 (2.6)

The ionic conductivities of LSM ($_{i\text{-LSM}}$) [22], the electronic conductivities of LSM ($_{e\text{-LSM}}$) [23,24], the ionic conductivities of YSZ ($_{i\text{-YSZ}}$) [25] and the electronic conductivities of YSZ ($_{e\text{-YSZ}}$) [26] were cited from the literatures and the values are summarized in **Table 2.1**.

However, these values of LaAlO are not available in literature. Due to the recombination and desorption of oxygen ions to form oxygen molecules at the LaAlO anode, the overall rate of these processes at LaAlO might be estimated from Eq. (2.7)

$$J_{O_2} = k_{O_2 - \text{perm}} \ln \left(\frac{P_{\text{rich}}}{P_{\text{lean}}} \right)$$
 (2.7)

where P_{rich} and P_{lean} represent partial pressure of oxygen at the rich and lean sides of LaAlO, respectively.

When the permeation is at steady state, the oxygen permeation flux across different parts of the cell is equal to the observed experimental results.

$$J_{O_2,Exp} = J_{O_2,LSM} = J_{O_2,YSZ} = J_{O_2,LaAIO}$$
 (2.8)

The values of $k_{\rm O2\text{-}perm}$ of LaAlO at different temperatures were determined by using an all-purpose equation solver, EQUATRAN-G (Omega Simulation, Japan). $P_{\rm rich}$ of LSM is partial pressure of oxygen at feed side (=101.3 kPa) while $P_{\rm lean}$ of LaAlO is partial pressure of oxygen at permeate side which calculated from the experiments. The estimated $k_{\rm O2\text{-}perm}$ value was shown as follows.

$$k_{\rm O_2-perm} = 0.413 \exp\left(\frac{-170400}{R_{\rm g}T}\right)$$
 (2.9)

In the case of methane feed without applied potential

Oxygen ions directly reacted with methane at the anode (Fig. 2.3(b)). It was expected that the oxygen permeation rate could be enhanced. Due to the chemical reaction at the anode catalyst surface, the overall reaction rate could depend on partial pressure of methane and surface oxygen concentration. The oxygen surface reaction coefficient (k_{O2-Rxn}) was estimated from experimental oxygen permeation flux by the following equation.

$$J_{\rm O_2} = k_{\rm O_2-Rxn} P_{\rm CH_4} \ln \left(\frac{P_{\rm rich}}{P_{\rm lean}} \right)$$
 (2.10)

No oxygen was observed in gas phase of the permeate side due to reactions with methane. The surface oxygen may not be in the equilibrium with oxygen in gas phase. However, the surface oxygen concentration in methane feed could be assumed similar to the helium case. Therefore, P_{lean} in the helium case was used in Eq. (2.10)

In the case of closed circuit with applied potential

It was expected that the oxygen transfer could be accelerated with increasing applied potential ((c)-(d) in Fig. 2.3). Linear relationship between applied potential and oxygen permeation flux was assumed and the following equation could be proposed.

$$J_{O_2} = J_{O_2,0V} + k_V V_{Per} (2.11)$$

The values of $J_{\rm O2,0V}$ without applied potential can be calculated by Eqs. (2.4)-(2.6) and (2.7) for the helium feed case and by Eqs. (2.4)-(2.6) and (2.10) for the methane feed case, respectively.

2.3.1 Steady state oxygen permeation results

2.3.1.1 Helium feed

Fig. 2.4 shows the effect of the applied potential on the oxygen flux at various temperatures. Linear relationships between the oxygen permeation flux and the applied potential were observed for all different temperatures. As shown in Fig. 2.4, the oxygen could be permeated without applied potential due to the system

possessed an internal "concentration cell" potential as a driving force. For example, the concentration cell potential is 0.225 V at 1223 K. This value agrees well with OCV value calculated from Nernst equation.

$$E = \frac{R_{\rm g}T}{4F} \ln \left(\frac{P_{\rm feed}}{P_{\rm perm}} \right)$$
 (2.12)

Therefore, we can assume surface oxygen concentration at the lean side of LaAlO is in equilibrium with oxygen in gas phase at the permeate side.

The proportional constants (k_v) from Eq. (2.11) could be determined from the slopes and expressed as Eq. (2.13).

$$k_{\text{V,He}} = 0.102 \exp\left(\frac{-122700}{R_{g}T}\right)$$
 (2.13)

Fig. 2.5 shows the plots between $\ln (J_{O2})$ and 1000/T at different levels of the applied potential. The solid lines represent the results calculated from Eqs. (2.4)-(2.7), (2.11) and (2.13). The oxygen flux increases with the increasing temperature and applied potential.

The solid lines in Fig. 2.5 can be approximated by straight lines of Arrhenius' plots by Eq. (2.14).

$$J_{\rm O_2} = A_{\rm Per} \exp\left(\frac{-E_{\rm Per}}{R_{\rm g}T}\right) \tag{2.14}$$

The overall activation energy of the oxygen transport through the cell (E_{Per}) was calculated from the slopes and the results are shown in **Table 2.2**. The activation energy is decreased from 170 kJ/mol in case of closed circuit with no applied potential to 119 kJ/mol with applied potential 2 V. TPD experiments have shown that the applied potential also decreased the activation energy of the oxygen desorption from 140 to 93 kJ/mol when applied potential 2 V [19]. Comparing these values, the activation energies of oxygen permeation are close to the activation energies of oxygen desorption.

The dashed line in Fig. 2.5 shows the results calculated from Han's model [9]. The comparison of our model with Han's model will be described later (Section 2.3.2.4).

2.3.2.2 Methane feed

Instead of helium, methane was fed to the anode chamber to react with the permeating oxygen. At 1273 K, the electromotive force from the experiment is 1.09 V, which is near to the theoretical value of ethylene formation (1.05 V). Linear relationships between the oxygen permeation flux and the applied potential were observed for all different temperatures as shown in **Fig. 2.6**. The proportional constants (k_v) from Eq. (2.11) could be determined from the slopes and the expression is shown in Eq. (2.15).

$$k_{\text{V,CH}_4} = 0.875 \exp\left(\frac{-104150}{R_{\text{g}}T}\right)$$
 (2.15)

Fig. 2.7 shows the plots between $\ln(J_{\rm O2})$ and 1000/T at different levels of the applied potential. The oxygen flux with the methane feed was estimated from the equivalent rate of oxygen required for the oxidation reaction. The oxygen surface reaction coefficient ($k_{\rm O2-Rxn}$) estimated from the experimental oxygen permeation flux by using Eq. (2.8) was shown as follows.

$$k_{\text{O}_2-\text{Rxn}} = 8.577 \times 10^{-3} \exp\left(\frac{-195100}{R_{\text{g}}T}\right)$$
 (2.16)

The solid line with $V_{Per} = 0$ V represents the calculated results by Eqs. (2.4)-(2.6), (2.10) and (2.16). The solid lines for $V_{Per} = 0.5$ V, 1 V and 2 V were calculated by Eqs. (2.4)-(2.6), (2.10)-(2.11) and (2.15)-(2.16).

The solid lines in Fig. 2.7 can be approximated by straight lines of Arrhenius' plots by Eq. (2.14). The overall activation energy of the oxygen transport through the cell (E_{Per}) was calculated from the slopes and the results are shown in **Table 2.3**. The applied potential increases the oxygen flux and also decreases the activation energy of the oxygen transport.

Compared with the helium feed case, the oxygen flux is significantly improved when methane is fed to the anode side. The oxygen permeation fluxes under the methane feed are 1-2 orders of magnitude higher than those under the helium feed. It is clear that the reaction of methane with the permeated oxygen at the anode catalyst significantly improves the overall oxygen permeation flux due to the surface oxygen kinetics with methane. The dashed line in Fig. 2.7 represents the Han's model.

2.3.2.3 Oxygen partial pressure profiles and permeation mechanism

Fig. 2.8 shows the oxygen partial pressure profile from the simulation results at 1223 K. In the case of the helium feed (solid line), it is obvious that the major oxygen permeation resistance through the cell or the rate-limiting step of this system is at the LaAlO electrode. Although the thickness of YSZ electrolyte is much more than the electrodes, the resistance of YSZ electrolyte is negligible. With the methane feed case (dashed lines), the resistances of three steps are comparable; consequently, the rate steps at the cathode and the electrolyte need to be taken into account.

In the case without methane, oxygen ions release electrons and recombine into oxygen molecules, which are then desorbed into the gas phase. On the other hand, with the methane feed, oxygen ions could directly react with methane to form CO_2 , CO and C_2 hydrocarbons.

Mechanisms of the oxygen activation on the LSM and the bulk transport of O²⁻ in YSZ might be the same as the helium feed case as shown in the previous sections. The change in the surface reaction step on the anode from the recombination and desorption of oxygen ion to the reaction of oxygen species with methane would be the main reason for the increase of oxygen flux for the methane feed.

2.3.2.4 Effect of YSZ thickness

The effect of YSZ thickness on the oxygen permeation flux is simulated and the results are shown in **Fig. 2.9**. In the case of helium feed, the oxygen permeation flux is independent on the YSZ thickness as noted in the previous section that LaAlO is the rate-limiting step. However, in the case of methane feed, the resistance of YSZ electrolyte is comparable to that of LaAlO. The rate of oxygen permeation depends on the YSZ electrolyte. The flux increases with decreasing the thickness of YSZ electrolyte membrane. However, for YSZ with thickness below 10 m, there is no significant improvement on the oxygen flux. The tendency is the same for T = 1223 K and 1273 K.

2.3.2.5 Estimation of oxygen permeation from a model proposed by Han et al. [9]

Han et al. [9] proposed Eqs. (2.1)-(2.3) for the permeation of oxygen through YSZ membrane but their system was tested under unusual conditions; i.e. very thin YSZ membrane of 2-15 m, low oxygen partial pressure in an oxygen source chamber of 5.33 kPa and without external circuit (open circuit). Dashed lines in Figs. 2.5 and 2.7 show the oxygen permeation flux calculated from Eqs. (2.1)-(2.3) using a YSZ with thickness of 1.5 mm. The estimated oxygen flux is much larger than that of the helium feed (compared with $V_{Per} = 0$ in Fig. 2.5) and far less than that of the methane feed (compared with $V_{Per} = 0$ in Fig. 2.7). This tendency can be understood by considering that the sweep gas of the permeate side contained 1% of hydrogen in their experiments [9].

Hydrogen in the sweep gas caused the promotion of the oxygen permeation by the surface reaction but the partial pressure was too low to complete the enhancement of the oxygen permeation. When hydrogen was mixed in the sweep gas, an electromotive force of about 1 V should be generated between the two electrodes. This may be the reason of the agreement with the plot of $V_{\text{Per}} = 1 \text{ V}$ in Fig. 2.5.

The differences in the activation energy should be caused by the differences in the surface reaction on the anode material. Further studies are required to find more details. All these results show that is essential for the model of the SOFC type reactor to include the permeation of oxygen though the cathode, the electrolyte and the anode.

2.4 Conclusion

The oxygen transport through the LSM/YSZ/LaAlO SOFC type reactor was studied at various operating conditions. The oxygen permeation flux was 8.90x10⁻⁸ mol m⁻² s⁻¹ at 1173 K with an activation energy of 170 kJ mol⁻¹. Increasing the applied potential increased the oxygen permeation fluxes in one order of magnitude and reduced the activation energy of the oxygen permeation. The oxygen permeation fluxes under the methane feed are 1-2 orders of magnitude higher than those under the helium feed. A model of oxygen permeation was proposed. In the helium case, the oxygen permeation at the LaAlO anode was the rate-limiting step for the oxygen permeation. However, by changing helium to reactant gas as methane, the resistances in the three parts (LSM/YSZ/LaAlO) become comparable.

Nomenclature

$A_{ m j}$	pre-exponential factor of conductivity	$(S K m^{-1})$
A_{Per}	pre-exponential factor of oxygen permeation	$(\text{mol m}^{-2} \text{ s}^{-1})$
E	electromotive force	(V)
E_{j}	activation energy of conductivity	(J mol ⁻¹)
$E_{ m Per}$	activation energy of oxygen permeation	$(J \text{ mol}^{-1})$
F	Faraday's constant, 96487	$(C \text{ mol}^{-1})$
$J_{ m O2}$	oxygen permeation flux	$(\text{mol m}^{-2} \text{ s}^{-1})$
$k_{\text{O2-perm}}$	overall oxygen ions recombination and diffusion co	
$k_{\text{O2-Rxn}}$	oxygen surface reaction coefficient	$(\text{mol m}^{-2} \text{ s}^{-1} \text{Pa}^{-1})$
$k_{ m V}$	proportional constant	$(\text{mol m}^{-2} \text{ s}^{-1} \text{ V}^{-1})$
L	thickness of material	(m)
$Per,_{\mathrm{O}_2}$	specific oxygen permeability	$(\text{mol m}^{-1} \text{ s}^{-1})$
$P_{ m feed}$	oxygen partial pressure at feed side (cathode side)	(Pa)
$P_{ m perm}$	oxygen partial pressure at permeate side (anode sid	e) (Pa)
P_{rich}	oxygen partial pressure at rich side of materials	(Pa)

P_{lean}	oxygen partial pressure at lean side of materials	(Pa)
$P_{\mathrm{O}_2(\mathrm{I})}$	oxygen partial pressure at the gas-membrane interface	(Pa)
$P_{\mathrm{O}_{2}(\mathrm{II})}$	oxygen partial pressure at membrane-gas interface	(Pa)
$R_{ m g}$	gas constant, 8.314	$(J \text{ mol}^{-1} \text{ K}^{-1})$
T	temperature	(K)
V_{Per}	applied external potential during steady state permeation	
α	permeation rate constants in interface diffusion step	$(\text{mol m}^{-2} \text{ s}^{-1} \text{ Pa}^{-1/2})$
β	permeation rate constants in bulk diffusion step	(mol m ⁻¹ s ⁻¹ Pa ^{-1/4})
	conductivities	$(S m^{-1})$

<Subscript>

e electronic i ionic

References

- [1] B.C.H. Steele, J.Material. Sci 36 (2001) 1053-1068.
- [2] O. Yamamoto, Electrochim. Acta 45 (2000) 2423-2435.
- [3] K.K. Moe, T. Tagawa, S. Goto, J. Ceram. Soc. Jpn. 106 (1998) 242-247.
- [4] K.K. Moe, T. Tagawa, S. Goto, J. Ceram. Soc. Jpn. 106 (1998) 754-758.
- [5] A.S. Carrillo, T. Tagawa, S. Goto, Mater. Res. Bull. 36 (2001) 1017-1027.
- [6] T. Tagawa, K.K. Moe, T. Hiramatsu, S. Goto, Solid State Ionics 106 (1998) 227-235.
- [7] T. Tagawa, K.K. Moe, M. Ito, S. Goto, Chem. Eng. Sci. 54 (1999) 1553-1557.
- [8] T. Tagawa, K. Kuroyanagi, S. Goto, S. Assabumrungrat, P. Praserthdam, Chem. Eng. J. 93 (2003) 3-9.
- [9] J. Han, G. Xomeritakis, Y.S. Lin, Solid State Ionics 93 (1997) 263-272.
- [10] Y. Nigara, J. Mizusaki, M. Ishigame, Solid State Ionics 79 (1995) 208-211.
- [11] Y. Teraoka, Y. Honbe, J. Ishii, H. Furukawa, I. Moriguchi, Solid State Ionics 152-153 (2002) 681-687.
- [12] S. Lee, K.S. Lee, S.K. Woo, J.W. Kim, T. Ishihara, D.K. Kim, Solid State Ionics 158 (2003) 287-296.
- [13] C.E. Platon, W.J. Thomson, Ind. Eng. Chem. Res. 41 (2002) 6637-6641.
- [14] F.T. Akin, Y.S. Lin, Y. Zeng, Ind. Eng. Chem. Res. 40 (2001) 5908-5916.
- [15] Z.Shao, G. Xiong, Y. Cong, W. Yang, J. Membr. Sci. 164 (2000) 167-176.
- [16] J. Tong, W. Yang, B. Zhu, R. Cai, J. Membr. Sci. 203 (2002) 175-189.
- [17] T. Ishihara, Y. Tsuruta, T. Todaka, H. Nishiguchi, Y. Takita, Solid State Ionics 152-153 (2002) 709-714.
- [18] Y. Zeng, Y.S. Lin, J. Catal. 193 (2000) 58-64.
- [19] W. Kiatkittipong, T. Tagawa, S. Goto, S. Assabumrungrat and P. Praserthdam, Solid State Ionics 166 (2004) 127-136.
- [20] S. Goto, T. Tagawa, S. Assabumrungrat, P. Praserthdam, Catal. Today 82 (2003) 223-232.
- [21] V.V. Kharton, A.V. Kovalevsky, A.P. Viskup, F.M. Figueiredo, J.R. Frade, A.A. Yaremchenko, E.N. Naumovich, Solid State Ionics 128 (2000) 117-130.
- [22] I. Yasuda, K. Ogasawara, M. Hishinuma, T. Kawada, M. Dokiya, Solid State Ionics 86-88 (1996) 1197-1201.
- [23] Z. Li, M. Behruzi., L. Fuerst, D. Stovet, in: S.C. Singhal, H. Iwahara (Eds.), SOFC-III, PV 93-4, The Electrochemical Society, Pennington, NJ, 1993, p.171

- [24] V.V. Kharton, A.P. Viskup, I.P. Marozau, E.N. Naumocich, Mater. Lett. 57 (2003) 3017-3021.
- [25] S.P.S. Badwal, Solid State Ionics 52 (1992) 23-32.
- [26] C. Xia, S. Zha, W. Yang, R. Peng, D. Peng and G. Meng, Solid State Ionics 133 (2000) 287-297.

Table 2.1 Values of parameters for the calculations of oxygen permeation flux

Parameters	$A_{\rm j}$ (S K m ⁻¹)	$E_{\rm j}$ (kJ mol ⁻¹)	Ref.
_{i-LSM} (S m ⁻¹)	2.311x10 ¹¹	284	[22] a)
_{e-LSM} (S m ⁻¹)	8.855×10^7	9	[23] ^{b)} , [24] ^{c)}
_{i-YSZ} (S m ⁻¹)	7.121×10^7	88	[25]
_{e-YSZ} (S m ⁻¹)	9.244×10^5	87.5	[26]

$$L_{LSM} = 1 \times 10^{-6} \text{ m}, L_{YSZ} = 1.5 \times 10^{-3} \text{ m}, L_{LaAIO} = 5 \times 10^{-6} \text{ m}.$$

- a) From Table 1 at 1173 K, the value was interpolated between $La_{0.95}Sr_{0.05}MnO_3$ and $La_{0.8}Sr_{0.2}MnO_3$, and at 1273 K between $La_{0.9}Sr_{0.1}MnO_3$ and $La_{0.8}Sr_{0.2}MnO_3$.
- b) _{e-LSM} was given at 1173 K.
- c) The activation energy was shown in Table 1.

Table 2.2 Summary of the values of pre-exponential factors of oxygen permeation and activation energy at different levels of applied potential from steady state permeation results using helium feed at anode side

V _{Per} (V)	$A_{\rm Per}$ (mol m ⁻² s ⁻¹)	E_{Per} (kJ mol ⁻¹)
0	3.499	170
0.5	1.280	154
1	0.675	144
2	0.157	119

Table 2.3 Summary of the values of pre-exponential factors of oxygen permeation and activation energy at different levels of applied potential from steady state permeation results using methane feed at anode side

V _{Per} (V)	A _{Per} (mol m ⁻² s ⁻¹)	E _{Per} (kJ mol ⁻¹)
0	$3.632x10^4$	219
0.5	186.9	157
1	82.84	145
2	15.77	124

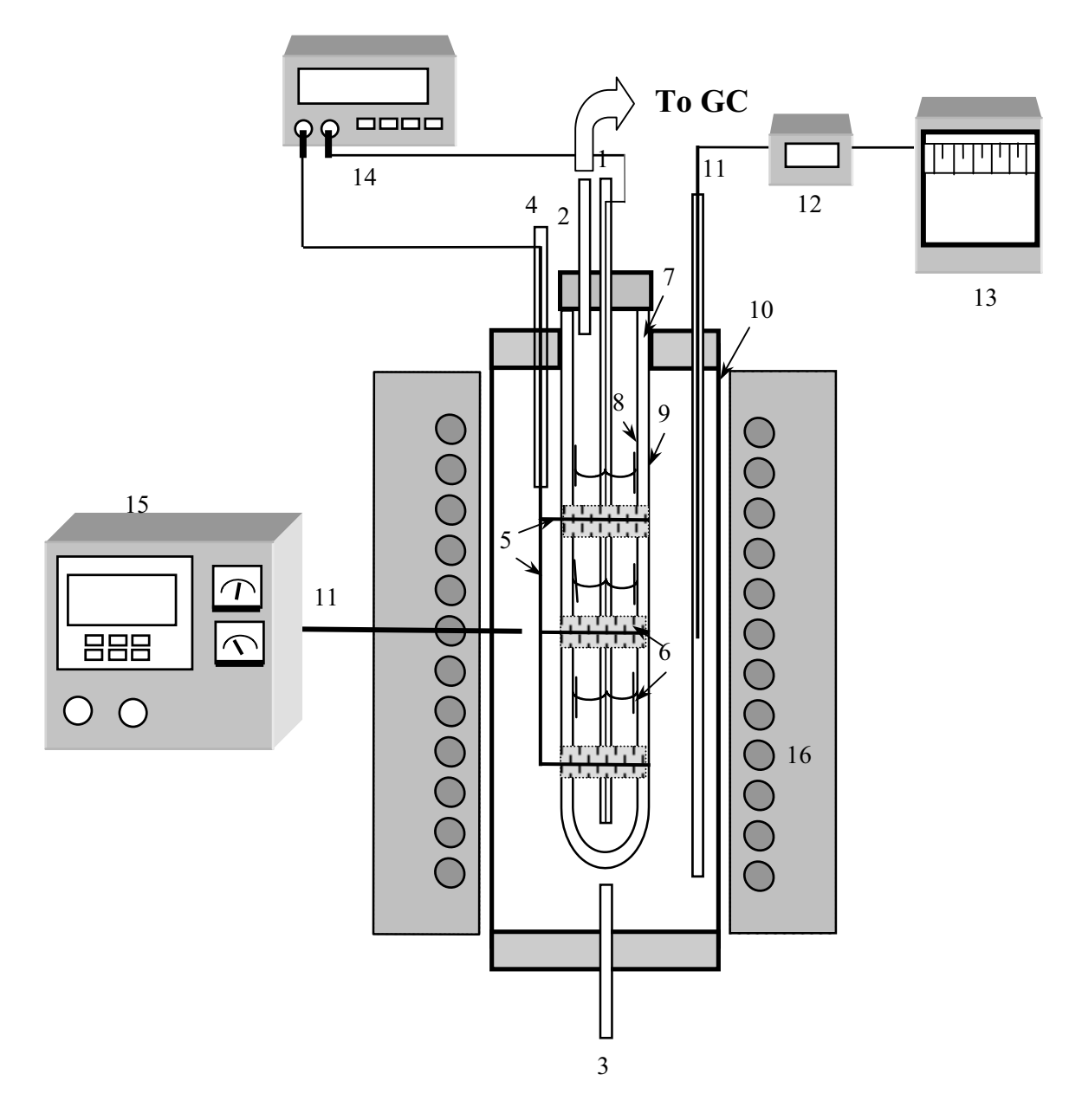


Fig. 2.1 Schematic diagram of the solid oxide fuel cell type reactor.

- 1. Anode side feed (He /CH₄)
- 4. Exit gas from cathode side
- 7. YSZ tube
- 10. Quartz tube
- 13. Temperature recorder
- 15. Temperature controller
- 2. Exit gas from anode side
- 5. Platinum wire
- 8. Anode (LaAlO)
- 11. Thermocouple
- 14. Ammeter/Voltmeter/Potentiostat
- 16. Furnace

3. Cathode side feed (O₂)

12. Temperature indicator

6. Platinum mesh

9. Cathode (LSM)

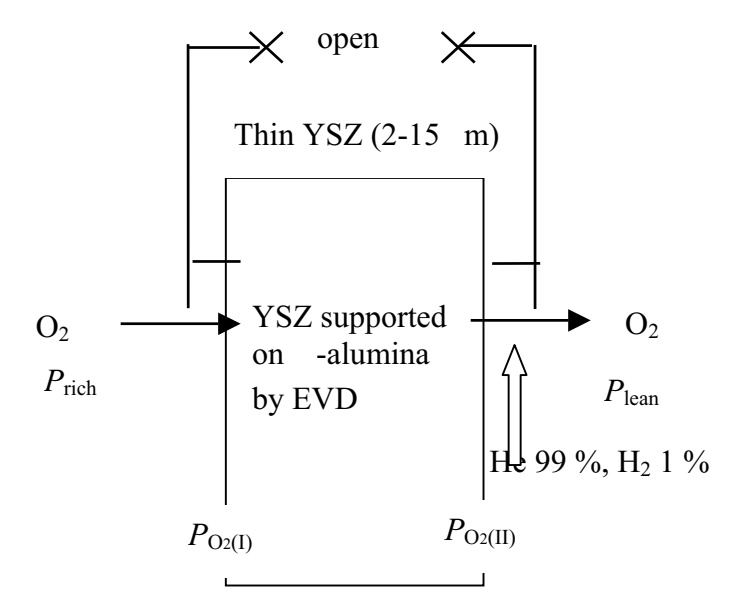
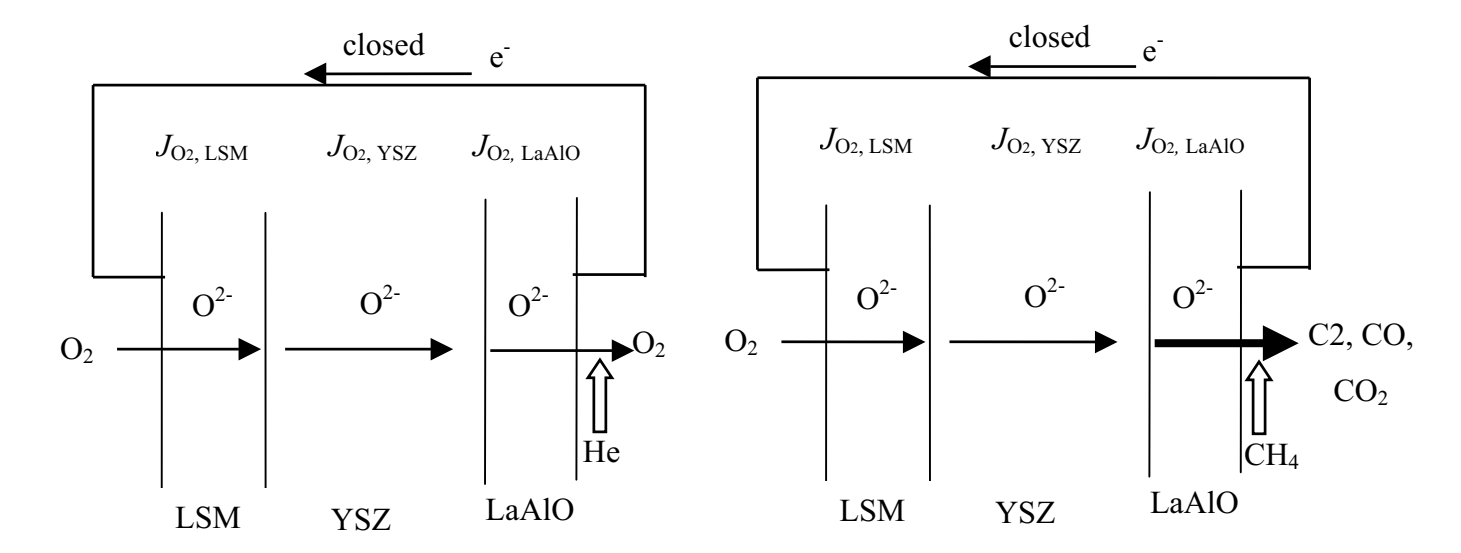
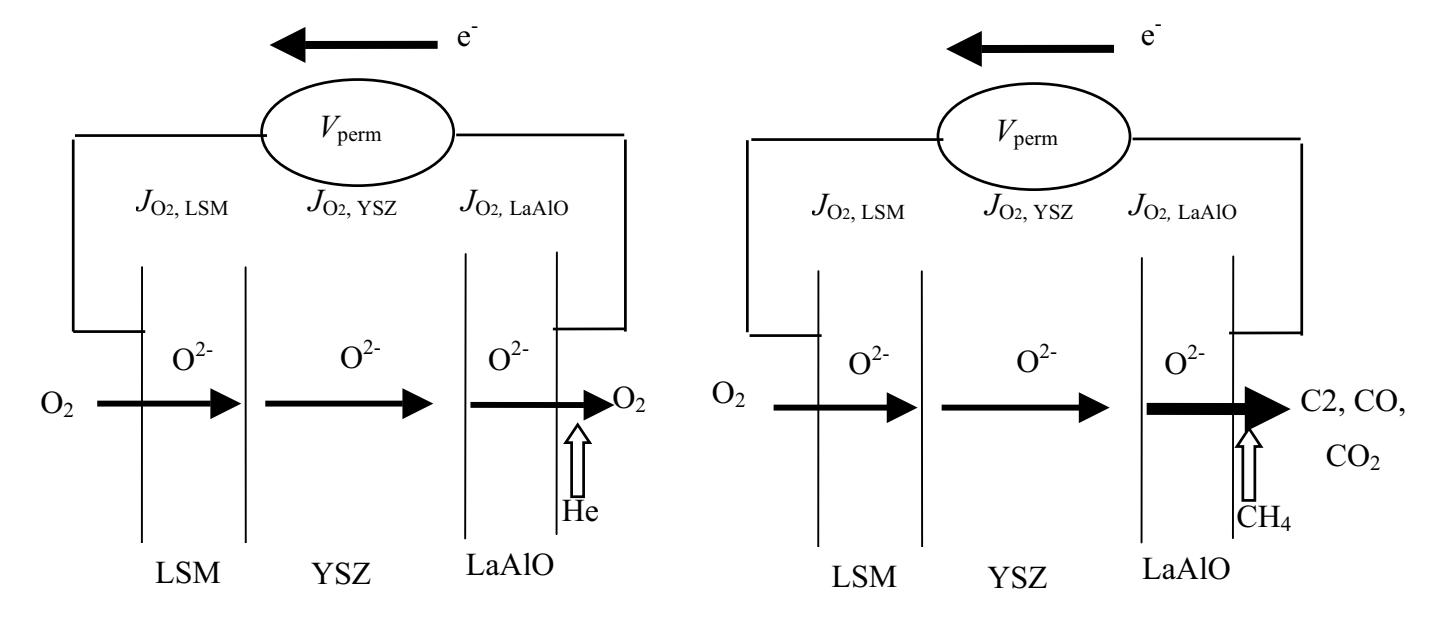


Fig. 2.2 Oxygen permeation process through thin YSZ membranes prepared by the electrochemical vapor deposition (EVD) method supported on α -alumina reported by Han *et al.* (1997).



- a) Helium feed at anode, closed circuit without applied potential
- b) Methane feed at anode, closed circuit without applied potential



- c) Helium feed at anode, closed circuit with applied potential
- d) Methane feed at anode, closed circuit with applied potential

Fig. 2.3 Proposed schemes for oxygen permeation through LSM/YSZ/LaAlO at various conditions.

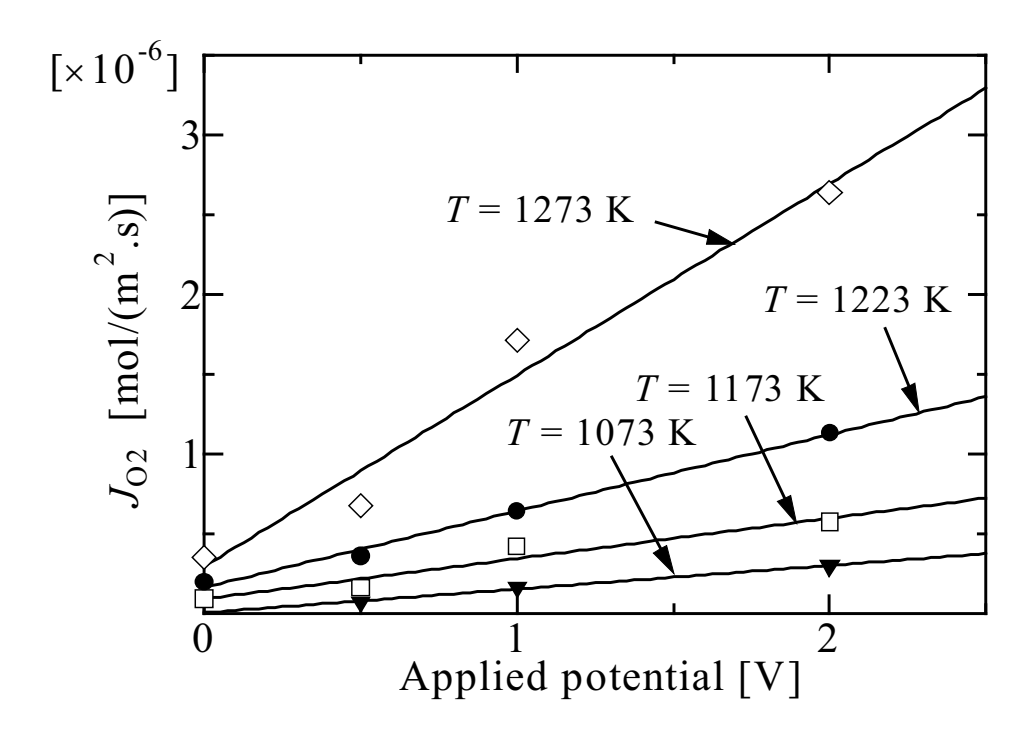


Fig. 2.4 Effect of applied potential on oxygen flux at various temperatures by steady state permeation experiments using helium feed at anode side.

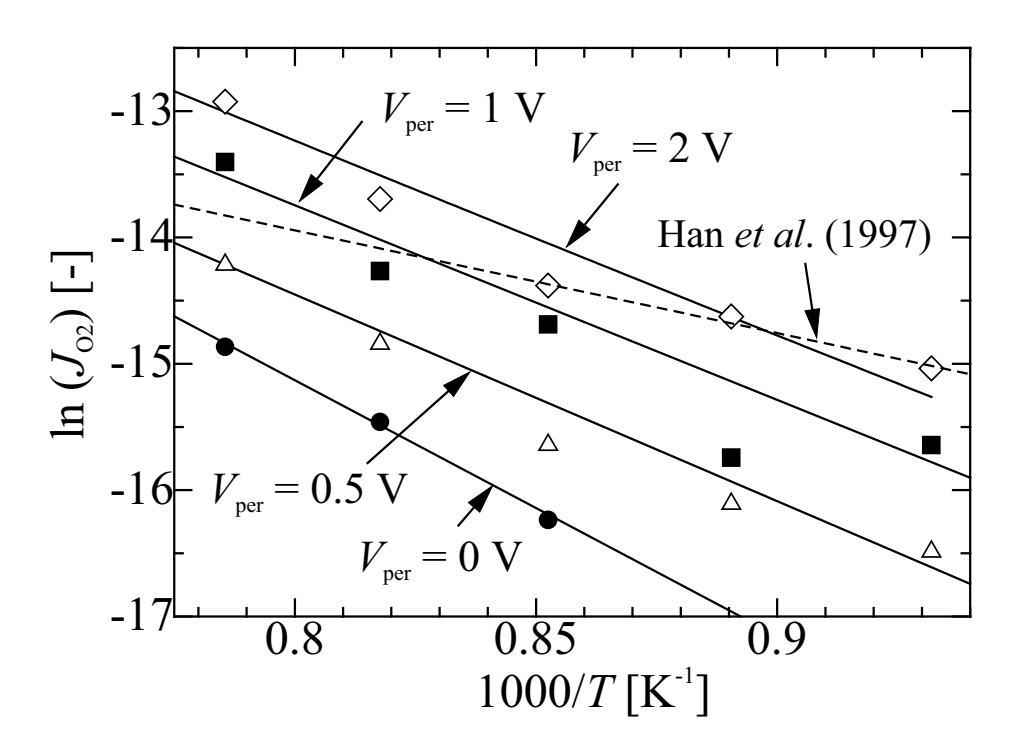


Fig. 2.5 Arrhenius' plot between $\ln (J_{O_2})$ and 1000/T at different levels of applied potential by steady state permeation experiments using helium feed at anode side.

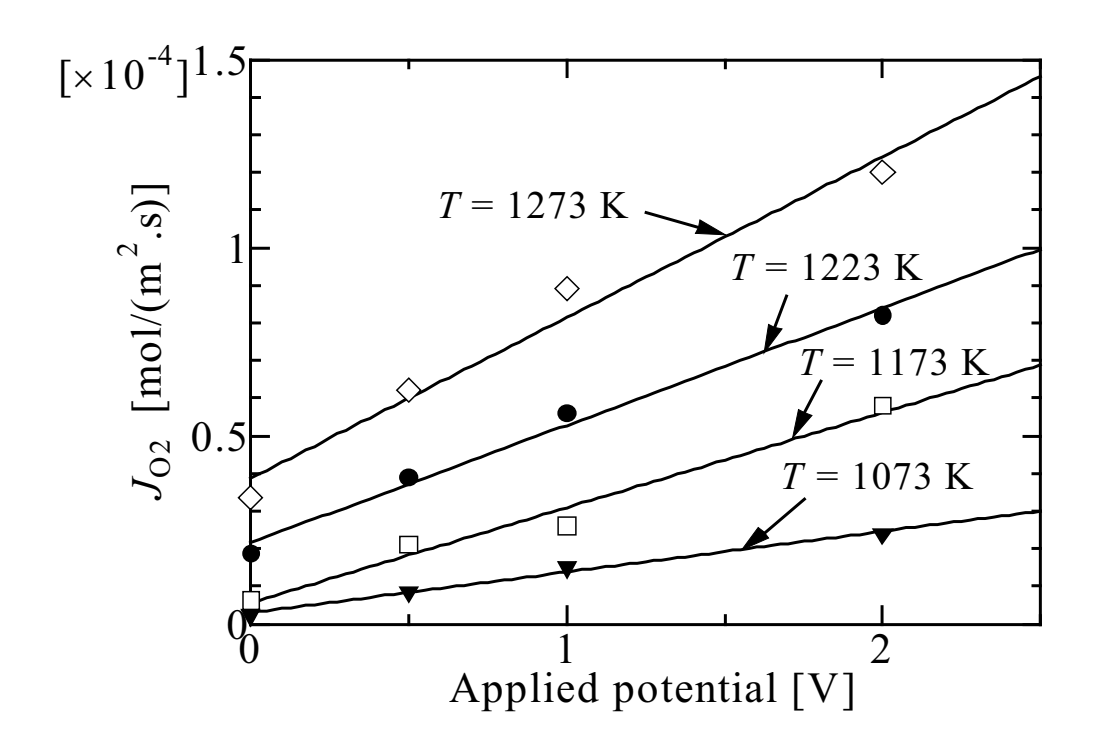


Fig. 2.6 Effect of applied potential on oxygen flux at various temperatures by steady state permeation experiments using methane feed at anode side.

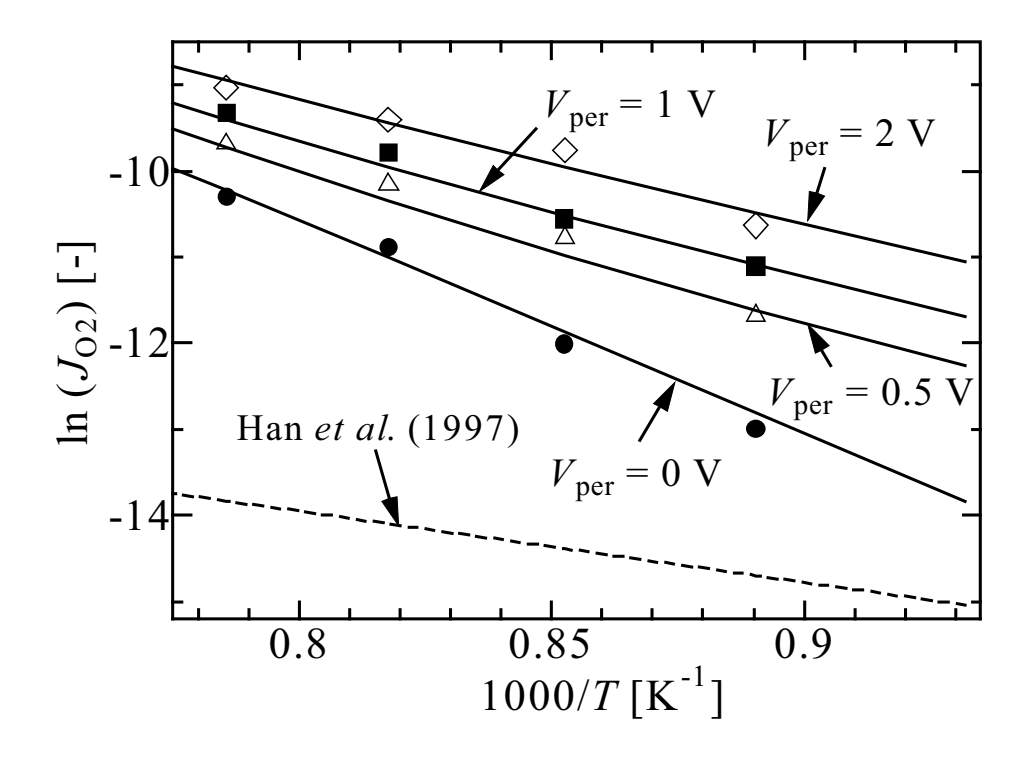


Fig. 2.7 Arrhenius' plot between $\ln (J_{O2})$ and 1000/T at different levels of applied potential by steady state permeation experiments using methane feed at anode side.

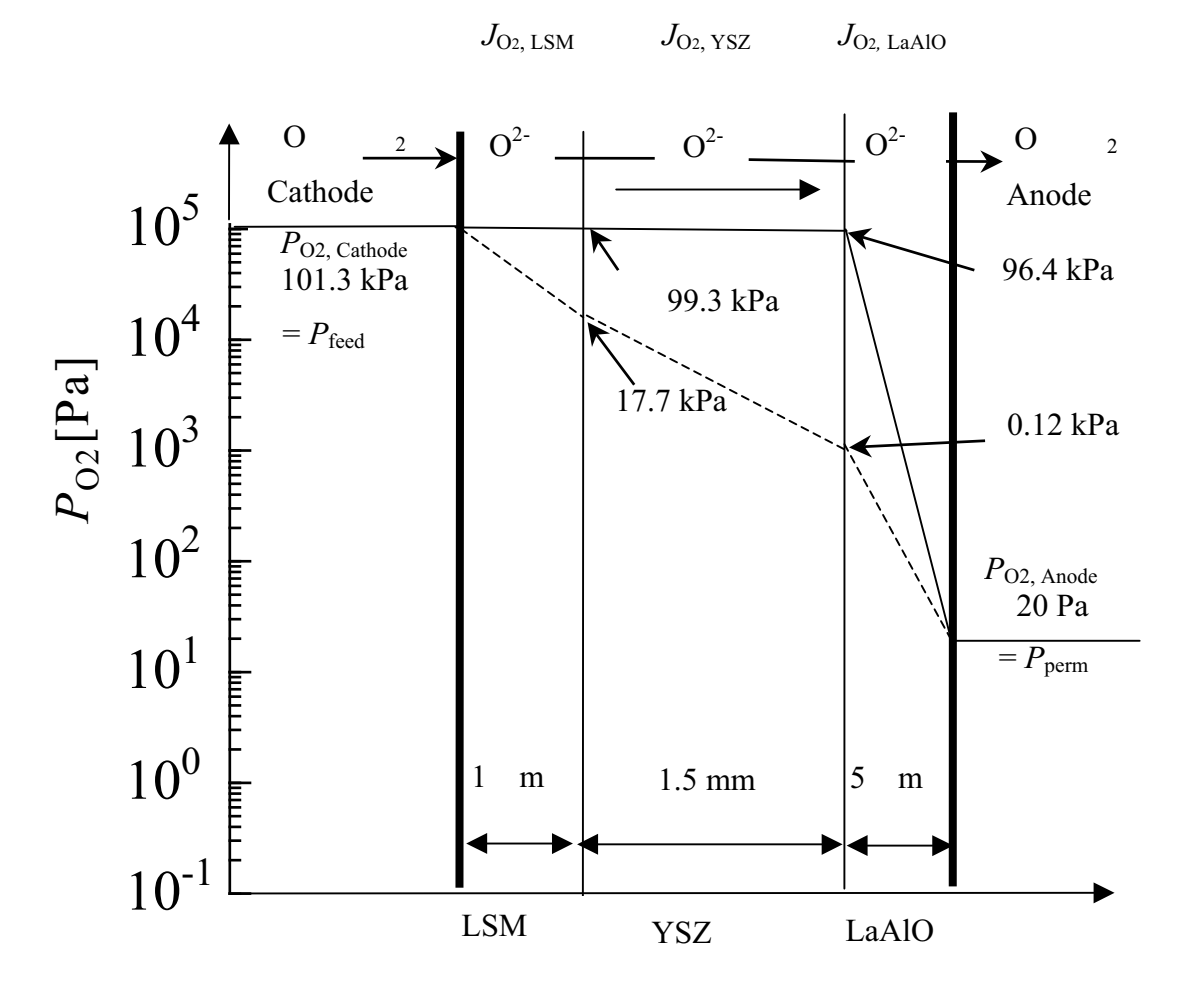


Fig. 2.8 The mechanism of oxygen permeation and the profile of oxygen partial pressure in LSM/YSY/LaAlO from the simulation results at 1223 K (solid line: helium feed, dashed line: methane feed).

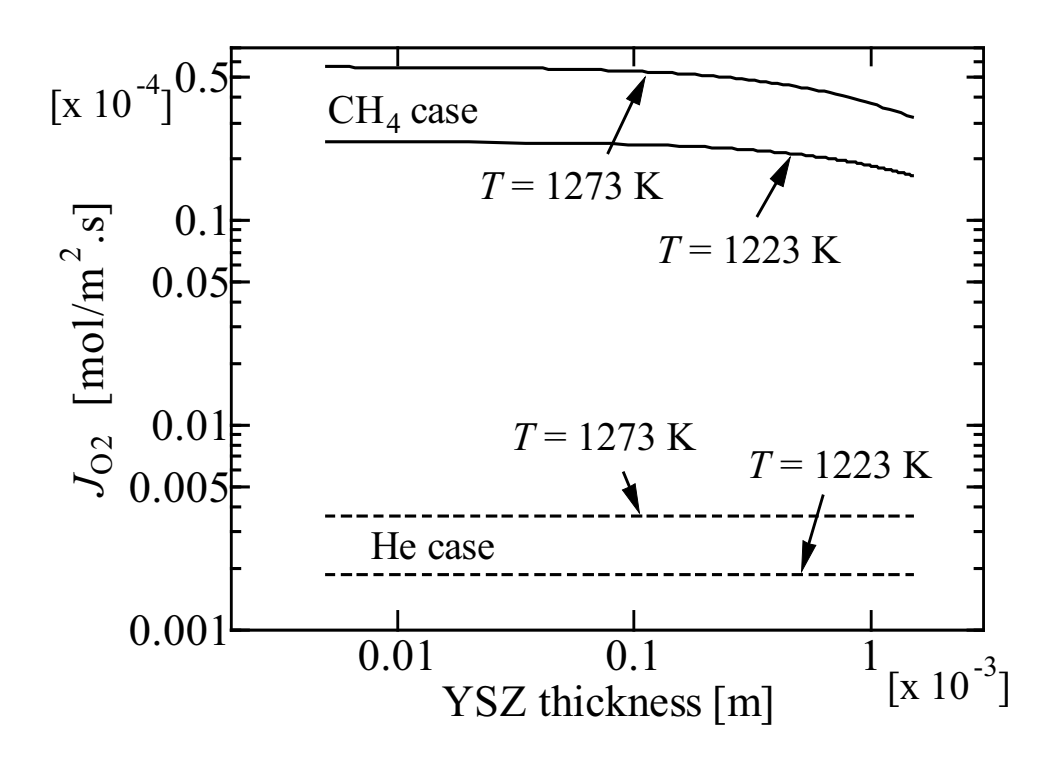


Fig. 2.9 Effect of YSZ thickness on oxygen permeation in helium and methane case.

Chapter 3
Oxidative Coupling of Methane in LSM/YSZ/LaAlO
SOFC Reactor

3.1 Introduction

Conversion of methane into other valuable hydrocarbons has significant industrial importance. Among the various schemes for methane conversion, the oxidative coupling of methane (OCM) to ethane and ethylene (C2) is a promising process to upgrade natural gas. Solid oxide fuel cell (SOFC) is one of the most attracting kinds of fuel cells (Yamamoto, 2000; Steele, 2001). As a reactor for the OCM reaction, a solid electrolyte was used as an oxygen separator and an oxygen distributor to achieve high C2 selectivity. A recent review (Stoukides, 2000) summarized the state of the art of this technology. It also provided a useful table comparing yields and selectivities of the OCM reaction on various catalysts. Most of the reported studies showed high selectivities but low yields.

In our previous papers, the OCM was studied in a SOFC reactor. Particular focuses were placed on catalyst preparation methods (Moe *et al.*, 1998a, 1998b; Carrillo *et al.*, 2001) and reactor performance test (Tagawa *et al.*, 1998, 1999, 2003). The oxygen temperature-programmed desorption (O₂-TPD) of the LaAlO powder sample was studied (Tagawa *et al.*, 1999) and it was proposed that oxygen species desorbed at low temperature (below 1000 K) were active for CO and CO₂ formation (oxygenate site) while those desorbed at higher temperature (above 1000 K) were active for the OCM to C2-hydrocarbon (coupling site). The fuel cell type temperature-programmed desorption (FC-TPD) measurements were employed to investigate (Kiatkittipong *et al.*, 2004a) oxygen species under the fuel cell operation. Both kinds of oxygen species were also observed.

Modeling is an important tool for design of SOFC and prediction of SOFC performances. Most attention has been given to the case where hydrogen or carbon monoxide is used as a fuel (Achenbach, 1994; Bessette *et al.*, 1995; Aguiar *et al.*, 2002; Yamada *et al.*, 2002). Very few investigators studied the modeling of the OCM reaction in SOFC reactors. Guo *et al.* (1999) proposed a mathematical model based on well mixed flow and plug flow. Although good agreement between their simulation and experimental results were observed, some parameters in the model are unclear.

In this paper, the OCM in a SOFC reactor with a cell of La_{0.85}Sr_{0.15}MnO₃/8 mol% Y₂O₃-ZrO₂/La_{1.8}Al_{0.2}O₃ (abbreviated as LSM/YSZ/LaAlO) was studied. An optimum condition for the anode preparation by the mist pyrolysis method was investigated to achieve high C2 selectivity. The knowledge of oxygen species from FC-TPD (Tagawa *et al.*, 1998; Kiatkittipong *et al.*, 2004a) and the oxygen permeation through the LSM/YSZ/LaAlO (Kiatkittipong *et al.*, 2004b) were taken into account to obtain the kinetic parameters of the reactions on the anode. The effect of external load resistance on the reactor performance was also considered. The model of overall OCM reaction in SOFC reactor was proposed.

3.2 Experimental

3.2.1 Apparatus

The schematic diagram of the solid oxide fuel cell type reactor was illustrated in **Figure 3.1**. A tube-type YSZ membrane (8 mol% Y_2O_3 , thickness = 1.5

mm, inside diameter = 18 mm, outside diameter = 21 mm, length = 500 mm, effective surface area = 0.0148 m^2) was used as an electrolyte. La_{1.8}Al_{0.2}O₃ (abbreviated as LaAlO) prepared by a mist decomposition method was used as an anode catalyst on the inner surface of the tube while La_{0.85}Sr_{0.15}MnO₃ (abbreviated as LSM) prepared by a conventional paste method on the outer side was used as the cathode. Platinum wire was connected to platinum meshes placed on both electrode surfaces to serve as current collectors. Current meter and voltmeter were used to measure closed circuit current (CCI) and open circuit voltage (OCV), respectively. Voltages at various current values were measured using a potentiostat. The standard operation was as follows.

Methane $(3.4x10^{-6} \text{ mol s}^{-1})$ was fed to the anode without dilution gases. Oxygen or air $(1.02x10^{-5} \text{ mol s}^{-1})$ was fed to the cathode. The operating temperatures were varied: i.e. T = 1073, 1123, 1173, 1223 and 1273 K. The flow rate of the anode exit gas was measured and its composition was analyzed by a gas chromatography with a TCD detector every 30 min until reaching a steady state condition.

It should be noted that carbon deposition on the anode is a typical phenomenon taken place in solid oxide fuel cells with hydrocarbon feed. However, all experimental results in this study were recorded at steady-state conditions and an apparent carbon deposition was not observed. The carbon balance was checked and found to be within 99.8%. In case of a possible carbon deposition, the cell was treated by feeding pure oxygen (1.02x10⁻⁵ mol s⁻¹) to the anode side, before running each set of experiments. The temperature was raised to 773 and 1223 K with a holding time of 6 h for each step.

3.2.2 Electrode preparation

The LSM powder was pounded and mixed with glycerol. It was pasted into thin film on the outside of the YSZ tube and heated at 1223 K for about 3 h in air (Tagawa *et al.*, 1999, 2003; Kiatkittipong *et al.*, 2004a, 2004b).

LaAlO anode material was prepared on the inside of the YSZ tube by the mist pyrolysis method as follows (Tagawa *et al.*, 1999, 2003; Kiatkittipong *et al.*, 2004a, 2004b).

Figure 3.2 shows the setup for the anode preparation. A mixed aqueous solution of lanthanum nitrate (La(NO₃)₃.6H₂O) and aluminum nitrate (Al(NO₃)₃.9H₂O), (La:Al=9:1) was placed in a reservoir. With a ceramic ultrasonic transducer (1.7MHz), mist of solution was generated. The mist was delivered to the YSZ tube with the air flow using an aspirator. A YSZ tube was placed in a furnace and heated. The pyrolysis was generally operated in periodic operations. In this periodic operation, the mist was intermittently sprayed to the YSZ tube and the optimum condition was summarized in **Table 3.1**.

3.3 SOFC Modelling

By assuming plug flow and isothermal condition, the mass balance equation in the anode side is given as

$$\frac{\mathrm{d}\gamma_i}{\mathrm{d}x} = \left\{ r_i + \left(\frac{S}{W} \right) J_i \right\} \left(\frac{W}{F_{\mathrm{CH},0}} \right) \tag{3.1}$$

where the permeation rate of component i except for oxygen is zero $(J_i = 0)$ because the YSZ membrane allows only oxygen to permeate.

At the entrance (x = 0), $\gamma_{CH_4} = 1$, $\gamma_i = 0$ (products)

The partial pressures in the anode side (AN) and the cathode side (CA) can be

determined as

$$P_{i,\text{AN}} = \frac{P_{t,\text{AN}}\gamma_i}{\sum \gamma_i} \tag{3.2}$$

 $P_{\text{O},CA} = 1.013 \times 10^5$ and 2.127×10^4 Pa for oxygen and air feed, respectively (3.3)

The oxygen permeation rate through the LSM/YSZ/LaAlO solid oxide fuel cell type reactor can be estimated from our model (Kiatkittipong *et al.*, 2004b). In the model, general reaction paths are 1) electrochemical reduction of molecular oxygen at the LSM surface to form oxygen ions, 2) incorporation of oxygen ions into the YSZ lattice, 3) oxygen ions directly reacted with methane at the anode. The permeation of oxygen depends upon ionic conductivity (σ_i) and electronic conductivity (σ_e) of the materials. The following set of equations is applied for LSM and YSZ with reported parameters.

$$J_{O_2} = \frac{Per_{O_2}}{L} \ln \left(\frac{P_{\text{rich}}}{P_{\text{lean}}} \right)$$

$$Per_{O_2} = \frac{R_g T}{16F^2} \frac{\sigma_i \sigma_e}{\sigma_i + \sigma_e}$$
(3.5)

$$\sigma_{j} = \left(\frac{A_{j}}{T}\right) \exp\left(\frac{-E_{j}}{R_{g}T}\right); j = i,e$$
 (3.6)

Although, these values of LaAlO are not available in literature, kinetic parameters were determined in the study. It is suggested in the study that the rate of oxygen permeation with helium flow on anode was determined by the surface desorption step from anode. On the other hand, these three rate steps are comparable with methane feed.

In our previous TPD work on LaAlO powder (Tagawa *et al.*, 1999), it was proposed that the oxygen species desorbed at low temperature (below 1000 K) were active for CO and CO₂ formation (oxygenate site) while the oxygen species desorbed at higher temperature (above 1000 K) were active for the OCM to C2-hydrocarbon (coupling site). From the fuel cell type temperature-programmed desorption (FC-TPD) measurements, the fraction of oxygen species for oxygenate site and coupling site were estimated by integration of oxygen FC-TPD results operated in closed circuit mode (as shown in Figure 3.7 in Kiatkittipong *et al.*, 2004a) and the values are summarized in **Table 3.2**.

When methane was fed on the anode and oxygen was permeated from the cathode to the anode side, the following oxidation reactions were proceeded.

Assuming the first order kinetics with respect to surface concentration of methane and oxygen, the rate equation for the product i can be expressed as follow.

$$r_i = k_i \varphi_{\mathrm{CH}_4} \varphi_{\mathrm{O}_2,j} \tag{3.12}$$

The surface concentration of methane (φ_{CH_4}) was supposed to have linear relationship with P_{CH_4} as follows.

$$\varphi_{\text{CH}_4} \propto P_{\text{CH}_4}$$
(3.13)

In the previous study on fuel cell type TPD of oxygen (Kiatkittipong *et al.*, 2004a), an important role of oxygen desorption from anode material has been pointed out. The activation energy of surface oxygen desorption (open circuit) and that of oxygen permeation (closed circuit) agreed with each other in both cases of oxygenate oxygen and coupling oxygen. These results suggested the permeation of oxygen strongly depended on the surface oxygen species. Thus linear relationship between surface concentration of oxygen ($\varphi_{O_2,j}$) and oxygen flux ($J_{O_2,j}$) was also supposed as follows.

$$\varphi_{\mathbf{O}_{2},i} \propto J_{\mathbf{O}_{2},i} \tag{3.14}$$

Where *j* represents either coupling oxygen (cou) or oxygenate oxygen (oxy). Then, the kinetic rate expressions determined for each of the above reactions are given as follows, respectively.

$$r_1 = k_1 P_{\text{CH}_4} J_{\text{O}_2,\text{cou}}$$
 (3.15)

$$r_2 = k_2 P_{\text{C,H}_6} J_{\text{O,,cou}}$$
 (3.16)

$$r_3 = k_3 P_{\text{CH}_4} J_{\text{O}_2,\text{oxy}}$$
 (3.17)

$$r_4 = k_4 P_{\text{CH}_4} J_{\text{O}_2,\text{oxy}}$$
 (3.18)

$$r_5 = k_5 P_{\text{CoHe}} J_{\text{Obloxy}}$$
 (3.19)

Therefore, the reaction rate of component i can be expressed by stoichiometric relations as follows:

$$r_{\rm CH_4} = -2r_1 - r_3 - r_4 \tag{3.20}$$

$$r_{\rm C_2H_6} = r_1 - r_2 - r_5 \tag{3.21}$$

$$r_{\rm C_2H_4} = r_2 \tag{3.22}$$

$$r_{\rm CO} = r_3 \tag{3.23}$$

$$r_{\text{CO}_2} = r_4 + r_5 \tag{3.24}$$

$$r_{O_2} = -\frac{1}{2}r_1 - \frac{1}{2}r_2 - \frac{3}{2}r_3 - 2r_4 - \frac{7}{2}r_5 \tag{3.25}$$

3.4 Results and Discussion

3.4.1 Selection of an optimum mist solution concentration for the anode preparation

Figure 3.3 shows the effect of the mist solution concentration on methane conversion (filled symbols) and C2 selectivity (open symbols). SOFC reactor was operated in a closed circuit mode without external resistance (short circuit, $R_L = 0$). The C2 selectivity increased with decreasing concentration of the mist solution or

with increasing reaction temperature. The solid lines represent calculated results, which will be described later. At lower concentration of the mist solution, particles with smaller sizes were obtained. The small particle sizes are effective for C2 product formation (Moe *et al.*, 1998a). As the mist solution concentration of 1.25 wt% showed the highest selectivity, it was chosen as an optimum concentration for the following studies. With the optimum anode preparation condition, the conversion and C2 selectivity were 23.7 % and 91.7 %, respectively, at 1273 K.

3.4.2 Permeation of oxygen

The amount of oxygen permeation is very important for selective oxidations. For a non-porous solid electrolyte, it can be related to current as described by Faraday's law as follows.

$$I = J_{O} Sx4F \tag{3.26}$$

Figure 3.4 shows the effect of temperature on the current. Three kinds of current were plotted as follows: 1) current recorded from the current meter, 2) equivalent current calculated from the oxygen consumption from product distribution and 3) equivalent current estimated from our permeation model (Kiatkittipong *et al.*, 2004b). Due to no oxygen in gas phase was detected from the anode exit gas; the permeated oxygen was all consumed in the reactions with methane.

As shown in Figure 3.4, the current values predicted from our model agreed well with those of experimental values from the current meter as well as those from the product distribution. These agreements indicated that the amount of reacted oxygen species (J_{0_2}) could be calculated from our permeation model (Kiatkittipong *et al.*, 2004b) and that the electrolyte used in the study was pin-hole free. Then, J_{0_2} was calculated with our permeation model (Kiatkittipong *et al.*, 2004b) for Section 4.3.

3.4.3 Reactor performance (short circuit, $R_L = 0$)

The SOFC reactor was operated in the closed circuit mode without external resistance (short circuit, $R_L = 0$). The kinetic rate expressions were determined for each of the above reaction by fitting the experimental data shown in Figure 3.3.

$$k_1 = 3.70 \times 10^7 \exp\left(\frac{-215000}{R_{\rm g}T}\right)$$
 (3.27)

$$k_2 = 2.96 \times 10^5 \exp\left(\frac{-110000}{R_g T}\right)$$
 (3.28)

$$k_3 = 4.14 \times 10^3 \exp\left(\frac{-124000}{R_{\rm g}T}\right)$$
 (3.29)

$$k_4 = 2.96 \times 10^3 \exp\left(\frac{-131000}{R_g T}\right)$$
 (3.30)

$$k_5 = 1.78 \times 10^5 \exp\left(\frac{-120000}{R_g T}\right)$$
 (3.31)

Figure 3.5 shows the reactor performance for the case with air feed on the cathode. Figure 3.5(a) shows the effect of temperature on methane conversion and C2 selectivity along with calculated results. The conversion and C2 selectivity increased with increasing temperature. These follow the same trend for the case with pure oxygen feed on the cathode; however, lower conversion was achieved. Figure 3.5(b) shows the selectivity of each product under the same conditions. It is worth noting that the selectivity of CO and CO_2 decreased with increasing temperature. The solid lines in Figures 3.3 and 3.5 represent calculated results which were carried out as follows: J_{O_2} was estimated from our model (Kiatkittipong *et al.*, 2004b). The amount of oxygen was divided into two different oxygen species; oxygenate and coupling oxygen by using mole fraction of oxygen species shown in Table 3.2 and the following relations

$$J_{O_{2},cou} = y_{O_{2},cou}J_{O_{2}}$$
 (3.32)

$$J_{\mathcal{O}_{2},\text{oxy}} = y_{\mathcal{O}_{2},\text{oxy}} J_{\mathcal{O}_{2}} \tag{3.33}$$

Then the C_2H_4 and C_2H_6 formations which use the oxygen species for coupling $(O_{2, \text{ cou}})$ were calculated by using Eqs. (3.15) and (3.16). CO and CO_2 formation which using the oxygen species for oxygenate $(O_{2, \text{ oxy}})$ were calculated by using Eqs. (3.17)-(3.19). Methane conversion and product selectivity were calculated by using Eqs. (3.1) and (3.2). The calculated results (solid lines) agreed well with the experimental results. The maximum C2 yield of 16.8 % was obtained at 1273 K in case of air feed at cathode side by multiply the conversion and the selectivity shown in Figure 3.5(a), where C2 yield of 21.7% was obtained in case of pure oxygen feed shown in Figure 3.3.

Effects of methane flow rate on methane conversion and C2 selectivity are shown in **Figure 3.6**. The calculated results in Figure 3.6 followed the same calculation method as used in Figure 3.5. As shown in Figure 3.6(a), the methane conversion increased with decreasing methane flow rate, which was in good agreement with the calculated values (solid lines).

As shown in Figure 3.6(b), the C2 selectivity was almost independent of methane flow rate. This suggested that oxygenate products and coupling products are formed in a parallel manner. On the other hand, C₂H₄/C₂H₆ ratio decreased with increasing methane flow rate. Because of shorter residence time, consecutive ethylene production from ethane decreased with increasing methane flow rate. Our developed model can predict the experimental results very well.

It should be noted that Guo *et al.* (1999) proposed the complex kinetic expressions to explain complicated changes in selectivity while this study proposed the simple kinetics by assuming two kinds of oxygen species with different activity.

3.4.4 Chemicals-energy cogeneration with SOFC reactor (closed circuit with external load, R_L)

The internal resistance of cell can be determined from the maximum power transfer theorem (Siskind, 1965) as described below. **Figure 3.7** shows a simplified

series circuit model, which consists of a voltage source (SOFC reactor unit) with a variable external load resistor (R_L) . If $R_L = \infty$ (open circuit), current $I_L = 0$ and power at load, $P_L = 0$; also, if $R_L = 0$ (short circuit), voltage $E_L = 0$ and $P_L = 0$. When R_L is neither ∞ or 0, P_L is not 0. A maximum power transferred to the load occurs when $R_L = R_{\text{int}}$. R_{int} is the overall resistance including ohmic, activation and concentration polarization resistances inside the cell unit. Therefore, R_{int} value varies with operating conditions such as temperature, $P_{O_2,CA}$ and should be experimentally estimated.

Figure 3.8 shows the load resistance-voltage and load resistance-power plots at various temperatures in case of (a) oxygen and (b) air feed on the cathode. The open circuit voltages were in range of 1.02-1.08 V, which is nearly equal to the theoretical value of the C₂H₄ formation from C₂H₆ (Tagawa *et al.*, 1999). Power increased with increasing temperature. With increasing the operating temperature, the chemical reaction could be enhanced as well as oxygen permeability through the YSZ. It should be noted that when the current-voltage was plotted for both cases as shown in **Figure 3.9**, a linear decrease of voltage with current was observed, indicating that the over-potential is mainly governed by the ohmic resistance of the cell.

Comparing between Figure 3.8(a) and Figure 3.8(b), changing oxygen to air feed on the cathode, the power decreased due to decreasing the driving force of oxygen gradient. However using air instead of oxygen could be competitive from a viewpoint of the oxygen purification cost.

Figure 3.10 shows the relation of internal cell resistance (R_{int}) and temperature. Following expressions can be obtained;

$$R_{\text{int}} = \frac{1.128 \times 10^{-2}}{P_{\text{O}_2,\text{CA}}^{0.2} T} \exp\left(\frac{166000}{R_{\text{g}}T}\right)$$
(3.34)

These results show that higher $P_{O_2,CA}$ gives lower R_{int} .

Figure 3.11(a) shows the relationship between load resistance and methane conversion. In the case of external load, the current can be calculated from

$$I = \frac{E}{R_{\text{int}} + R_{\text{I}}} \tag{3.35}$$

Then, the calculated current was used to estimate the amount of oxygen permeated to anode by Eq. (3.26).

The filled symbol represents pure oxygen feed on the cathode case while the open symbol represents air feed on the cathode case. The solid line represents calculated results. I was estimated from R_L value with Eqs. (3.34) and (3.35) using E values shown as a voltage in Figure 3.8 for oxygen and air feed on the cathode. Using mole fraction of oxygen species shown in Table 3.2 and Eqs. (3.32) and (3.33), the amount of oxygen for oxygenate and coupling site were estimated, respectively. Then C_2H_4 and C_2H_6 formation were calculated by using Eqs. (3.15) and (3.16), while CO and CO_2 formation were calculated by using Eqs. (3.17)-(3.19) as described in the previous section. Methane conversion was calculated by using Eqs. (3.1) and (3.2). The calculated results are shown in Figure 3.11(a) as solid lines. With increasing load resistance, oxygen hardly permeated due to increasing electron transfer resistance. This resulted in decrease of methane conversion. Changing oxygen to air feed on

the cathode, the methane conversion decreased due to decreasing the amount of permeated oxygen.

Figure 3.11(b) shows the relationship between R_L and the selectivity. Load resistance showed insignificantly effect on C2 selectivity while operating temperature showed strong effect. The selectivity was calculated by the same method mentioned above. Changing oxygen to air feed on the cathode, the C2 selectivity was insignificantly affected. The calculated results agreed well with the experimental results.

3.5 Conclusion

Oxidative coupling of methane was studied in LSM/YSZ/LaAlO SOFC tube type reactor. The C2 selectivity increased with increasing temperature. The C2 selectivity and methane conversion were 91.7% and 23.7% at 1273 K with the optimum preparation of anode catalyst. A set of reaction model was proposed with distinguished oxygen species such as oxygenate species and coupling species. The equivalent current calculated from oxygen consumption and the simulation results agreed well with the current values read from current meter showing that oxygen transport could be estimated by simulation. The internal resistance of cell could be lumped and estimated by maximum power transfer theorem. The effect of external load on reactor performance was investigated both experimental and simulation. Increasing the external load, decreased oxygen transport, resulting in decreased methane conversion. However, the C2 selectivity kept constant. The calculated results agreed well with the experimental results. A set of the simple kinetic model by using two different oxygen species is useful to evaluate the oxidative coupling of methane in SOFC type reactor.

Nomenclature

A_j	=	pre-exponential factor of conductivities	[S K m ⁻¹]
\vec{E}	=	cell voltage	[V]
F	=	Faraday's constant, 96485	[C mol ⁻¹]
$F_{\mathrm{CH_4,0}}$	=	feed molar flow rate of methane	$[\text{mol s}^{-1}]$
I	=	current	[A]
$J_{{ m O}_2}$	=	oxygen permeation flux	$[\text{mol m}^{-2} \text{ s}^{-1}]$
k	=	reaction rate constant	$[m^2 kg^{-1} Pa^{-1}]$
L	=	thickness of material	[m]
$N_{ m O_2}$	=	oxygen consumption	$[\text{mol s}^{-1}]$
Per , O_2	=	specific oxygen permeability	[mol m ⁻¹ s ⁻¹]
P_i	=	pressure of component i	[Pa]
P_{rich}	=	oxygen partial pressure at rich side of materi	als [Pa]
P_{lean}	=	oxygen partial pressure at lean side of mater	ials [Pa]
$P_{ m O_2,CA}$	=	pressure of oxygen in the cathode side	[Pa]
$P_{ m t,AN}$	=	total pressure in the anode side, 1.013×10^5	[Pa]
r_j	=	rate of reaction <i>j</i>	$[\text{mol kg}^{-1} \text{ s}^{-1}]$
R	=	resistance	[ohm]
$R_{ m g}$	=	gas constant, 8.314	[J mol ⁻¹ K ⁻¹]
S	=	membrane surface area	$[m^2]$
T	=	temperature	[K]

W	=	mass of anode catalyst	[kg]
X	=	dimensionless axial length divided by the to	otal
		length of reactor	[-]
$\mathcal{Y}_{\mathrm{O}_2,\mathrm{cou}}$	=	mole fraction of oxygen for coupling site	[-]
$\mathcal{Y}_{\mathrm{O}_2,\mathrm{oxy}}$	=	mole fraction of oxygen for oxygenate site	[-]
γ	=	molar flow rate ratio $(=F_i/F_{CH_4,0})$	[-]
arphi	=	surface concentration	$[\text{mol m}^{-2}]$
σ	=	conductivities	[S m ⁻¹]

<Subscript>

AN	=	anode side
CA	=	cathode side
cou	=	coupling site
e	=	electronic
i	=	ionic
i	=	component i
int	=	internal
j	=	reaction j
L	=	load
oxy	=	oxygenate site
0	=	feed

References

- Achenbach, E.; "Three-Dimensional and Time-Dependent Simulation of a Planar Solid Oxide Fuel Cell Stack," *J. Power. Sources*, **49**, 333-348 (1994)
- Aguiar, P., D. Chadwick and L. Kershenbaun; "Modelling of an Indirect Internal Reforming Solid Oxide Fuel Cell," *Chem. Eng. Sci.*, **57**, 1665-1677 (2002)
- Bessette, N. F., W. J. Wepfer and J. Winnick; "A Mathematical Model of a Solid Oxide Fuel Cell," *J. Electrochem. Soc.*, **142**, 3792-3800 (1995)
- Carrillo, A. S., T. Tagawa and S. Goto; "Application of Mist Pyrolysis Method to Preparation of Ni/ZrO₂ Anode Catalyst for SOFC Type Reactor," *Mater. Res. Bull.*, **36**,1017-1027 (2001)
- Guo, X. M., K. Hidajat and C. B. Ching; "Simulation of a Solid Oxide Fuel Cell for Oxidative Coupling of Methane," *Catal. Today*, **50**, 109-116 (1999)
- Kiatkittipong, W., T. Tagawa, S. Goto, S. Assabumrungrat and P. Praserthdam; "TPD Study in LSM/YSZ/LaAlO System for the Use of Fuel Cell Type Reactor," *Solid State Ionics*, **166**, 127-136 (2004a)
- Kiatkittipong, W., T. Tagawa, S. Goto, S. Assabumrungrat and P. Praserthdam; "Oxygen Transport through LSM/YSZ/LaAlO System for Use of Fuel Cell Type Reactor," the Proc. of the 10th APCChE, Kitakyushu, Japan (2004b) to be published
- Moe, K. K., T. Tagawa and S. Goto; "Preparation of Electrode Catalyst for SOFC Reactor by Ultrasonic Mist Pyrolysis of Aqueous Solution," *J. Ceram. Soc. Jpn.*, **106**, 242-247 (1998a)
- Moe, K. K., T. Tagawa and S. Goto; "Preparation of Electrode Catalyst for SOFC Reactor by Ultrasonic Mist Pyrolysis: Effect of Spray Time," *J. Ceram. Soc. Jpn.*, **106**, 754-758 (1998b)

- Siskind, C. S.; Electrical Circuits: Direct and Alternating Current, 2nd ed., McGraw-Hill Book, Tokyo, Japan (1965)
- Steele, B. C. H.; "Material Science and Engineering: The Enabling Technology for the Commercialisation of Fuel Cell Systems," *J.Material. Sci.*, **36**, 1053-1068 (2001)
- Stoukides, M; "Solid-Electrolyte Membrane Reactors: Current Experience and Future Outlook," *Catal. Rev. Sci. Eng.*, **42**, 1-70 (2000)
- Tagawa, T., K. K. Moe, T. Hiramatsu and S. Goto; "Design of Electrode for Solid Oxide Fuel Cells Reactor," *Solid State Ionics*, **106**, 227-235 (1998)
- Tagawa, T., K. K. Moe, M. Ito and S. Goto; "Fuel Cell Type Reactor for Chemicals-Energy Co-Generation," *Chem. Eng. Sci.*, **54**, 1553-1557 (1999)
- Tagawa, T., K. Kuroyanagi, S. Goto, S. Assabumrungrat and P. Praserthdam; "Selective Oxidation of Methane in an SOFC-Type Reactor: Effect of Applied Potential," *Chem. Eng. J.*, **93**, 3-9 (2003)
- Yamada, K., N. Takahashi and C. J. Wen; "Design and Evaluation of an Electric Vehicle Using Solid Oxide Fuel Cells," *J. Chem. Eng. Japan*, **35**, 1290-1297 (2002)
- Yamamoto, O.; "Solid Oxide Fuel Cells: Fundamental Aspect and Pospects," *Electrochim. Acta*, **45**, 2423-2435 (2000)

 Table 3.1 Optimum condition for the anode preparation

YSZ temperature	503 K
Concentration of salt solution	1.25 wt%
Spray time	30 s
Interval time	30 s
Total spray time	2 h

Table 3.2 Mole fraction of oxygen species for oxygenate site and coupling site

Reaction temperature	1073 K	1123 K	1173 K	1223 K	1273 K
${\mathcal Y}_{{ m O}_2,{ m oxy}}$	0.704	0.601	0.490	0.319	0.235
${\mathcal Y}_{{ m O}_2,{ m cou}}$	0.296	0.399	0.510	0.681	0.765

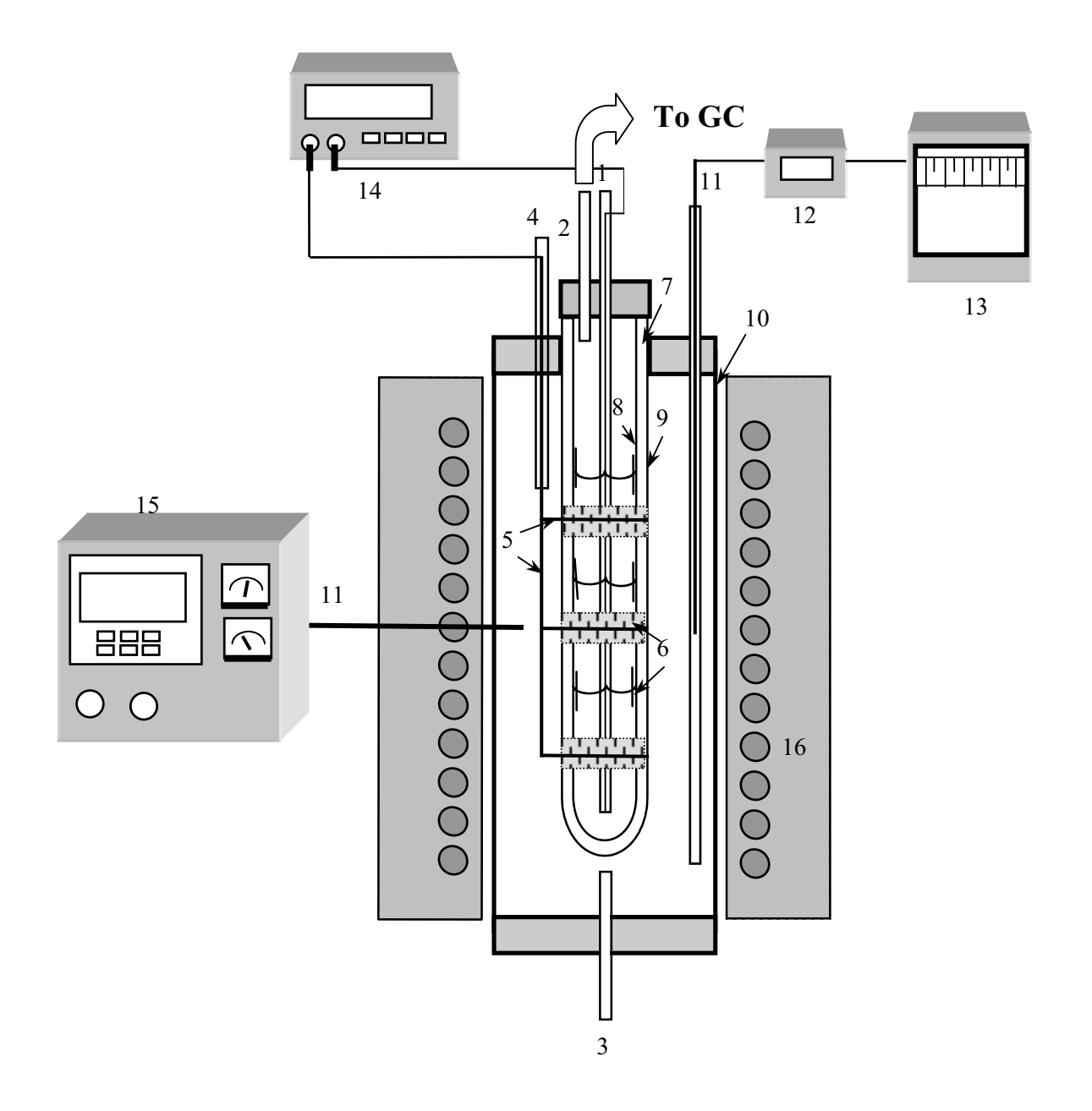


Fig. 3.1 Schematic diagram of the solid oxide fuel cell type reactor.

1. Anode side feed (CH₄)

2. Exit gas from anode side

3. Cathode side feed (O₂/air)

4. Exit gas from cathode side

5. Platinum wire

6. Platinum mesh

7. YSZ tube

9. Cathode (LSM)

10. Quartz tube

8. Anode (LaAlO)

13. Temperature recorder

11. Thermocouple

12. Temperature indicator 14. Current meter/Voltmeter/Potentiostat

15. Temperature controller

16. Furnace

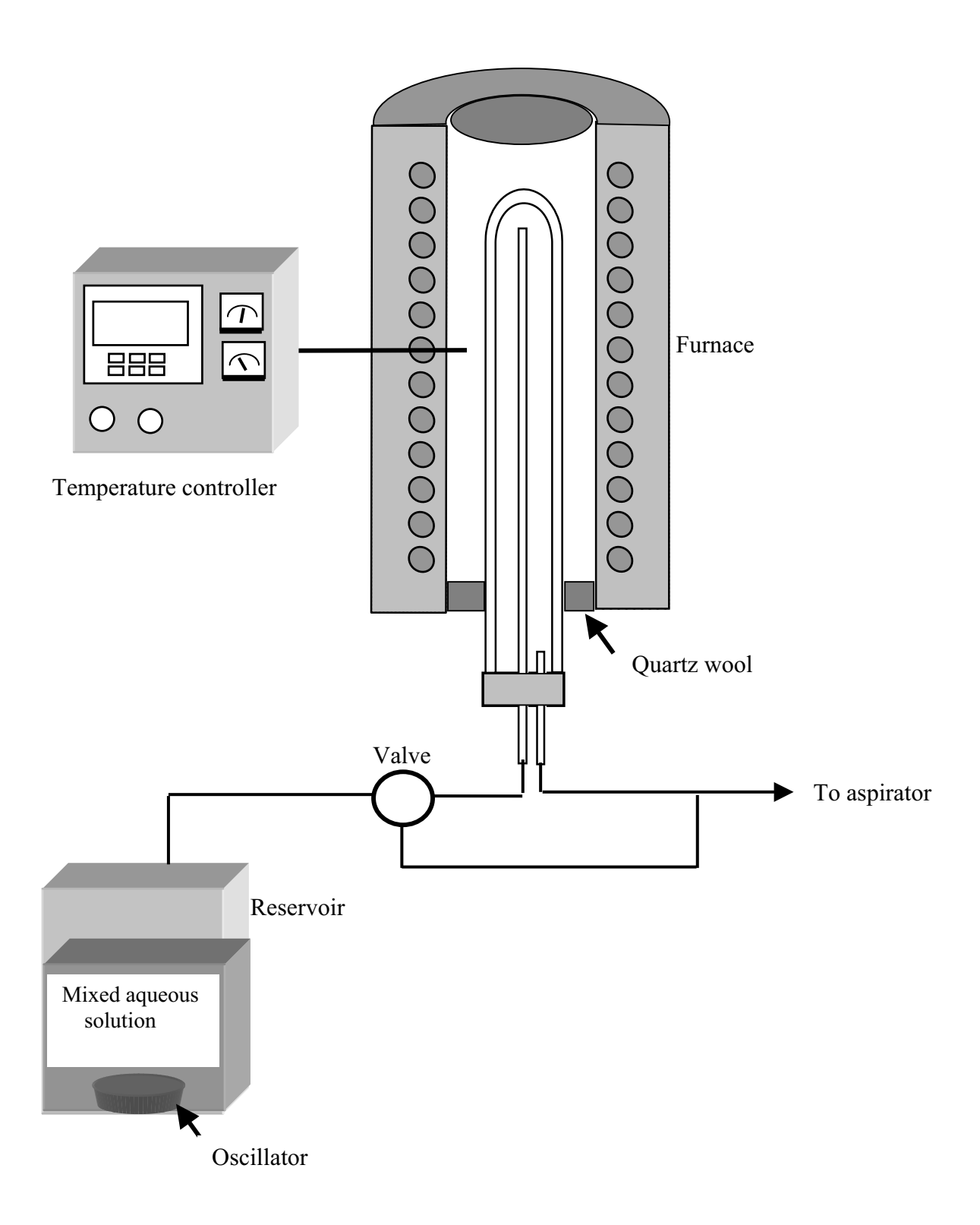


Fig. 3.2 Schematic diagram of the setup for the anode preparation

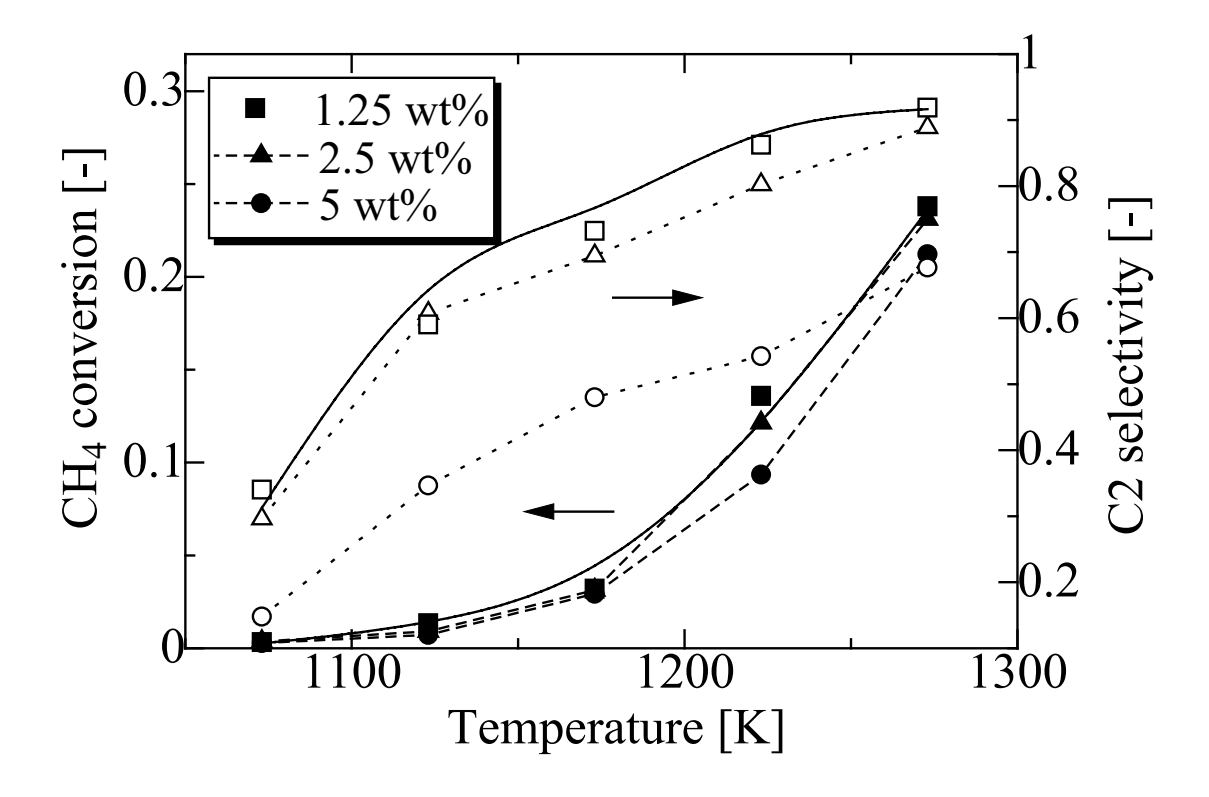


Fig. 3.3 Effect of temperature on methane conversion and C2 selectivity at difference anode preparation: $F_{\rm CH_4,0} = 3.4 {\rm x} 10^{-6} \ {\rm mol \ s}^{-1}, \ W = 4.0 {\rm x} 10^{-5} \ {\rm kg}$, pure oxygen feed on the cathode

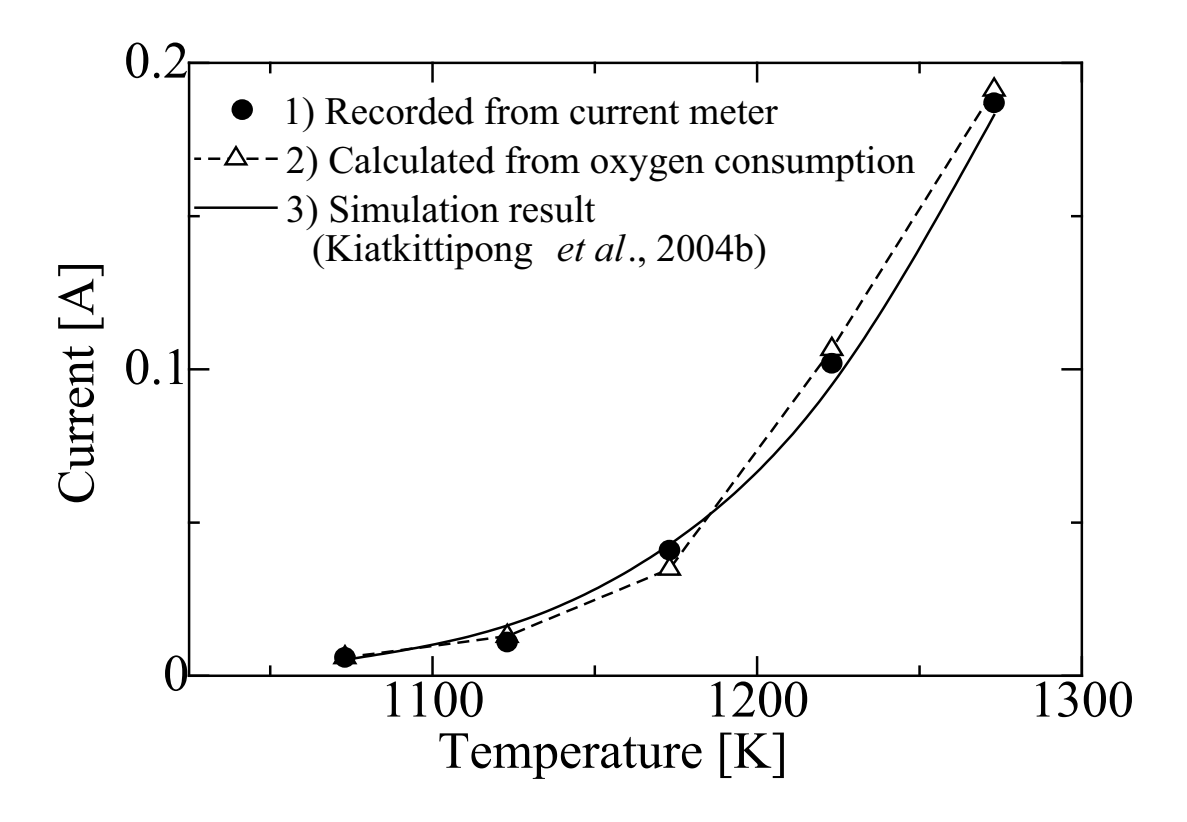
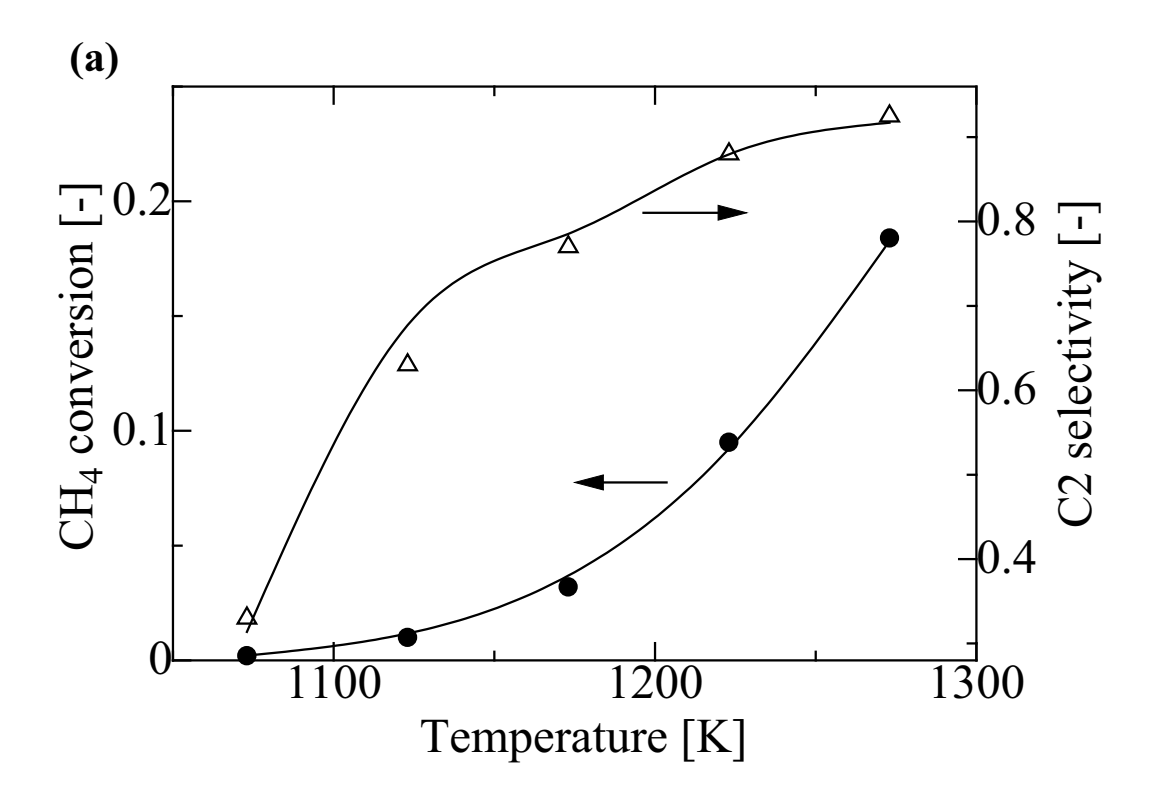


Fig. 3.4 Effect of temperature on current with short circuit mode: $F_{\rm CH_4,0} = 6.8 \times 10^{-6}$ mol s⁻¹, $W = 4.0 \times 10^{-5}$ kg, pure oxygen feed on the cathode



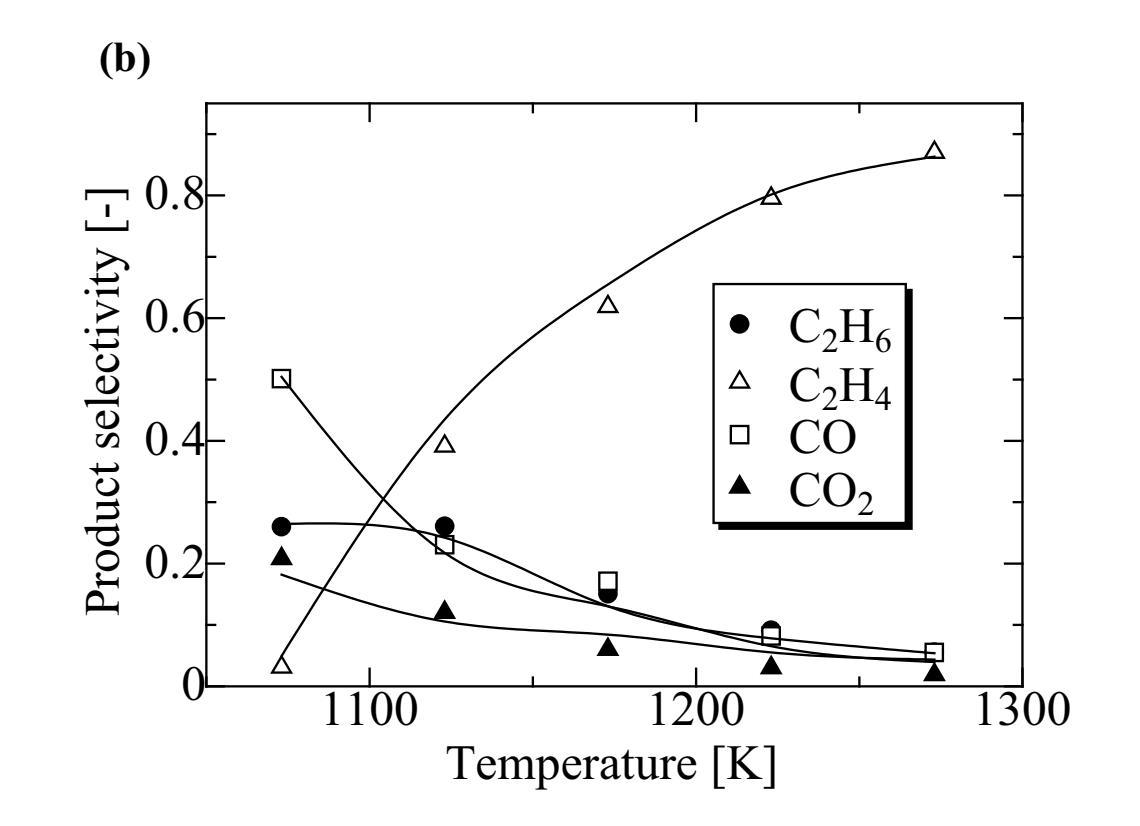


Fig. 3.5 Effect of temperature (a) on methane conversion and C2 selectivity and (b) on the product selectivity distribution: $F_{\rm CH_4,0} = 3.4 \times 10^{-6} \,$ mol s⁻¹, $W = 4.0 \times 10^{-5} \,$ kg, air feed on the cathode

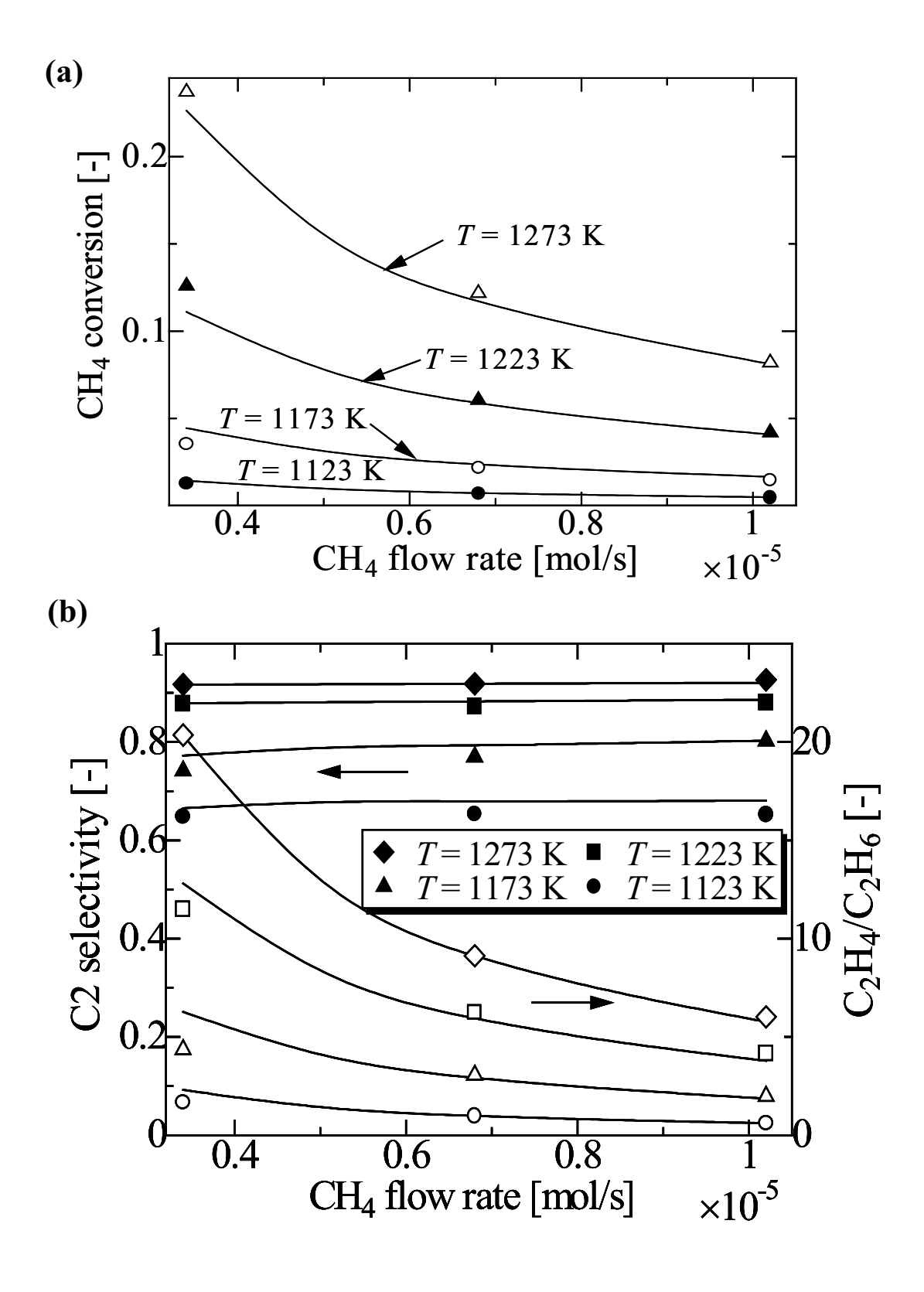


Fig. 3.6 Effect of methane flow rate (a) on methane conversion and (b) on C2 selectivity and C_2H_4/C_2H_6 ratio at various temperatures: $W = 4.0 \times 10^{-5}$ kg, pure oxygen feed on the cathode

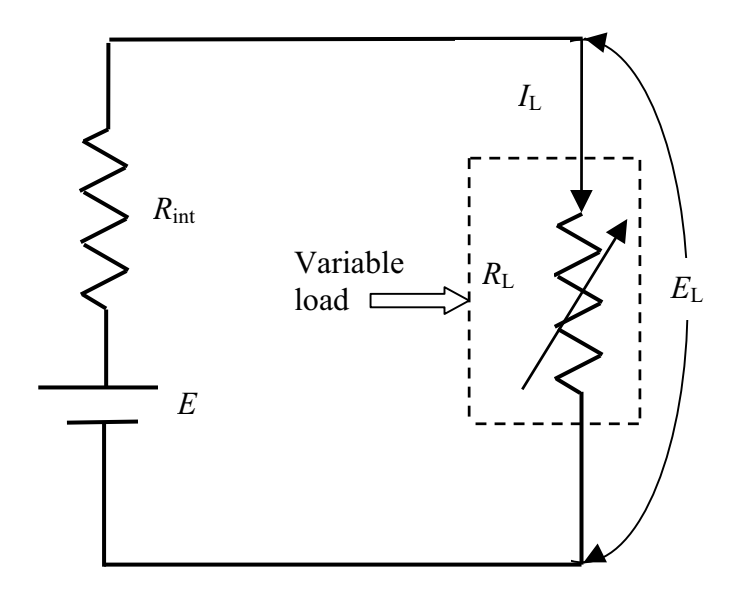


Fig. 3.7 Simplified circuit diagram to illustrate SOFC involving a variable load resistor

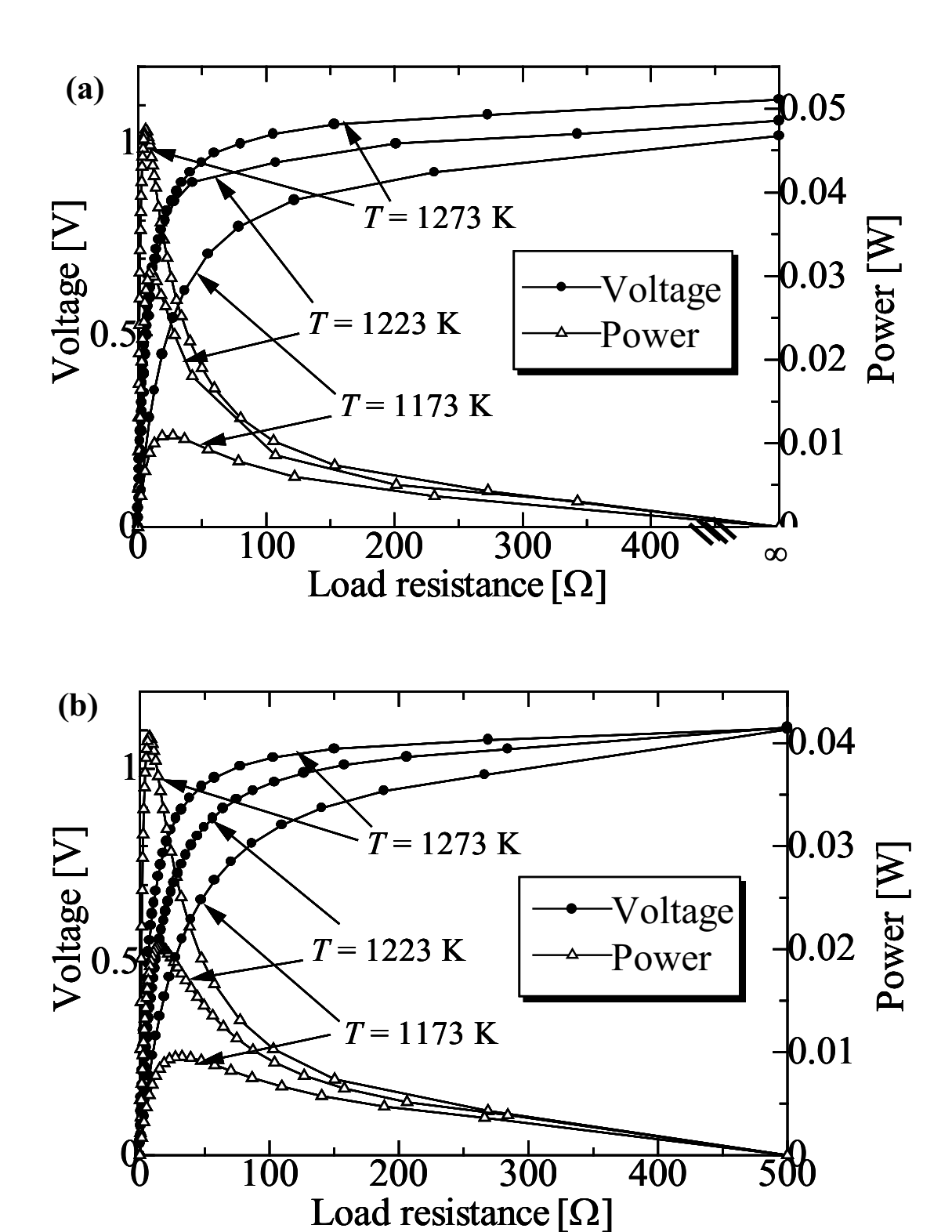


Fig. 3.8 Load resistance-voltage and load resistance-power at various temperatures in the case of (a) pure oxygen feed on the cathode and (b) air feed on the cathode: $F_{\text{CH}_4,0} = 6.8 \times 10^{-6} \text{ mol s}^{-1}$, $W = 4.0 \times 10^{-5} \text{ kg}$

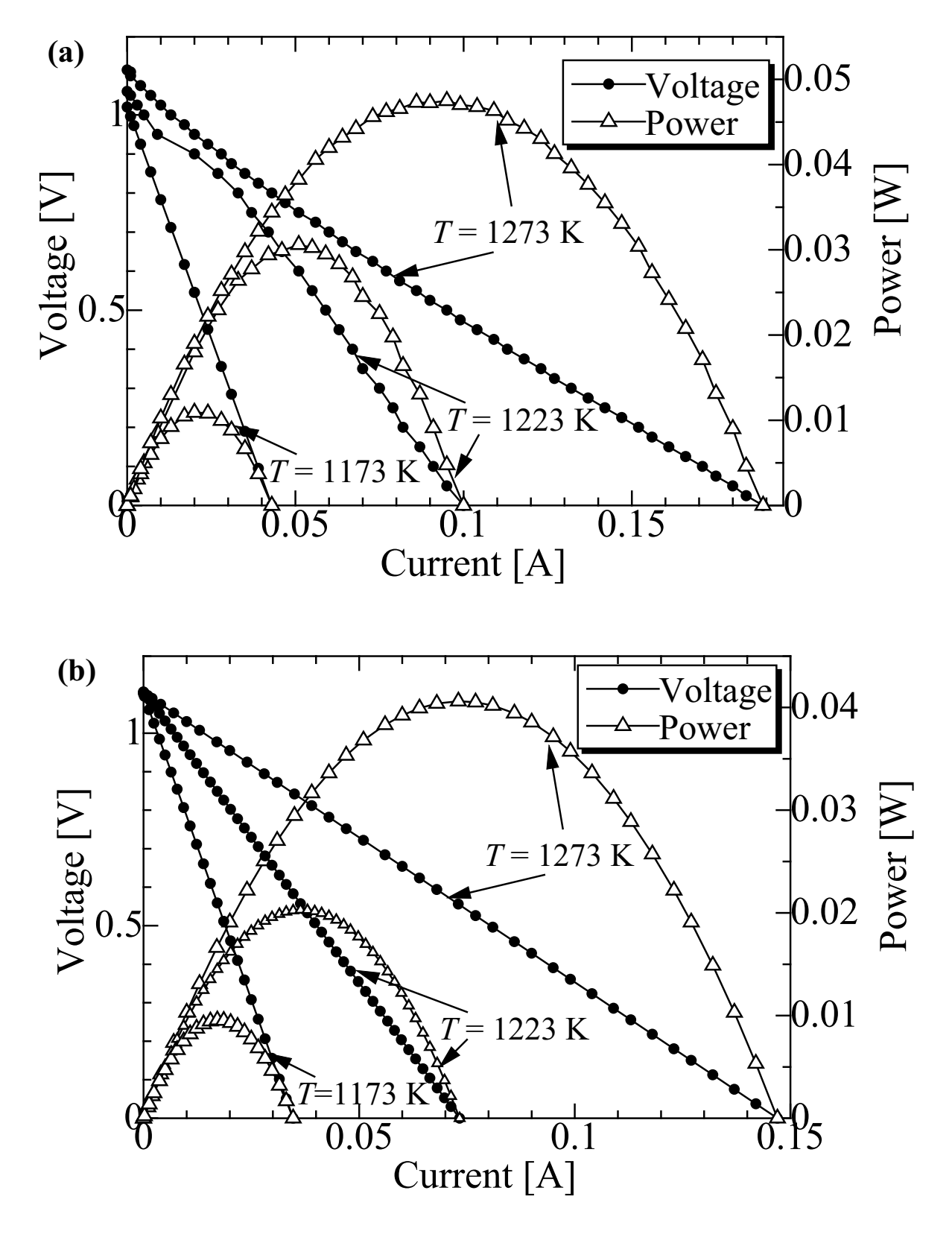


Fig. 3.9 Current-voltage and current-power at various temperatures in the case of (a) pure oxygen feed on the cathode and (b) air feed on the cathode: $F_{\text{CH}_4,0} = 6.8 \times 10^{-6} \text{ mol s}^{-1}$, $W = 4.0 \times 10^{-5} \text{ kg}$

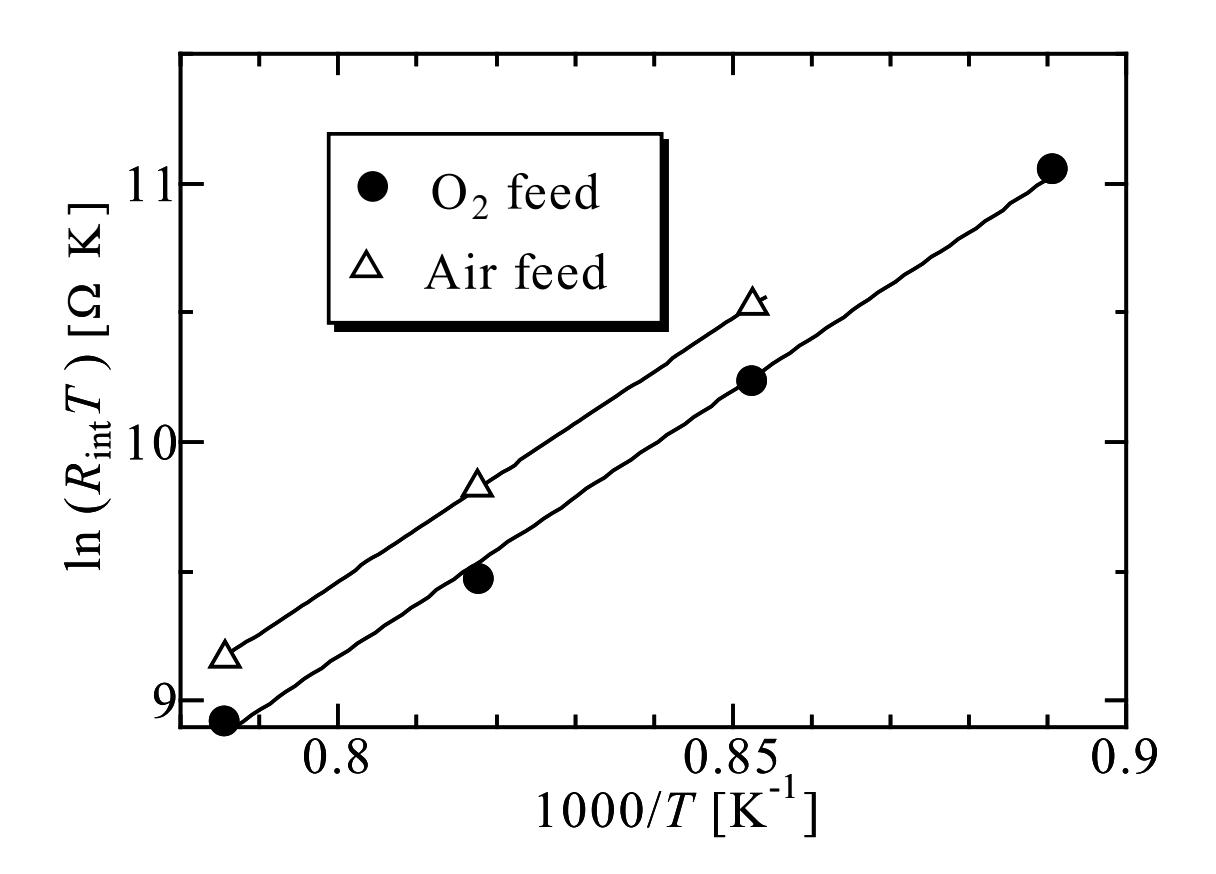


Fig. 3.10 Arrhenius' plot between $\ln{(R_{int}T)}$ and 1000/T

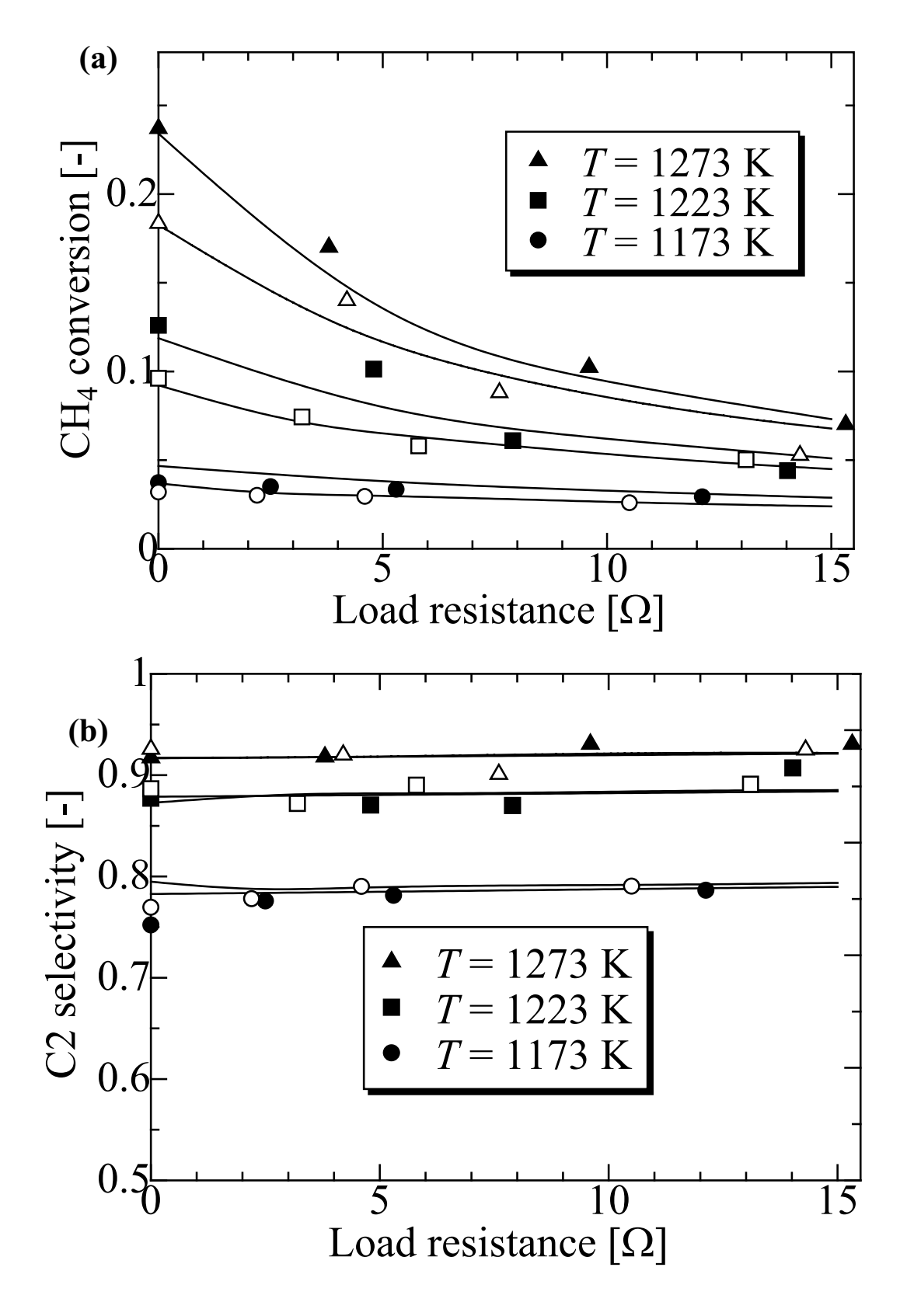


Fig. 3.11 Effect of load resistance (a) on methane conversion and (b) on C2 selectivity at various temperatures: $F_{\rm CH_4,0} = 3.4 \times 10^{-6} \, {\rm mol \ s^{-1}}, \, W = 4.0 \times 10^{-5} \, {\rm kg}, \, {\rm filled \ symbol} = {\rm pure \ oxygen \ feed \ on \ the \ cathode}$

Chapter 4
Simulation of Oxidative Coupling of Methane in Solid Oxide
Fuel Cell Type Reactor for C2 Hydrocarbon and Electricity
Co-Generation

4.1 Introduction

Solid oxide fuel cell (SOFC) is one of the most efficient ways to generate power from fuel (Yamamoto, 2000; Steele, 2001). Most attention has been given to the case where hydrogen or carbon monoxide are either directly fed to SOFC to be electrochemically oxidized or produced through direct or indirect internal steam reforming of methane (Achenbach, 1994; Bessette *et al.*, 1995; Nakagawa *et al.*, 2001; Aguiar *et al.*, 2002; Yamada *et al.*, 2002). Recent investigators used other types of fuel such as methane, methanol and ethanol. Among these studies, chemicals and power co-generation is one of the outstanding topics. The conversion of methane into higher hydrocarbons, which are more valuable, attracts a lot of attention. Among the various schemes for converting methane into more valuable feed stocks, the oxidative coupling of methane (OCM) to ethane and ethylene (C2) is a promising process to upgrade natural gas. For SOFC as a reactor for OCM reaction, a solid electrolyte was used as an oxygen separator and an oxygen distributor to achieve higher C2 selectivity.

In our previous papers, OCM was studied in SOFC reactor. Particular focuses were on catalyst preparation methods (Moe *et al.*, 1998a, 1998b; Carrillo *et al.*, 2001; Kiatkittipong *et al.*, 2004a) and reactor performance test (Tagawa *et al.*, 1998, 1999, 2003; Kiatkittipong *et al.*, 2004a). The fuel cell type temperature-programmed desorption (FC-TPD) measurements were employed to investigate oxygen species under the fuel cell operation (Kiatkittipong *et al.*, 2004b). The knowledge of oxygen species from FC-TPD (Tagawa *et al.*, 1998; Kiatkittipong *et al.*, 2004c) and the oxygen permeation through the LSM/YSZ/LaAlO (Kiatkittipong *et al.*, 2004c) were taken into account to obtain the kinetic parameters of the reactions on the anode (Kiatkittipong *et al.*, 2004a). A set of the kinetic model considering two different oxygen species; i.e. oxygenate and coupling species, was useful to evaluate the oxidative coupling of methane in a tubular SOFC type reactor. The effect of external load on reactor performances was investigated (Kiatkittipong *et al.*, 2004a).

In this paper, the performances in C2 and electricity productions of SOFC reactor operated at maximum power at load, is simulated. The effect of operating conditions; i.e., operating temperature, methane feed flow rate and concentration on the anode, oxygen concentrations on the cathode, and operating pressure were investigated.

4.2 Single unit of SOFC reactor configuration

The schematic diagram of the single solid oxide fuel cell type reactor was illustrated elsewhere (Kiatkittipong *et al.*, 2004a-2004c). A tube-type YSZ membrane (8 mol% Y₂O₃, thickness = 1.5 mm, inside diameter = 18 mm, outside diameter = 21 mm, total length = 500 mm) was used as an electrolyte. La_{1.8}Al_{0.2}O₃ (abbreviated as LaAlO) prepared by a mist decomposition method was used as an anode catalyst on the inner surface of the tube while La_{0.85}Sr_{0.15}MnO₃ (abbreviated as LSM) prepared by a conventional paste method on the outer side was used as the cathode. The electrodes were coated in the length of 0.242 m and the effective surface area is 0.0148 m². Platinum wire was connected to platinum meshes placed on both electrode surfaces to serve as current collectors. Current meter and voltmeter were used to measure closed circuit current (CCI) and open circuit voltage (OCV), respectively. Voltages at various current values were measured using a potentiostat.

4.3 SOFC modelling

By assuming plug flow and isothermal condition, the mass balance equation in the anode side is given as

$$\frac{\mathrm{d}\gamma_i}{\mathrm{d}x} = \left\{r_i + \left(\frac{S}{W}\right)J_i\right\} \left(\frac{W}{F_{\mathrm{CH_4,0}}}\right) \tag{4.1}$$

where the permeation rate of component i except for oxygen is zero ($J_i = 0$) because the YSZ electrolyte allows only oxygen to permeate.

At the entrance (x = 0), $\gamma CH_4 = 1$, $\gamma_i = 0$ (i = products)

The partial pressures in the anode side (AN) and the cathode side (CA) can be determined as

$$P_{i,\text{AN}} = \frac{P_{t,\text{AN}} \gamma_i}{\sum_{i} \gamma_i}$$
 (4.2)

 $P_{\rm O_2,CA} = 1.013 \times 10^5$ and 2.127×10^4 Pa for pure oxygen and air feed, respectively.

It should be noted that since the radiation is a very efficient for heat transfer due to high temperature as 1073-1273 K in the oven (Kiatkittipong *et al.*, 2004 a), the temperature is uniform. The isothermal behavior of SOFC has already been reported in the literature (Costamagna *et al.*, 1998, 2004). Therefore, the simulations are considered isothermal and the energy balances are not included in this work.

The oxygen permeation rate through the LSM/YSZ/LaAlO solid oxide fuel cell type reactor can be estimated from our model (Kiatkittipong *et al.*, 2004c). The permeation of oxygen depends upon ionic conductivity (σ_i) and electronic conductivity (σ_e) of the materials. The following set of equations is applied for LSM and YSZ with reported parameters.

$$J_{O_2} = \frac{Per_{O_2}}{L} \ln \left(\frac{P_{\text{rich}}}{P_{\text{loan}}} \right)$$
 (4.3)

$$Per_{,O_2} = \frac{R_g T}{16F^2} \frac{\sigma_i \sigma_e}{\sigma_i + \sigma_e}$$
(4.4)

$$\sigma_{j} = \left(\frac{A_{j}}{T}\right) \exp\left(\frac{-E_{j}}{R_{g}T}\right); j = i,e$$
 (4.5)

Although these values of LaAlO are not available in literature, the kinetic parameters were determined in our previous study.

The oxygen permeation rate was divided into two different types of oxygen species; i.e., oxygenate and coupling oxygen, by using mole fraction of oxygen species as shown below.

$$y_{0,,\text{oxy}} = -2.381x10^{-3}T + 3.2661$$
 (4.6)

$$J_{O_2, oxy} = y_{O_2, oxy} J_{O_2} \tag{4.7}$$

$$J_{O_{2},\text{cou}} = y_{O_{2},\text{cou}} J_{O_{2}} = (1 - y_{O_{2},\text{oxy}}) J_{O_{2}}$$
(4.8)

Eq. (4.6) was determined from the FC-TPD experimental results of our previous work in Table 2 (Kiatkittipong *et al.*, 2004a).

The reactions taking place in the system are summarized in Eqs. (4.9)–(4.13).

The rate expressions are provided in our previous work (Kiatkittipong et al., 2004a).

$$2CH_4 + 1/2O_2 \rightarrow C_2H_6 + H_2O$$
 (4.9)

$$C_2H_6 + 1/2O_2 \rightarrow C_2H_4 + H_2O$$
 (4.10)

$$CH_4 + 3/2O_2 \rightarrow CO + 2H_2O$$
 (4.11)

$$CH_4 + 2O_2 \rightarrow CO_2 + 2H_2O$$
 (4.12)

$$C_2H_6 + 7/2O_2 \rightarrow 2CO_2 + 3H_2O$$
 (4.13)

The current density and its average value can be related to oxygen permeation flux as described by Faraday's law as follows.

$$I_{\text{CCI}} = J_{\text{O}_2} \times 4F \tag{4.14}$$

$$\overline{I_{\text{CCI}}} = \frac{\int_{0}^{Z_{\text{T}}} I_{\text{CCI}} dx}{Z_{\text{T}}}$$
(4.15)

The internal cell resistance ($R_{\rm int}$) is almost independent on partial pressure of methane in the range of our previous study (Kiatkittipong *et al.*, 2004a). However, at intermediate and low values of partial pressure of methane, the dependency of the $R_{\rm int}$ on the partial pressure of methane needs to be taken into account. Other sets of experiments were carried out, and the following expression is obtained;

$$R_{\text{int}} = \frac{0.0567}{P_{\text{O}_{2},\text{CA}}^{0.51} P_{\text{CH}_{4}}^{0.51} T} \exp\left(\frac{166000}{R_{g}T}\right)$$
(4.16)

A simplified short circuit model is shown in **Fig. 4.1(a)**. In normal fuel cell operation, an external load is connected to the cell for power utilization. A simplified series circuit model is proposed in **Fig. 4.1(b)**. Assuming the cell is operated at maximum power at load which occurs when $R_L = R_{int}$. Then the corresponding current density (I_L) and voltage across the load (E_L) are estimated as follows (Siskind, 1965).

$$I_{\rm L} = \frac{\overline{I_{\rm CCI}}}{2} \tag{4.17}$$

$$E_{\rm L} = \frac{E}{2} = I_{\rm L} R_{\rm L} \tag{4.18}$$

Then the power at load operated at the maximum power transfer is

$$P_{\rm L} = (I_{\rm L} \times S) \times E_{\rm L}$$
 (4.19)

The values of overall efficiency can be based on heat of reaction of methane combustion $(-\Delta H_{\rm CO_2})$ and on that of the selective coupling to ethylene $(-\Delta H_{\rm C_2H_4})$ as follows;

$$CH_4 + 2O_2 \rightarrow CO_2 + 2H_2O$$
 (4.20)

 $(-\Delta H_{\rm CO_2})$ at operating temperature T =

$$-802600 + 15.884(T - T_{st}) - 1.698 \times 10^{-2} \left(\frac{T^2 - T_{st}^2}{2}\right) - 1.227 \times 10^{-5} \left(\frac{T^3 - T_{st}^3}{3}\right) + 8.660 \times 10^{-9} \left(\frac{T^4 - T_{st}^4}{4}\right) (4.21)$$

where $T_{\rm st}$ is standard temperature (298 K)

$$CH_4 + 1/2O_2 \rightarrow 1/2C_2H_4 + H_2O$$
 (4.22)

 $(-\Delta H_{C,H_a})$ at operating temperature T =

$$-141050 + 1.588(T - T_{st}) + 2.226 \times 10^{-2} \left(\frac{T^2 - T_{st}^2}{2}\right) - 4.025 \times 10^{-5} \left(\frac{T^3 - T_{st}^3}{3}\right) + 1.558 \times 10^{-8} \left(\frac{T^4 - T_{st}^4}{4}\right) (4.23)$$

The definition of the overall efficiency is defined as follows.

$$\eta_{\text{OV, k}} = \frac{P_{\text{T}}}{(-\Delta H_{\text{k}})F_{\text{CH}_4,0}}; k = \text{CO}_2, \text{C}_2\text{H}_4$$
(4.24)

4.4. Results and Discussion

4.4.1 Comparison between simulation and experimental results

The mathematical model was verified by comparing simulation results with the experimental results. EQUATRAN-G (Omega Simulation, Japan), all-purpose equation solver, was employed to solve the equations. **Table 4.1** shows the current (I_L x S), voltage (E_L) and power (P_L) obtained from the experiments and simulations when the cell is operated at maximum power at load. The voltage and current at maximum power for the cases of pure oxygen and air feeds on the cathode are obtained from reported data of our previous paper in Fig. 9 (Kiatkittipong *et al.*, 2004a). Good agreements between simulation and experimental results are obtained. Then the effects of various operating conditions are investigated. The simulation results are shown as lines while some of the experimental results are shown as symbols.

4.4.2 Effect of operating temperature

Figure 4.2(a) shows the effect of temperature on methane conversion and C2 selectivity in both cases of pure oxygen and air feeds on the cathode. The conversion and C2 selectivity increase with increasing temperature. Slightly higher conversion is achieved in the case of pure oxygen feed on the cathode due to the increased driving force of oxygen partial pressure. However, the values of C2 selectivity are almost the same for both cases. Figure 4.2(b) shows the effect of temperature on power at load and overall efficiency. They increase with increasing operating temperature due to the increased oxygen permeation rate. It should be noted that the overall efficiency is low because the calculation is based on the overall heat of combustion of methane to carbon dioxide. In addition, the differences in the power and the overall efficiency between the cases with air feed and pure oxygen feed are not significant, indicating that the effort to purify air to achieve high oxygen concentration is unnecessary.

4.4.3 Effect of feed flow rate and methane feed concentration

Figure 4.3 shows the effect of feed flow rate on the reactor performances at various levels of methane feed concentration. Methane was diluted with inert gas and fed to the reactor. As shown in Fig. 4.3, the methane conversion decreases with increasing total molar flow rate for all methane feed concentration due to the decreased residence time. In addition, the C2 selectivity is only slightly decreased with decreasing total molar flow rate or increasing the inert mole fraction. It is explained by that the oxygenate products and coupling products are mainly formed in a parallel manner. The filled and open symbol represent to methane conversion and C2 selectivity from the experiment, respectively. The simulation results agreed well with the experimental results. However, most of our simulation conditions were extended from the range of our experiments, only one of experiments was shown in this figure. In our system, most of C2 production is ethylene, which is more favored

than ethane. The mole fraction profiles along the reactor length are shown in **Fig. 4.4**. In Fig. 4.4, the different range of Y-axis (until 0.04) is also shown to clarify the products profiles. The profiles of the products C₂H₆, CO and CO₂, which are at small values, are magnified inside the figure. CO and CO₂ slightly increase while C₂H₆ decreases with the increasing reactor length. Although inert gas is not participated in the reaction, the mole fraction of inert gas slightly decreases due to the increase of gas mole from the reaction. It is worthy to note that LaAlO, anode catalyst, is very effective for C2 production (especially, C₂H₄) from OCM in SOFC reactor. Our previous work studied both of normal SOFC mode and mixed flow mode with different anode preparation method (Tagawa et al., 2003). The C2 selectivity in the case of mixed flow mode is much lower than the normal SOFC mode.

Power at load increases with increasing methane feed concentration while it slightly increases with increasing the total molar flow rate as shown in **Fig. 4.5**. It is important to note that the power at load in case of dilution with inert gas is obviously lower than that with pure methane because the internal cell resistance is influenced by partial pressure of methane; i.e., it increases with the decrease of methane partial pressure. In addition, the current, which is corresponding to oxygen permeation, increases with increasing methane partial pressure (Kiatkittipong *et al.*, 2004c). Figure 4.5 also provides the overall efficiency based on the heat of selective oxidation to ethylene. The value as high as 17% can be obtained. This value is corresponding to the overall efficiency based on the heat of combustion of 2.9%. It might be difficult to define the overall efficiency for this SOFC system because there are many reactions involved. For example, at T = 1273 K, the Gibbs' free energy of the methane conversion to carbon dioxide and to ethylene are 7.958×10^5 and 1.533×10^5 J mol⁻¹, respectively. The extent of undesired complete oxidation reaction can significantly increase the value of the overall efficiency based on the ethylene production.

4.4.4 Effect of operating pressure

In order to avoid cell damages, the operating pressures in both sides of the cells are maintained at the same value. The results shown in **Fig. 4.6** indicate that the methane conversion increases with increasing operating pressure while the C2 selectivity is insignificantly affected. The factors controlling the selectivity are mainly the oxygen species and their amount which depend on the operating temperature. Therefore, the operating temperature indicates the strongest effect on C2 selectivity as shown in Fig. 4.2 (a).

Corresponding to the increased conversion, the power and the overall efficiency shown in **Fig. 4.7** become higher. As the operating pressure increases, the driving force for oxygen permeation through the cell increases. This tendency can be explained by the increased oxygen partial pressure in the cathode and the acceleration of reaction rate from the increased methane partial pressure. In addition, the internal cell resistance becomes smaller with increasing the partial pressures of methane and oxygen as shown in Eq. (4.12). It is clear that operation at high pressure is beneficial to SOFC performances; however, other considerations such as problems on seals and mechanical properties of the cells at high pressure should be taken into account for selection of a suitable operating pressure.

4.4.5 Comparison of SOFC performances among different systems

Typical SOFCs are used for power generation. It is desired to operate SOFC at high power density. The value of 960 W m⁻² was reported for the complete oxidation of methane in SOFC with YSZ electrolyte at 1073 K (Liu *et al.*, 2003). The lower value of 375 W m⁻² was reported for the partial oxidation of methane to synthesis gas using YSZ electrolytes (Sobyanin *et al.*, 2000). In this study, the maximum power density obtained with pure methane feed at atmospheric pressure and 1273 K is 3.34 W m⁻². This value is in the same range reported by other investigators. Guo *et al.* (1999) studied OCM in tube type SOFC reactor with YSZ electrolyte of 1 mm thickness. The maximum power density of 3.89 W m⁻² was obtained at 1003 K. Tagawa *et al.* (1999) studied OCM in a similar system of this study (LSM/YSZ/LaAlO) but using a plate type electrolyte. The maximum power density was 13.85 W m⁻². This is due to the smaller thickness of the YSZ electrolyte used in their study (0.3 mm).

It is obvious that with the present technology on OCM in SOFC, the obtained power density is much lower than the conventional SOFC. However, our SOFC system is attractive in that it offers high selectivity to C2 hydrocarbon and electricity is obtained simultaneously.

4.5 Conclusion

The simulation was carried out for OCM in LSM/YSZ/LaAlO SOFC reactor. The plug flow reactor model (PFRM) was developed using kinetic parameters of the oxidative coupling of methane and oxygen permeability through LSM/YSZ/LaAlO from our previous works. The mathematical model was verified by comparing simulation results with the experimental results of the single unit cell operated at maximum power at load. Methane conversion and C2 selectivity increase with increasing operating temperature. Methane conversion increases with decreasing total molar flow rate or decreasing methane feed concentration while C2 selectivity is only slightly decreased. No effort on air purification is required in the system. Operation at higher pressure seems to be attractive to obtain higher power and C2 production. The results suggest that our SOFC system is an excellent reactor for C2 production where electric power is generated simultaneously.

Nomenclature

E	=	cell voltage	[V]
F	=	Faraday's constant, 96485	[C mol ⁻¹]
$F_{\mathrm{CH_4,0}}$	=	feed molar flow rate of methane	$[\text{mol s}^{-1}]$
$-\Delta H_{ m k}$	=	heat of reaction	[J mol ⁻¹]
I	=	current density	$[A m^{-2}]$
\overline{I}	=	average current density	$[A m^{-2}]$
$J_{\scriptscriptstyle{\mathrm{O}_2}}$	=	oxygen permeation flux	$[\text{mol m}^{-2} \text{ s}^{-1}]$
L	=	thickness of material	[m]
Per, _{O2}	=	specific oxygen permeability	$[\text{mol m}^{-1} \text{ s}^{-1}]$
P_i	=	pressure of component i	[Pa]
$P_{ m rich}$	=	oxygen partial pressure at rich side of materi	als [Pa]
P_{lean}	=	oxygen partial pressure at lean side of mater	ials [Pa]
$P_{ m O_2,CA}$	=	pressure of oxygen in the cathode side	[Pa]

$P_{ m t,AN}$	=	total pressure in the anode side	[Pa]	
$P_{ m L}$	=	power at load	[W]	
P_{T}	=	total power output	[W]	
r_j	=	rate of reaction <i>j</i>	$[\text{mol kg}^{-1} \text{ s}^{-1}]$	
Ř	=	resistance	[ohm m ²]	
$R_{ m g}$	=	gas constant, 8.314	$[J \text{ mol}^{-1} \text{ K}^{-1}]$	
S	=	effective surface area	$[m^2]$	
T	=	temperature	[K]	
$T_{ m st}$	=	standard temperature, 298	[K]	
W	=	mass of anode catalyst	[kg]	
\boldsymbol{x}	=	dimensionless axial length divided by the to	tal length of reactor	[-]
y	=	mole fraction	[-]	
Z_{T}	=	total length of reactor	[m]	
η	=	efficiency	[-]	
γ	=	molar flow rate ratio (= $F_i / F_{CH_4,0}$)	[-]	
σ	=	conductivities	$[S m^{-1}]$	

<Subscript>

AN = anode side CA = cathode side

CCI = closed circuit current

 $egin{array}{lll} \mathbf{e} & = & & & & & & \\ \mathbf{FC} & = & & & & & & \\ \mathbf{i} & = & & & & & \\ \mathbf{i} & = & & & & & \\ \mathbf{i} & = & & & & & \\ \mathbf{component} \ \mathbf{i} & & & & \\ \end{array}$

int = internal
I = inert gas
L = load

 $O_{2, \text{ cou}} = oxygen \text{ for coupling site}$ $O_{2, \text{ oxy}} = oxygen \text{ for oxygenate site}$

 $egin{array}{lll} \mathrm{OV} &=& \mathrm{overall} \ \mathrm{T} &=& \mathrm{total} \ 0 &=& \mathrm{feed} \ \end{array}$

References

- Achenbach, E.; "Three-Dimensional and Time-Dependent Simulation of a Planar Solid Oxide Fuel Cell Stack," *J. Power. Sources*, **49**, 333-348 (1994)
- Aguiar, P., D. Chadwick and L. Kershenbaun; "Modelling of an Indirect Internal Reforming Solid Oxide Fuel Cell," *Chem. Eng. Sci.*, **57**, 1665-1677 (2002)
- Bessette, N. F., W. J. Wepfer and J. Winnick; "A Mathematical Model of a Solid Oxide Fuel Cell," *J. Electrochem. Soc.*, **142**, 3792-3800 (1995)
- Carrillo, A. S., T. Tagawa and S. Goto; "Application of Mist Pyrolysis Method to Preparation of Ni/ZrO₂ Anode Catalyst for SOFC Type Reactor," *Mater. Res. Bull.*, **36**, 1017-1027 (2001)
- Costamagna, P., K. Honegger; "Modeling of solid oxide heat exchanger integrated stacks and simulation at high fuel utilization," *J. Electrochem. Soc.*, **145**, 3995–4007 (1998)
- Costamagna, P., A. Selimovic, M. D. Borghi, G. Agnew; "Electrochemical model of the integrated planar solid oxide fuel cell (IP-SOFC)," *Chem. Eng. J.*, **102**, 61–69 (2004)

- Guo, X. M., K. Hidajat and C. B. Ching; "Simulation of a Solid Oxide Fuel Cell for Oxidative Coupling of Methane," *Catal. Today*, **50**, 109-116 (1999)
- Kiatkittipong, W., T. Tagawa, S. Goto, S. Assabumrungrat and P. Praserthdam; "Oxidative Coupling of Methane in LSM/YSZ/LaAlO SOFC Reactor," *J. Chem. Eng. Japan.*, **37**, 1461-1470 (2004a)
- Kiatkittipong, W., T. Tagawa, S. Goto, S. Assabumrungrat and P. Praserthdam; "TPD Study in LSM/YSZ/LaAlO System for the Use of Fuel Cell Type Reactor," *Solid State Ionics*, **166**, 127-136 (2004b)
- Kiatkittipong, W., T. Tagawa, S. Goto, S. Assabumrungrat and P. Praserthdam; "Oxygen Transport Through LSM/YSZ/LaAlO System for Use of Fuel Cell Type Reactor," *Chem. Eng. J.*, (in press, 2004c)
- Liu, J., S. Barnett; "Operation of Anode-Supportde Solid Oxide Fuel Cells on Methane and Natural Gas," *Solid State Ionics*, **158**, 11-16 (2003)
- Moe, K. K., T. Tagawa and S. Goto; "Preparation of Electrode Catalyst for SOFC Reactor by Ultrasonic Mist Pyrolysis of Aqueous Solution," *J. Ceram. Soc. Japan.*, **106**, 242-247 (1998a)
- Moe, K. K., T. Tagawa and S. Goto; "Preparation of Electrode Catalyst for SOFC Reactor by Ultrasonic Mist Pyrolysis: Effect of Spray Time," *J. Ceram. Soc. Japan.*, **106**, 754-758 (1998b)
- Nakagawa, N., H. Sagara and K. Kato; "Catalytic Activity of Ni-YSZ-CeO₂ Anode for the Steam Reforming of Methane in a Direct Internal-Reforming Solid Oxide Fuel Cell," *J. Power. Sources*, **92**, 88-94 (2001)
- Siskind, C. S.; Electrical Circuits: Direct and Alternating Current, 2nd ed., McGraw-Hill Book, Tokyo, Japan (1965)
- Sobyanin, V. A. and V. D. Belyaev; "Gas-Phase Electrocatalysis; Methane Oxidation to Syngas in a Solid Oxide Fuel Cell Reactor," *Solid State Ionics*, **136-137**, 747-752 (2000)
- Steele, B. C. H.; "Material Science and Engineering: The Enabling Technology for the Commercialisation of Fuel Cell Systems," *J. Material. Sci.*, **36**, 1053-1068 (2001)
- Tagawa, T., K. K. Moe, T. Hiramatsu and S. Goto; "Design of Electrode for Solid Oxide Fuel Cells Reactor," *Solid State Ionics*, **106**, 227-235 (1998)
- Tagawa, T., K. K. Moe, M. Ito and S. Goto; "Fuel Cell Type Reactor for Chemicals-Energy Co-Generation," *Chem. Eng. Sci.*, **54**, 1553-1557 (1999)
- Tagawa, T., K. Kuroyanagi, S. Goto, S. Assabumrungrat and P. Praserthdam; "Selective Oxidation of Methane in an SOFC-Type Reactor: Effect of Applied Potential," *Chem. Eng. J.*, **93**, 3-9 (2003)
- Yamada, K., N. Takahashi and C. J. Wen; "Design and Evaluation of an Electric Vehicle Using Solid Oxide Fuel Cells," *J. Chem. Eng. Japan.*, **35**, 1290-1297 (2002)
- Yamamoto, O.; "Solid Oxide Fuel Cells: Fundamental Aspect and Pospects," *Electrochim. Acta.*, **45**, 2423-2435 (2000)

Table 4.1 Comparison of current ($IL \times S$), voltage (EL) and power (PL) between experimental and simulation results ($F_{CH_4,0} = 6.8 \times 10^{-6} \text{ mol s}^{-1}$, ZT = 0.242 m and operation at maximum power at load)

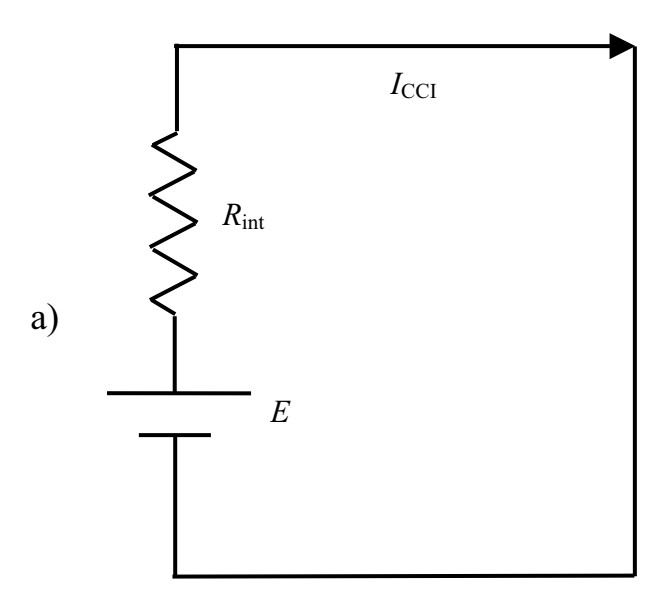
a) In the case of pure oxygen feed on the cathode

	1 70			
Temperature				
	Experiment (Simulation)*			
[K]	$(IL \times S)[A]$	EL [V]	PL [W]	
1173	0.020 (0.021)	0.546 (0.483)	0.011 (0.010)	
1223	0.051 (0.047)	0.562 (0.512)	0.029 (0.024)	
1273	0.095 (0.090)	0.500 (0.501)	0.048 (0.045)	

b) In the case of air feed on the cathode

Temperature	Experiment (Simulation)*			
[K]	/L [A]	EL [V]	PL [W]	
1173	0.017 (0.017)	0.559 (0.539)	0.010 (0.009)	
1223	0.036 (0.038)	0.557 (0.550)	0.020 (0.021)	
1273	0.073 (0.073)	0.556 (0.550)	0.041(0.040)	

^{*} Parentheses show the simulation results



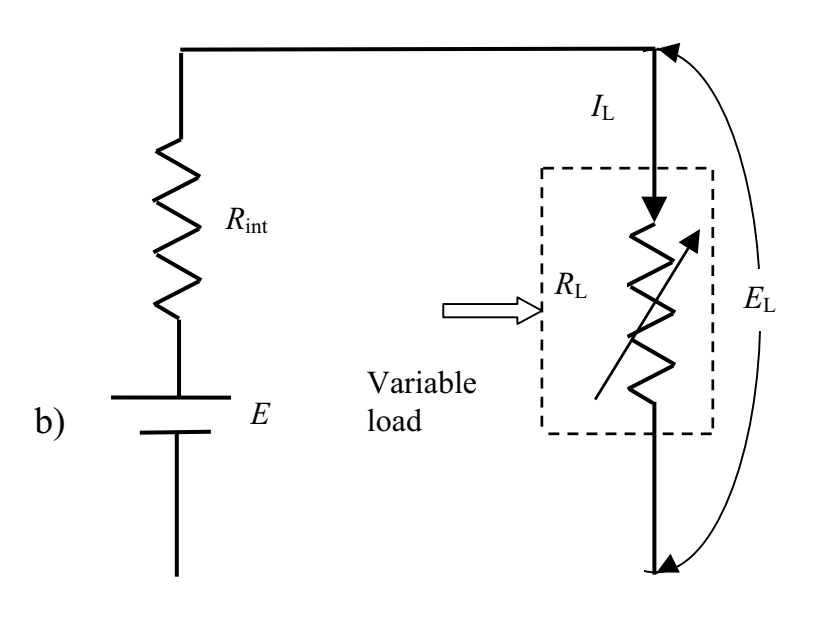


Fig. 4.1 Simplified circuit diagram to illustrate SOFC reactor

- a) Operation with short circuit mode
- b) Operation with an external variable load resistor.

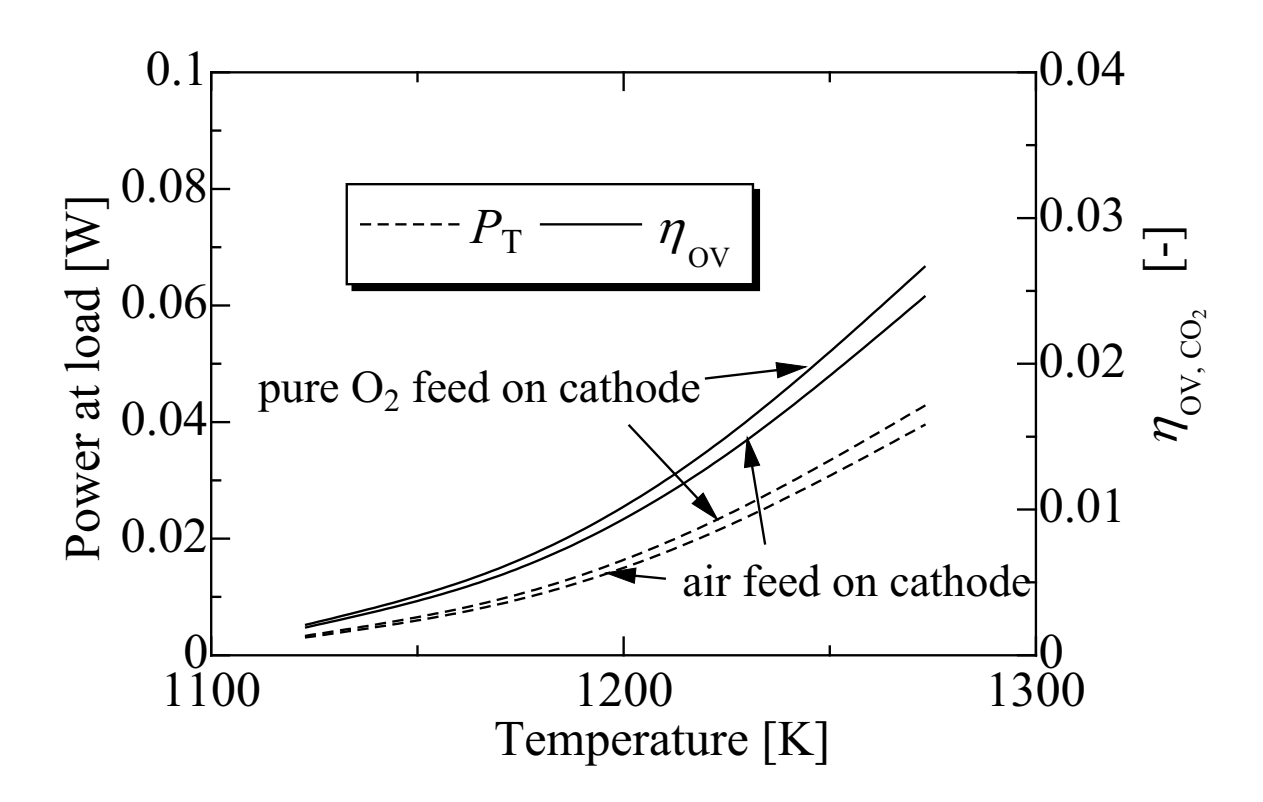


Fig. 4.2 Effect of operating temperature on a) methane conversion and C2 selectivity and b) power at load and overall efficiency; the lines represent the simulation results ($F_{\text{CH}_4,0} = 2.0 \times 10^{-6} \text{ mol s}^{-1}$, $Z_{\text{T}} = 0.242 \text{ m}$, $P_{\text{t, AN}} = P_{\text{t, CA}} = 1.013 \times 10^{5}$ Pa, pure methane feed on the anode).

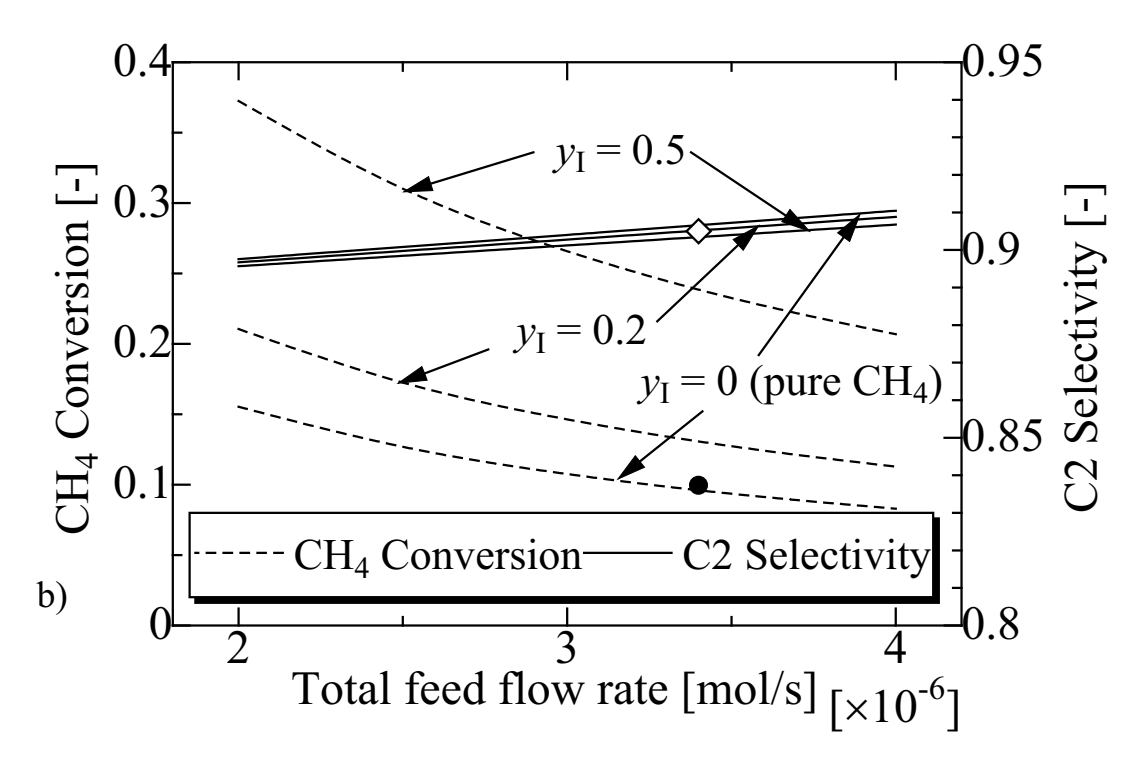


Fig. 4.3 Effect of total feed flow rate on methane conversion and C2 selectivity at various methane feed concentration; the lines represent the simulation results, the symbols represent the experimental results ($Z_T = 0.242 \text{ m}$, $P_{t, AN} = P_{t, CA} = 1.013 \times 10^5 \text{ Pa}$, T = 1273 K, air feed on the cathode).

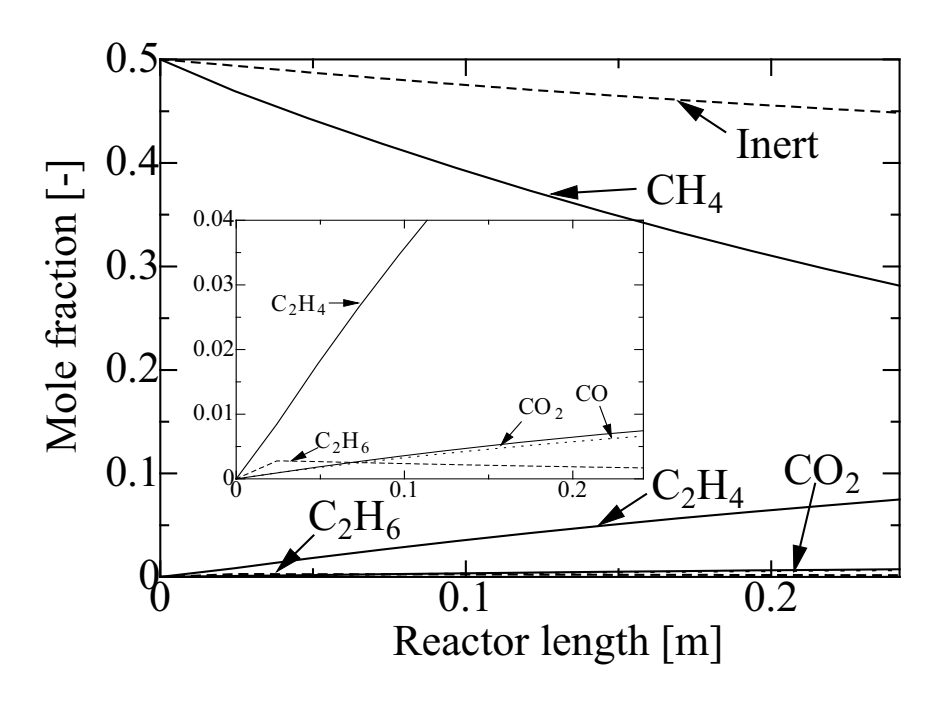
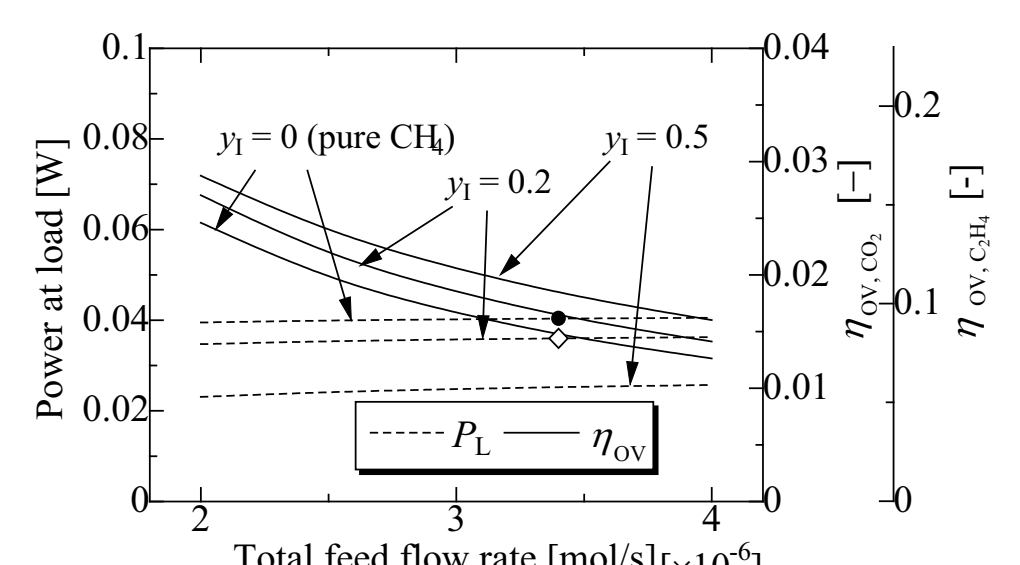


Fig. 4.4 Mole fraction profiles with reactor length; the lines represent the simulation results $(Z_T = 0.242 \text{ m}, P_{t, AN} = P_{t, CA} = 1.013 \times 10^5 \text{ Pa}, T = 1273 \text{ K}, \text{ air feed on the})$ cathode, $y_I = 0.5$).



Total feed flow rate [mol/s] $[\times 10^{-6}]$ Fig. 4.5 Effect of total feed flow rate on power at load and overall efficiency at various methane feed concentration; the lines represent the simulation results, the symbols represent the experimental results ($Z_T = 0.242 \text{ m}$, $P_{t, AN} = P_{t, CA} = 1.013 \times 10^5$ Pa, T = 1273 K, air feed on the cathode).

75

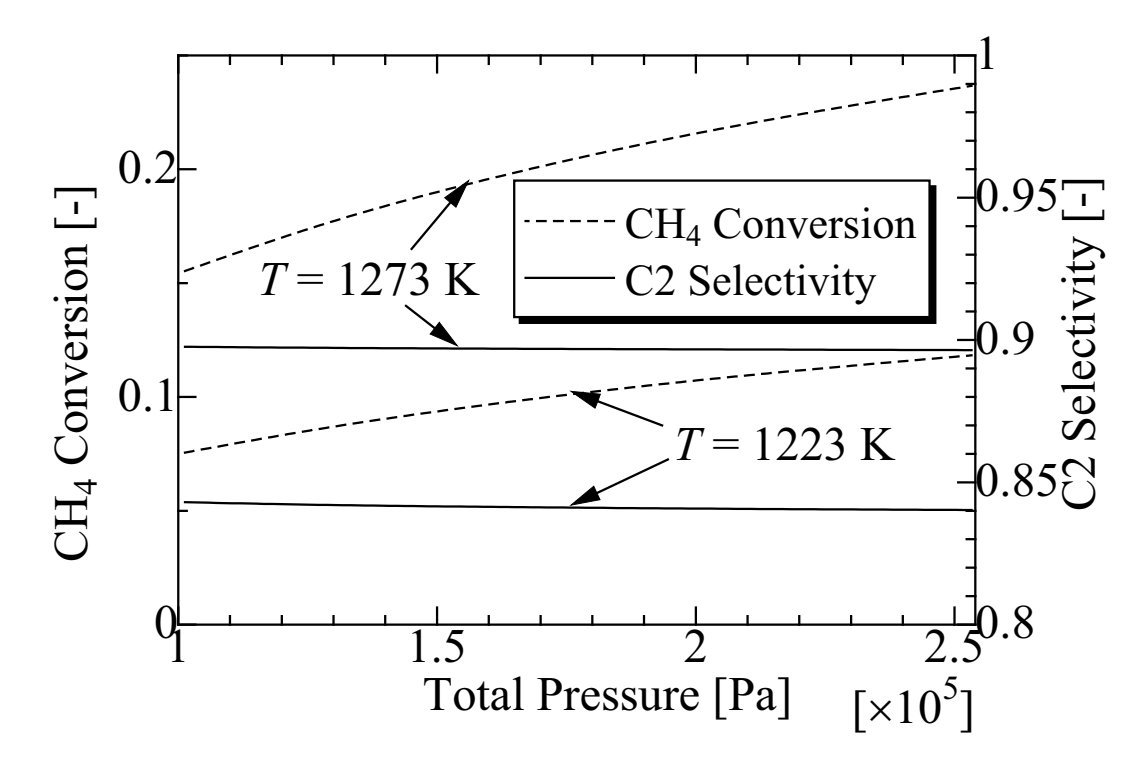


Fig. 4.6 Effect of operating pressure on methane conversion and C2 selectivity; the lines represent the simulation results ($F_{\text{CH}_4,0} = 2.0 \text{x} 10^{-4} \text{ mol s}^{-1}$, $Z_{\text{T}} = 0.242 \text{ m}$, pure methane feed on the anode, air feed on the cathode).

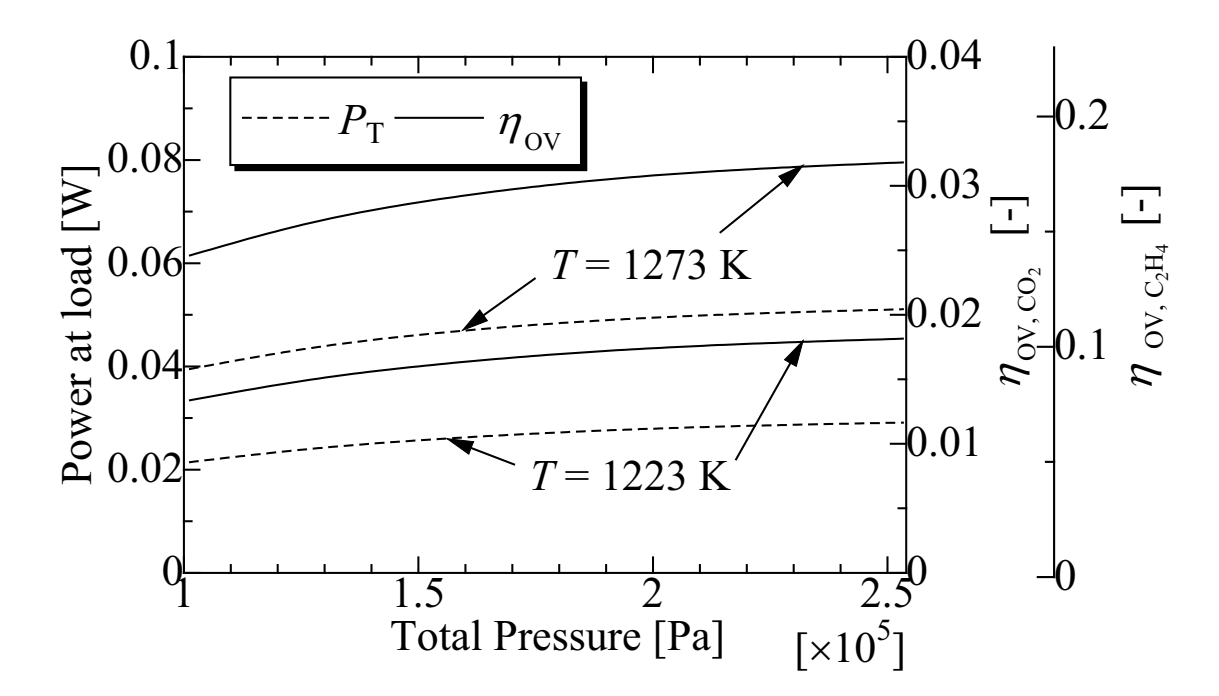


Fig. 4.7 Effect of operating pressure on power at load and overall efficiency; the lines represent the simulation results ($F_{\text{CH}_4,0} = 2.0 \text{x} 10^{-4} \text{ mol s}^{-1}$, $Z_{\text{T}} = 0.242 \text{ m}$, pure methane feed on the anode, air feed on the cathode).

Chapter 5
Comparative Study of Oxidative Coupling of Methane
Modeling in Various Types of Reactor

5.1 Introduction

The conversion of methane into other valuable hydrocarbons has significant industrial importance. Among various schemes for methane conversion, oxidative coupling of methane (OCM) to C2 hydrocarbons (ethane and ethylene) is a promising process to upgrade natural gas. After a pioneer work of Keller and Bhasin [1], there have been extensive research and development efforts in this area. However, the yield of C2 hydrocarbons achieved in a conventional fixed-bed reactor (FBR) was limited to about 25% [2, 3] due to the presence of undesired complete oxidation reactions in the gas phase and partially on the catalyst surface. An application of membrane reactor to control oxygen concentration along the reactor offers a possibility to achieve a much higher C2 hydrocarbons selectivity and yield for OCM. Santamaria and co-workers [4-7] reported that a porous ceramic membrane reactor gave a considerably better selectivity than a fixed-bed reactor (FBR); however, the improvement in C2 yield was usually small. Lin and co-workers [8] investigated the performance of OCM reaction in a conventional FBR and a mixed ionic and electronic membrane reactor (MIEMR) packed with Li/MgO catalyst. The kinetic equations over Li/MgO were obtained from their previous work [2]. It was found that the use of the MIEMR significantly improved C2 selectivity and yield. They also studied the reaction using a membrane reactor with a catalytically active membrane such as $Bi_{1.5}Y_{0.3}Sm_{0.2}$ $O_{3-\delta}$ (BYS) [9-11] and 25 mol% yttria doped bismuth oxide (BY25) [12]. It was found that the best single-pass C2 yield was achieved in BYS doping with Y and Sm membrane reactor [10]. C2 yield of 35% and C2 selectivity of 54% at 1173 K could be obtained in their system [10].

Some researchers employed a solid oxide fuel cell reactor (SOFCR) for the electrochemical selective oxidation of methane to C2 hydrocarbons [13-15]. Electric power was generated simultaneously with the selective production of C2 hydrocarbons.

In our previous papers, OCM was studied in SOFCR. Particular focuses were on catalyst preparation methods [15-18] and reactor performance test [13, 15, 19]. The fuel cell type temperature-programmed desorption (FC-TPD) technique was proposed to investigate types of oxygen species under the fuel cell operation [20]. The knowledge of oxygen species from FC-TPD [19-21] and the oxygen permeation through LSM/YSZ/LaAlO [22] were taken into account to obtain the kinetic parameters of the reactions on the anode [15]. A set of the kinetic model using two different oxygen species; i.e., oxygenate and coupling species, was useful to evaluate OCM in a tubular SOFCR. SOFCR for OCM was considered as the good reactor for C2 production although the obtained electricity was quite far from a typical SOFC [23].

Nowadays, mixed ionic and electronic conductors with high oxygen permeability have been developed, offering an opportunity for use in a membrane reactor. Perovskite-type (A,La)(Co,Fe)O_{3-δ} membranes (where A is alkaline-earth element) are among the well-known mixed conductors with highest oxygen permeability; however most of them are thermodynamically and/or dimensionally unstable under large oxygen chemical potential gradient typically encountered in membrane reactor operation conditions [24-25]. At temperatures below 1000–1070 K, the membrane performance is degraded with time. Moreover, it has a very high thermal expansion [24-25]. One alternative group of the membrane materials is a LaGaO₃-based mixed conductor with perovskite-type structure. Substitution of La with alkaline-earth cations (Sr, Ca, Ba) and Ga with bivalent cations (Mg, Ni) results

in high ionic conduction. One of the highest oxygen ionic conductor is a La(Sr)Ga (Mg) $O_{3-\delta}$ (LSGM) solid solution [25-26]. Even though the use of this conductor in MIEMR is less complicated than SOFCR, no electricity is obtained as a byproduct unlike SOFCR.

In this paper, the comparative study of the performances of various reactors for the OCM to C2 hydrocarbons was investigated by simulations. Kinetic data of Li/MgO catalyst [8] was used in FBR, PMR and MIEMR. The data on permeation rates of gases through a commercial "Membralox" membrane with 10 nm pore size [27] and "La_{0.40}Sr_{0.60}Ga_{0.40}Fe_{0.60}O_{3- δ}" mixed conductor [25] were used for modeling PMR and MIEMR, respectively. Permeation data [21] and the kinetic expressions [15] of the $La_{0.85}Sr_{0.15}MnO_3/8$ mol% Y_2O_3 - $ZrO_2/La_{1.8}Al_{0.2}O_3$ (abbreviated as LSM/YSZ/LaAlO) were used in the modeling of SOFCR.

5.2 Modelling

Fig. 5.1 (a) shows the scheme of FBR. Methane, oxygen/air and inert gas were mixed and co-fed to an impermeable tube reactor. The membrane reactors in this study are double tubular reactors as shown in Fig. 5.1 (b)-(d). The inner tube is made of a γ -alumina membrane, a $La_{0.40}Sr_{0.60}Ga_{0.40}Fe_{0.60}O_{3-\delta}$ membrane and a LSM/YSZ/LaAlO cell for PMR, MIEMR and SOFCR, respectively. The outer shell is an impermeable wall. The simulations were carried out using a reactor length of 20 cm, inner diameter of the inner tube of 1.8 cm and inner diameter of the shell tube of 4 cm.

By assuming plug flow and isothermal condition, the mass balance equation in the tube side is given as

$$\frac{d\gamma_{t,i}}{dx} = \left\{ r_{t,i} + \left(\frac{S}{W} \right) J_i \right\} \left(\frac{W}{F_{t,T0}} \right) \tag{5.1}$$

For FBR, the permeation rate of component i is zero $(J_i = 0)$ because the tube is made of an impermeable wall.

For PMR, all of component i can permeate through the membrane because the γ-alumina membrane is not highly selective. The permeation data for PMR is based on the permeation data of gases through a commercial "Membralox" membrane. The membrane consists of porous α -alumina supports and a separative layer of γ -alumina with pore size of 1×10^{-8} m and thickness of 5×10^{-6} m. Both Knudsen and viscous flow mechanisms are important and can be expressed as follows [27-28]. $J_i = \frac{a}{\sqrt{M_i T}} (P_{s,i} - P_{t,i}) + \frac{b}{2\mu T} (P_{s,i}^2 - P_{t,i}^2)$ (5.2)

$$J_{i} = \frac{a}{\sqrt{M_{i}T}} (P_{s,i} - P_{t,i}) + \frac{b}{2\mu T} (P_{s,i}^{2} - P_{t,i}^{2})$$
(5.2)

where
$$a = 2.298 \times 10^{-4}$$
 mol $K^{1/2}$ Pa⁻¹ m⁻² s⁻¹ (5.3)
 $b = 4.779 \times 10^{-14}$ mol K Pa⁻¹ m⁻² (5.4)

$$b = 4.779 \times 10^{-14}$$
 mol K Pa⁻¹ m⁻² (5.4)

The gas viscosity can be estimated by Wilke's correlation [29].

For MIEMR and SOFCR, the permeation rate of component i except oxygen is zero $(J_i = 0)$ due to the highly selective property of the membranes.

The oxygen permeation rate through the La_{0.40}Sr_{0.60}Ga_{0.40}Fe_{0.60} O_{3-δ} mixed ionic and electronic conductor with thickness (d) of 1×10^{-4} m is expressed as follows [25].

 $J_{O_2} = \frac{Per_{O_2}}{d} \ln \left(\frac{P_{s,O_2}}{P_{t,O_3}} \right)$ (5.5)

$$Per_{O_2} = 0.0645 \exp\left(\frac{-108400}{R_o T}\right)$$
 (5.6)

The $Per_{,O_2}$ of the La_{0.40}Sr_{0.60}Ga_{0.40}Fe_{0.60} O_{3- δ} membrane was determined from Fig.6 of ref. [25].

The kinetic data of Li/MgO obtained from Kao *et al.* [8] was used in the cases of FBR, PMR and MIEMR. The simulation results of FBR agree excellently with those reported in the previous work [8]. Our simulations were performed by using an all-purpose equation solver, EQUATRAN-G (Omega Simulation, Japan). The catalyst was packed in the tube. The solid density of catalyst with the size of $100-200 \, \mu m$ is about 2,022 kg m⁻³ [30]. Because the catalyst particle diameter is much smaller than the tube diameter, void fraction of 0.34 can be assumed [31].

For LSM/YSZ/LaAlO SOFCR, the rate expressions were provided in our previous work [15] and the oxygen permeation rate through the LSM/YSZ/LaAlO can be estimated from our model [22]. The thickness of the YSZ membrane was represented by 1.5×10^{-3} m in this study.

At the entrance (x = 0),
$$\gamma_{t,CH_4} = \frac{F_{t,CH_40}}{F_{t,T0}}$$
, $\gamma_i = 0$ (products)

The mass balance equation in the shell side is given as

$$\frac{d\gamma_{s,i}}{dx} = \left\{ r_{s,i} - \left(\frac{S}{V}\right) J_i \right\} \left(\frac{V}{F_{s,T0}}\right) \tag{5.7}$$

where $r_{s,i}$ is homogeneous gas phase reaction rate on the shell side [32]. The partial pressures in the tube side and the shell side can be determined as follows.

$$P_{t,i} = \frac{P_{t,T} \cdot \gamma_{t,i}}{\sum \gamma_{t,i}} \tag{5.8}$$

$$P_{s,i} = \frac{P_{s,T} \cdot \gamma_{s,i}}{\sum \gamma_{s,i}} \tag{5.9}$$

Because OCM is a highly exothermic reaction, the hot spot temperature might occur for the FBR case. Even though, the energy balance was not considered in the FBR model using Li/MgO catalyst by Kao *et al.* [8], good agreement between their simulation results and the previous experimental results could be obtained [8]. The membrane reactors can be maintained at nearly isothermal condition by distributing the oxygen feed along the reactors with excellent heat transfer characteristics. The isothermal behavior of PMR and SOFCR has already been reported in the literature [23, 33-34]. Therefore, the simulations in this study are considered isothermal and the energy balance equations are not included in this work.

It should be noted that the feed molar flow rate of methane, oxygen and inert gas are the same for FBR, PMR and MIEMR for each simulation condition. For SOFCR, the amount of catalyst is not same as the others; however, *WHSV* and methane to oxygen ratio of all simulation are fixed at 1.8x10⁻³ mol s⁻¹ kg⁻¹ and 2.0, respectively.

5.3 Results and Discussion

5.3.1 Effect of operating temperature

Fig. 5.2 shows the effect of temperature on C2 yield and selectivity of various types of reactors. Li/MgO OCM catalysts are packed in FBR, PMR and MIEMR while LaAlO is used as the anode catalyst for SOFCR. Pure methane and oxygen are fed with a molar ratio of 2.0. The temperatures of FBR, PMR and MIEMR are considered in a range of 1023-1173 K, corresponding to the validation limit of the kinetic expressions [8]. C2 yield and selectivity increase with increasing temperature for all reactors. It is obvious that both PMR and MIEMR give higher C2 yield and selectivity than FBR as expected. It should be noted that methane conversion of PMR are higher than MIEMR (the results are not shown) because of higher oxygen permeability. On the other hand, C2 selectivity of MIEMR is higher than PMR because the mixed conductor is a purely oxygen conductor in which only oxygen can permeate from the shell side to the tube side while the porous alumina membrane in PMR allows all component to permeate through it from both sides. Methane reactant was allowed to permeate through the shell side and homogeneous gas phase reactions in the shell side can take place. Considering in the tube side, the decrease of methane partial pressure in the tube side due to methane loss leads to low methane and oxygen ratio which is not favorable. Even though C2 selectivity in SOFCR dramatically increases with increasing temperature, C2 yield is very low. This suggests that SOFCR should be operated at higher temperature than the others in order to obtain enough oxygen permeability, which is nature of this electrolyte. This high temperature requirement may be the main disadvantage of SOFCR; however, the electricity which is simultaneously generated may compensate and make SOFCR still challenging. From this reason, SOFCR was simulated at higher temperature than the others in the following sections.

5.3.2 Effect of inert feed concentration

According to a viewpoint of the oxygen purification cost, air is considered to use as an oxidant in the system. Methane and oxygen feeds are kept at a mole ratio of 2.0 and *WHSV* is maintained at 1.8×10^{-3} mol s⁻¹ kg⁻¹ for all simulations. The inert mole fraction was increased from 0 to 0.55, corresponding to mole fraction of methane: oxygen: inert as 0.667:0.333:0 for pure oxygen feed and 0.3:0.15:0.55 for air feed. In the case of FBR, inert was mixed and co-fed with methane and oxygen. As shown in Fig. 5.3, the increase in the inert mole fraction does not significantly affect C2 selectivity. Even though, methane residence time increases with increasing inert feed concentration, methane conversion may not be improved because of insufficient oxygen supply, and therefore, C2 yield only slightly increases. It is worthy to note that oxygen is completely consumed within the initial part of FBR, while at the same oxygen feed flow rate, it is enough to supply along the reactor for the other membrane reactors. However, C2 selectivity and, therefore, yield may be possibly improved when using very diluent feed because the formation rate of C2 can be greater than that of CO_x [8]. For the membrane reactors, the oxygen partial pressure in the shell side is decreased with increasing inert mole fraction and thus decreases the driving force for the oxygen permeation. It results in high methane and oxygen molar ratio in the reactor side which leads to higher C2 selectivity as shown in PMR case. However, when oxygen permeation decreases, the overall reaction rate decreases. In addition, even though the residence time increases with decreasing methane feed flow rate, methane conversion may not be efficiently improved because of the significant loss of methane to the shell side in the case of PMR.

For the MIEMR case, increase in the inert mole fraction in the shell side is insignificantly affected C2 selectivity. Because no methane losses to the shell side like in the PMR, methane can be converted more completely with increasing the residence time. It results in an increase of C2 yield. The same results are also observed in the SOFCR case. However, it should be noted that SOFCR was simulated at 1273 K which is 200 K higher than the other cases.

The effect of inert feed concentration on reactor performance was extended to the case with diluted reactant in the tube side. **Fig. 5.4** shows the reactor performances at various values of inert feed concentration in the tube side.

In the PMR case, as the inert mole fraction in the tube side increases, the partial pressure of methane decreases and then C2 selectivity decreases. However, it results in reduction of methane loss to the shell side. These effects make C2 yield to be traded off and shown some optimum conditions.

For the MIEMR case, the effect of increasing of residence time which leads to higher methane conversion plays more important role than the effect of reduction of methane partial pressure which leads to the decrease of C2 selectivity. Consequently, an increase of C2 yield is obtained. Similar tendency can be observed for the SOFCR case.

5.3.3 Effect of operating pressure

Effect of total operation pressure was studied. In order to avoid cell damages, the operating pressures in both sides of the cells are maintained at the same value in the cases of MIEMR and SOFCR. The results shown in Fig. 5.5 indicate that the C2 yield increases with increasing operating pressure for all types of reactor except FBR. For the membrane reactors, as the operating pressure increases, the driving force for the oxygen permeation through the membrane increases. This tendency can be explained by the increase of oxygen partial pressure in the shell side of the reactors and also the acceleration of the reaction rate with increasing methane partial pressure. However, in the cases of FBR and PMR whose C2 selectivity strongly depends on partial pressure of methane and oxygen, C2 selectivity decreases with increasing operating pressure. C2 yield in the case of PMR shows trade off between the increase in methane conversion and the decrease in C2 selectivity with increasing operating pressure. From the results, it is suggested that operation at high pressure is obvious beneficial to the MIEMR and SOFCR; however, other considerations such as problems on seals and mechanical properties of the oxide conductor should be taken into account for operating at high pressure.

5.4 Conclusion

Oxidative coupling of methane (OCM) was simulated using plug flow reactor models in several types of reactors: i.e. fixed-bed reactor (FBR), porous membrane reactor (PMR), mixed ionic and electronic membrane reactor (MIEMR) and solid oxide fuel cell reactor (SOFCR). FBR, PMR and MIEMR were packed with Li/MgO catalyst. SOFCR used La_{0.85}Sr_{0.15}MnO₃/8mol%Y₂O₃-ZrO₂/La_{1.8}Al_{0.2}O₃ (abbreviated as LSM/YSZ/LaAlO) as cathode, electrolyte and anode, respectively. It was found that FBR was not recommended for OCM while PMR and MIEMR were suggested

when operating at temperature lower than 1150 K and higher than 1150 K, respectively. Operation at high pressure is beneficial only to MIEMR and SOFCR. The drawback of PMR is the methane loss through the non-selective porous membrane while that of SOFCR is the requirement of higher operating temperature of approximately 200 K compared to the others. However, the electricity simultaneously generated as by-product may make SOFCR still challenging.

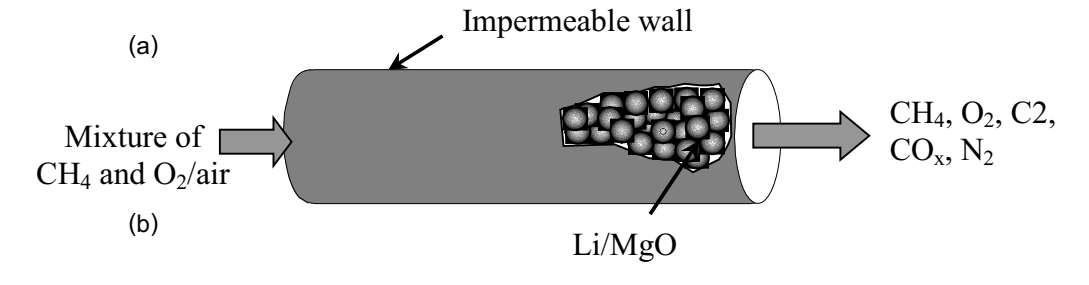
Nomenclature

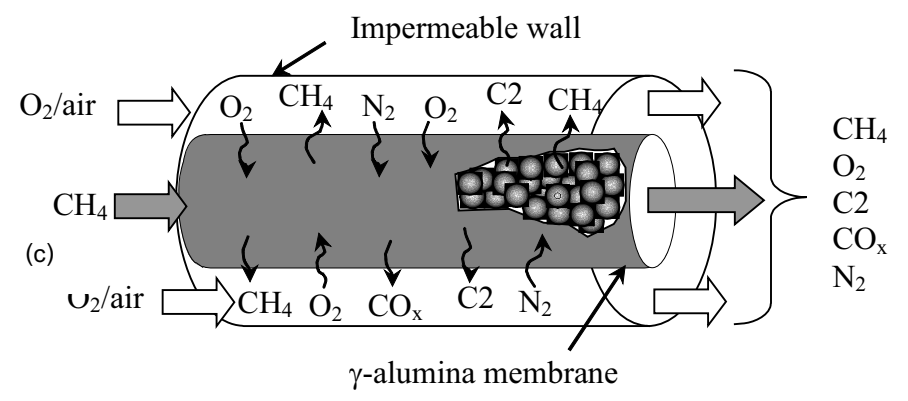
a	Knudsen parameter defined in Eq. (5.2)	$(\text{mol } K^{1/2} \text{ Pa}^{-1} \text{ m}^{-2} \text{ s}^{-1})$
b	Viscous flow parameter defined in Eq.(5.2)	1 2
d	thickness of material	(m)
F_i	molar flow rate of component i	(mol s^{-1})
j_i	molar permeation flux of component i acros	ss the membrane
	$(\text{mol m}^{-2} \text{ s}^{-1})$	
L	reactor length (m)	
M_i	molecular weight of component i	(kg mol ⁻¹)
$Per,_{{ m O}_2}$	specific oxygen permeability	$(\text{mol m}^{-1} \text{ s}^{-1})$
P_{i}	pressure of component i	(Pa)
r_i	rate of formation of component i	$(\text{mol kg}^{-1} \text{ s}^{-1})$
$rac{R_{ m g}}{S}$	gas constant, 8.314	$(J \text{ mol}^{-1} \text{ K}^{-1})$
S	membrane surface area	(m^2)
T	temperature	(K)
V	volume of reactor	(m^3)
W	mass of anode catalyst	(kg)
WHSV	weight hour space velocity	$(\text{mol s}^{-1} \text{kg}^{-1})$
X	dimensionless axial length divided by the to	tal length of reactor (-)
γ	molar flow rate ratio (= $F_i/F_{T,0}$)	(-)
<subscript></subscript>		
i	component i	
S	shell side	
t	tube side	
T	total	
0	feed	

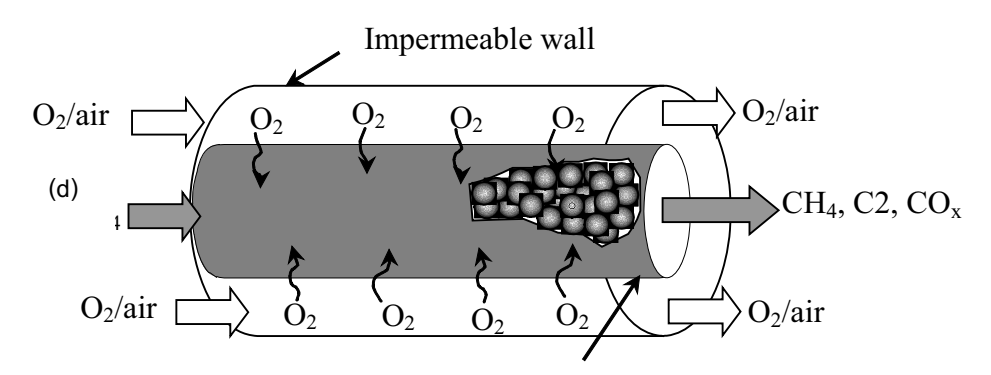
References

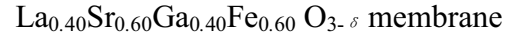
- [1] G.E. Keller, M.M. Bhasin, J. Catal. 73 (1982) 9-19.
- [2] W. Wang, Y.S. Lin, J. Memb. Sci. 103 (1995) 219-233.
- [3] J. H. Lunsford, Catal. Today 63 (2000) 165-174.
- [4] J. Coronas, M. Menendez, J. Santamaria, Chem. Eng. Sci. 49 (1994) 2015-2025.
- [5] D. Lafarga, J. Santamaria, M. Menendez, Chem. Eng. Sci. 49 (1994) 2005-2013.
- [6] J. Coronas, M. Menendez, J. Santamaria, Chem. Eng. Sci. 49 (1994) 4749-4757.
- [7] J. Herguido, D. Lafarga, M. Menendez, J. Santamaria, C. Guimon, Catal. Today., 25 (1995) 263-269.
- [8] Y.K. Kao, L. Lei, Y.S. Lin, Ind. Eng. Chem. Res. 36 (1997) 3583-3593.
- [9] F.T. Akin, Y. S. Lin, Y. Zeng, Ind. Eng. Chem. Res. 40 (2001) 5908-5916.
- [10] F.T. Akin, Y. S. Lin, AIChE. J. 48 (2002) 2298-2306.
- [11] Y. Zeng, Y. S. Lin, AIChE. J. 47 (2001) 436-444.

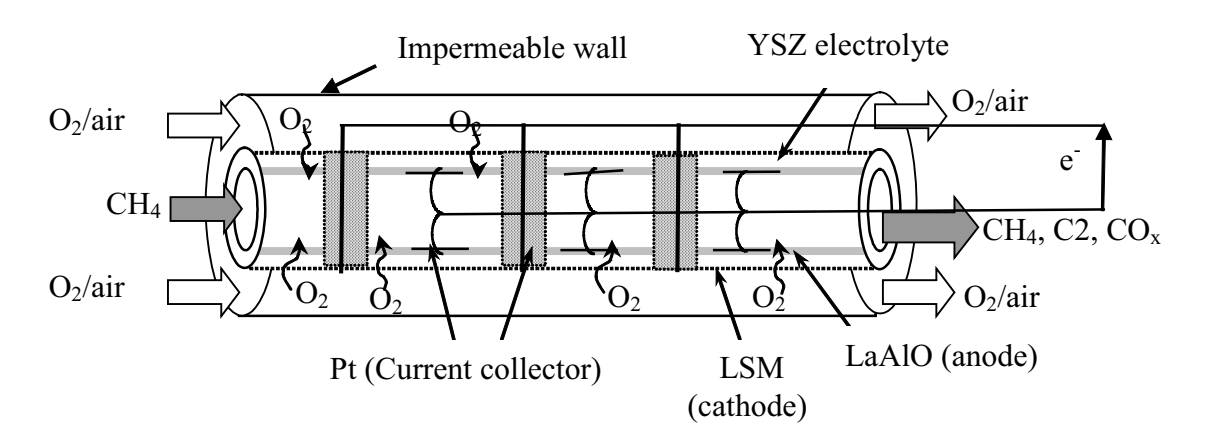
- [12] Y. Zeng, Y. S. Lin, J. Catal., 193 (2000) 58-64.
- [13] T. Tagawa, K.K. Moe, M. Ito, S. Goto, Chem. Eng. Sci. 54 (1999) 1553-1557.
- [14] X.M. Guo, K. Hidajat and C. B. Ching, Catal. Today 50 (1999) 109-116.
- [15] W. Kiatkittipong, T. Tagawa, S. Goto, S. Assabumrungrat, P. Praserthdam, J. Chem. Eng. Japan. 37 (2004) 1461-1470.
- [16] K.K. Moe, T. Tagawa, S. Goto, J. Ceram. Soc. Japan. 106 (1998) 242-247.
- [17] K.K. Moe, T. Tagawa, S. Goto, J. Ceram. Soc. Japan. 106 (1998) 754-758.
- [18] A.S. Carrillo, T. Tagawa, S. Goto, Mater. Res. Bull. 36 (2001) 1017-1027.
- [19] T. Tagawa, K.K. Moe, T. Hiramatsu, S. Goto, Solid State Ionics 106 (1998) 227-235.
- [20] W. Kiatkittipong, T. Tagawa, S. Goto, S. Assabumrungrat, P. Praserthdam, Solid State Ionics 166 (2004) 127-136.
- [21] T. Tagawa, K. Kuroyanagi, S. Goto, S. Assabumrungrat, P. Praserthdam, Chem. Eng. J. 93 (2003) 3-9.
- [22] W. Kiatkittipong, T. Tagawa, S. Goto, S. Assabumrungrat, P. Praserthdam, Chem. Eng. J., 106 (2005) 35-42.
- [23] W., Kiatkittipong, S. Goto, T. Tagawa, S. Assabumrungrat, P. Praserthdam (2005) (submitted to J. Chem. Eng. Japan.)
- [24] V.V. Kharton, A.A. Yaremchenko, A.V. Kovalevsky, A.P. Viskup, E.N. Naumovich, P.F. Kerko, J. Memb. Sci. 163 (1999) 307-317.
- [25] A.L., Shaula, A.A. Yaremchenko, V.V. Kharton, D.I. Logvinovich, E.N. Naumovich, A.V. Kovalevsky, J.R. Frade, F.M.B. Marques, J. Memb. Sci. 221 (2003) 69-77.
- [26] T. Ishihara, H. Matsuda, Y. Takita, Solid State Ionics 79 (1995) 147-151.
- [27] S. Assabumrungrat, D.A. White, Chem. Eng. Sci. 51 (1996) 5241-5250.
- [28] Assabumrungrat, S. "Mechanisms and Modelling of Gas separations Through Ceramic Membrane in Chemical Reaction Processes" Ph.D. Thesis, London (1996).
- [29] Bird, R.B., W.E. Steward, E.N. Lightfoot, Transport Phenomena, Wiley, New York, 1960.
- [30] E. Marco, A. Santos, M. Menendez, J. Santamaria, Powder Tech. 92 (1997) 47-52.
- [31] McCabe, W.L., J.C. Smith, P. Harriott, Unit Operations of Chemical Engineering, McGraw-Hill, Singapore, 2001.
- [32] G.S. Lane, E.E. Wolf, J. Catal., 113 (1988) 144-163.
- [33] Y.K., Kao, L. Lei, Y.S. Lin, Catal. Today 82 (2003) 255-273.
- [34] P. Costamagna, A. Selimovic, M. D. Borghi, G. Agnew, Chem. Eng. J. 102 (2004) 61–69.











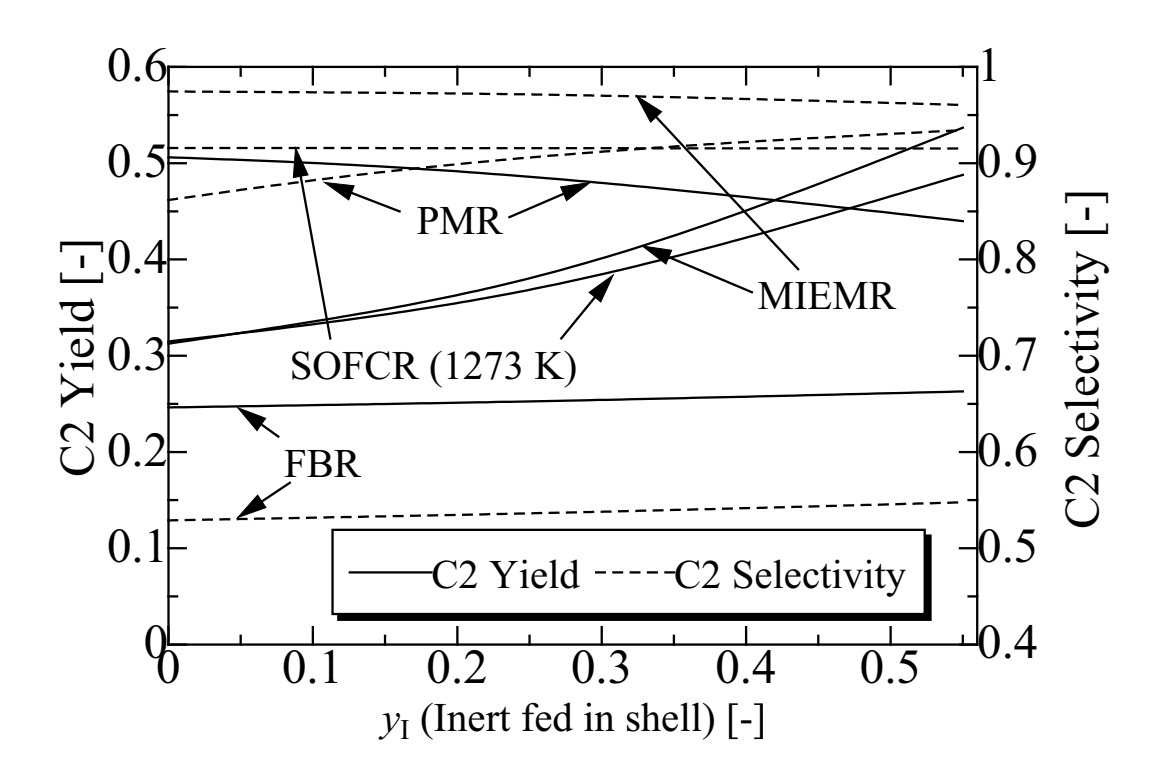


Fig. 5.1 Proposed schemes for various OCM reactors: (a) FBR (b) PMR (c) MIEMR and (d) SOFCR.

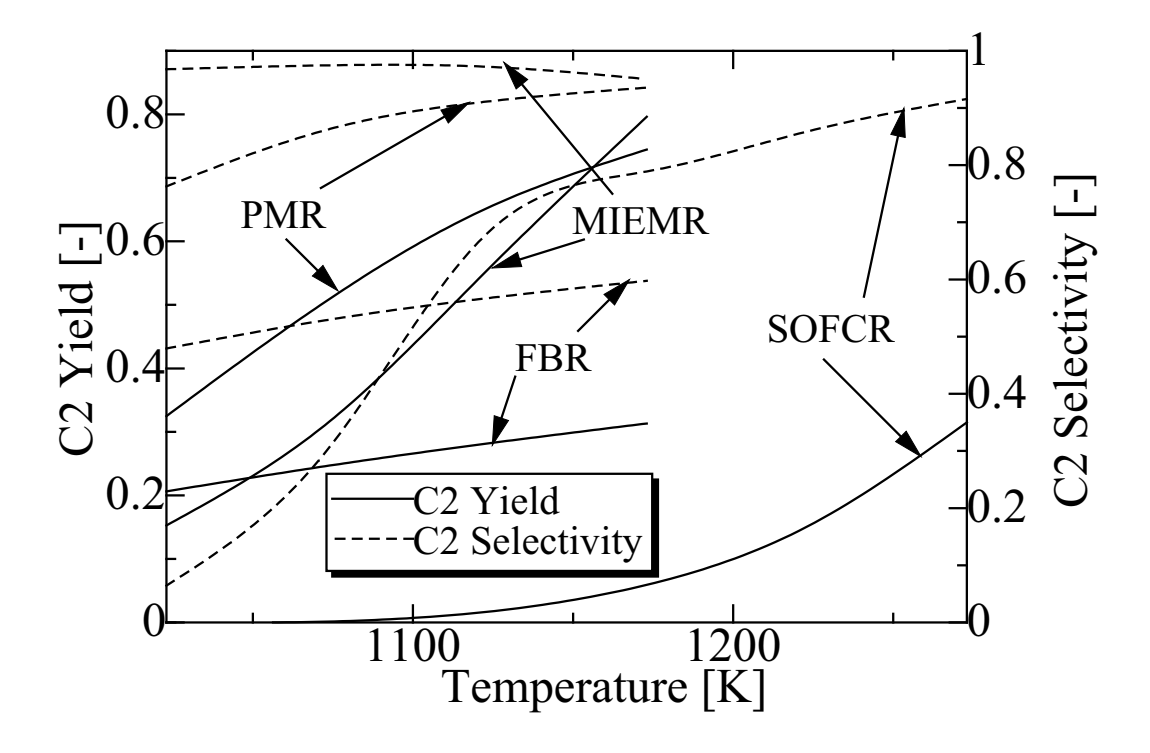


Fig. 5.2 Effect of temperature on C2 yield and selectivity for various types of reactor $(y_I = 0, WHSV = 1.8 \times 10^{-3} \text{ mol s}^{-1} \text{ kg}^{-1}, L = 0.2 \text{ m and } P_{t,T} = P_{s,T} = 1.013 \times 10^{5} \text{ Pa}).$

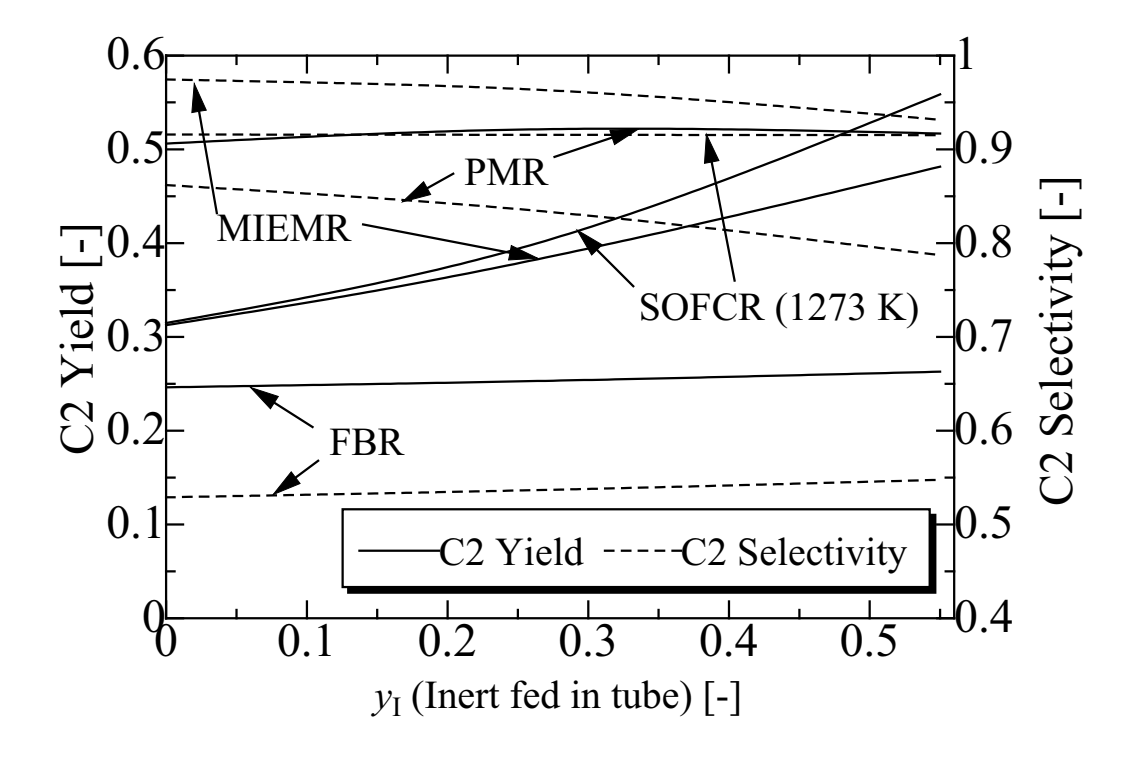
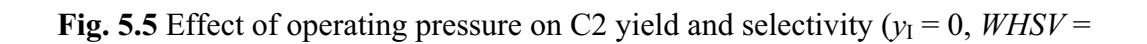
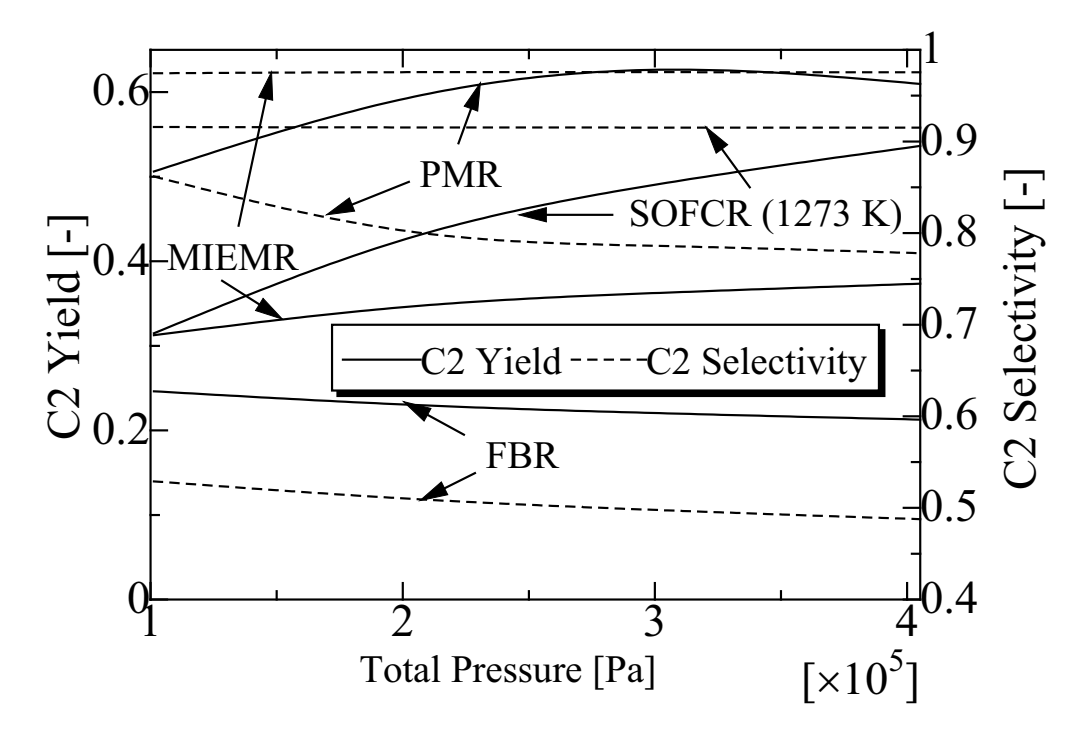


Fig. 5.3 Effect of inert mole fraction in shell side on C2 yield and selectivity for various types of reactor ($WHSV = 1.8 \times 10^{-3} \text{ mol s}^{-1} \text{ kg}^{-1}$, L = 0.2 m, $P_{t,T} = P_{s,T} = 1.013 \times 10^{5} \text{ Pa}$, T = 1073 K for FBR, PMR and MIEMR, and T = 1273 K for SOFCR).

Fig. 5.4 Effect of inert mole fraction in tube side on C2 yield and selectivity for various types of reactor ($WHSV = 1.8 \times 10^{-3} \text{ mol s}^{-1} \text{ kg}^{-1}$, L = 0.2 m, $P_{t,T} = P_{s,T} = 1.013 \times 10^{5} \text{ Pa}$, T = 1073 K for FBR, PMR and MIEMR, and T = 1273 K for SOFCR).





 1.8×10^{-3} mol s⁻¹ kg⁻¹, L = 0.2 m, T = 1073 K for FBR, PMR and MIEMR, and T = 1273 K for SOFCR).

Summary of Research Outputs

International Paper

- 1) Worapon Kiatkittipong, Tomohiko Tagawa, Shigeo Goto, Suttichai Assabumrungrat and Piyasan Praserthdam "TPD study in LSM/YSZ/LaAlO system for the use of fuel cell type reactor" Solid State Ionics, 166 (1-2), 15 January 2004, 127-136 (Impact Factor-2004 = 1.862).
- 2) Worapon Kiatkittipong, Tomohiko Tagawa, Shigeo Goto, Suttichai Assabumrungrat and Piyasan Praserthdam "Oxidative Coupling of Methane in LSM/YSZ/LaAlO SOFC Reactor" Journal of Chemical Engineering of Japan, 37 (12) (2004) 1461-1470 (Impact Factor-2004 = 0.515).
- 3) Worapon Kiatkittipong, Tomohiko Tagawa, Shigeo Goto, Suttichai Assabumrungrat and Piyasan Praserthdam "Oxygen transport through LSM/YSZ/LaAlO system for the use of fuel cell type reactor" Chemical Engineering Journal, 106 (1) (2005), 35-42 (Impact Factor-2004 = 1.383).
- 4) Worapon Kiatkittipong, Tomohiko Tagawa, Shigeo Goto, Suttichai Assabumrungrat and Piyasan Praserthdam "Simulation of Oxidative Coupling of Methane in Solid Oxide Fuel Cell Type Reactor for C2 Hydrocarbon and Electricity Co-Generation" Journal of Chemical Engineering of Japan, in press (Impact Factor-2004 = 0.515).
- 5) Worapon Kiatkittipong, Tomohiko Tagawa, Shigeo Goto Suttichai Assabumrungrat and Piyasan Praserthdam "Comparative Study of Oxidative Coupling of Methane Modeling in Various Types of Reactor" Chemical Engineering Journal, under revision (Impact Factor-2004 = 1.383).

International Conferences

- 1) Kampol Silpasup, Pattanawit Preechasanongkit, Suttichai Assabumrungrat, Worapon Kiatkittipong, Piyasan Praserthdam, Tomohiko Tagawa and Shigeo Goto "Effect of metal composition of Sm_{2-x}Al_xO anode catalysts for SOFC reactors" Regional Symposium on Chemical Engineering (RSCE) 2002 In conjunction with 16th Symposium of Malaysian Chemical Engineers (SOMChE) Kuala Lumpur, MALAYSIA 28-30th October 2002 (oral presentation)
- 2) Worapon Kiatkittipong, Tomohiko Tagawa, Shigeo Goto, Suttichai Assabumrungrat and Piyasan Praserthdam "Oxygen Transport Through LSM/YSZ/LaAlO System for Use of Fuel Cell Type Reactor" APCChE 2004, Kitakyushu, Japan, October 17-21, 2004. (poster presentation)
- 3) W. Kiatkittipong, S. Goto, T. Tagawa, S. Assabumrungrat and P. Praserthdam "SCALE-UP SIMULATION OF LSM/YSZ/LaAlO SOFC REACTOR FOR OXIDATIVE COUPLING OF METHANE" Regional Symposium on Chemical Engineering (RSCE 2004), Bangkok, December 1 3, 2004 (oral presentation).
- 4) Worapon Kiatkittipong, Tomohiko Tagawa, Shigeo Goto, Suttichai Assabumrungrat and Piyasan Praserthdam "SIMULATION OF OXIDATIVE COUPLING OF METHANE IN SOLID OXIDE FUEL CELL TYPE REACTOR FOR C2 HYDROCARBONS AND ELECTRICITY CO-GENERATION" 5th International Symposium on Catalysis in Multiphase Reactors (CAMURE-5) & 4th International Symposium on Multifunctional Reactors (ISMR-4), Slovenia, June 15-18, 2005 (poster presentation).

Graduate students

PhD graduate
1. Dr. Worapon Kiatkittipong

MEng graduate 2. Mr. Kampol Silpasup

Appendix A
Manuscript "TPD study in LSM/YSZ/LaAlO system for the
use of fuel cell type reactor"



Available online at www.sciencedirect.com



Solid State Ionics 166 (2004) 127-136



TPD study in LSM/YSZ/LaAlO system for the use of fuel cell type reactor

Worapon Kiatkittipong ^{a,1}, Tomohiko Tagawa ^{b,*}, Shigeo Goto ^b, Suttichai Assabumrungrat ^a, Piyasan Praserthdam ^a

 *Center of Excellence on Catalysis and Catalytic Reaction Engineering, Department of Chemical Engineering, Chulalongkorn University, Bangkok 10330, Thailand
 *Department of Chemical Engineering, Nagoya University, Chikusa, Nagoya 464-8603, Japan

Received 26 August 2003; received in revised form 10 October 2003; accepted 31 October 2003

Abstract

Behaviors of oxygen species in the LSM/YSZ/LaAlO SOFC type reactor were investigated. The fuel cell type temperature-programmed desorption (FC-TPD) measurements were employed in three operating modes; i.e. (1) open circuit, (2) closed circuit without applied potential and (3) closed circuit with applied potential modes. Various pretreatment conditions, i.e. (a) open circuit, (b) closed circuit without applied potential and (c) closed circuit with applied potential, were investigated. The FC-TPD technique enables to discuss the oxygen species responsible for a combustion reaction and those for a coupling reaction, separately. The open circuit type FC-TPD showed that the applied potential during the pretreatment caused the increase in the amount of surface oxygen and the decrease in activation energy of desorption of oxygen at the anode catalyst. The closed circuit FC-TPD provided the combined effects of desorption and permeation. In addition, the FC-TPD analysis could correlate the behavior of adsorbed oxygen species to the NEMCA effect observed in the oxidative coupling of methane in the SOFC reactor.

© 2003 Elsevier B.V. All rights reserved.

PACS: 84.60.D: Fuel cell

Keywords: Solid oxide fuel cell; Oxygen permeation; Temperature-programmed desorption; NEMCA

1. Introduction

Solid oxide fuel cell (SOFC) is a promising energy-conversion technology for future application [1,2]. In our previous papers, the SOFC system was applied as a selective oxidation reactor for chemicals-energy co-generation [3–9]. In these studies, the oxidative coupling of methane to ethane and ethylene was studied. The solid electrolyte is used as an oxygen separator and an oxygen distributor to achieve high C2 selectivity. In this electro-catalytic system, combined effects of activation of oxygen on an anode and permeation of oxygen through the electrolyte control the

performance of reactor. A number of reviews were published on this topic [10-12].

The use of external potential is also of recent interest. Special attention has been focused on the effect of non-Faradaic electrochemical modification of catalytic activity (NEMCA) [13,14] observed for a wide range of reactions in the presence of metals such as Pt, Pd, Rh, Au, Ag and Ni, and those of oxides such as IrO₂ and RuO₂. Conventional solid electrolytes used in most studies are O²⁻ conductors like YSZ [15–17] or CeO₂ [18].

Temperature-programmed desorption (TPD) technique is usually used to investigate behaviors of oxygen species on the selective oxidation catalyst by detecting gas phase oxygen desorbed from pretreated oxide surface with increasing temperature of the sample oxide. However, very limited studies on TPD in SOFC reactor are reported. Tsiplakides et al. [16] investigated oxygen TPD on metal electrode (e.g. Pt and Ag) deposited on YSZ. Two oxygen

0167-2738/S - see front matter © 2003 Elsevier B.V. All rights reserved. doi:10.1016/j.ssi.2003.10.018

^{*} Corresponding author. Tel./fax: +81-52-789-3388.

E-mail address: tagawa@nuce.nagoya-u.ac.jp (T. Tagawa).

1 Nagoya University Program For Academic Exchange (NUPACE)-

¹ Nagoya University Program For Academic Exchange (NUPACE)-PhD student supported by AIEJ.

adsorption states, i.e. strongly bonded anionic oxygen and weakly bonded atomic oxygen, were generated by applied potential [16]. Baker et al. [19] studied TPD in system of solid oxide fuel cell by using CaO-stabilized zirconia (CSZ) tube as a solid oxide electrolyte and Ag as a cathode. Two anode systems were used, La_{0.8}Ca_{0.2}Cr_{0.9} Co_{0.1}O₃ with Au current collector and Au alone. A new low-temperature desorption peak was electrochemically generated [19]. The formation of new oxygen species, at lower desorption temperature, under electrochemical oxygen pumping conditions were observed in both cases [16,19].

As a tool for designing anode catalysts for the oxidative coupling of methane in the SOFC reactor, the conventional TPD technique has been successfully applied [5]. A novel fuel cell type temperature-programmed desorption (FC-TPD) was proposed and proved to be a very useful tool for characterization of the SOFC type reactors [8]. In the same report [8], the effect of applied potential on reactivity was also investigated. The change in the selectivity with applied potential, when the selective oxidation catalyst was employed as the anode with a pre-mixed feed of air and methane, gave a new aspect to the NEMCA phenomena. In this study, unsteady state experiments with FC-TPD technique on open circuit,

closed circuit with and without applied potential were conducted and the reactivity of oxygen species was correlated to surface active sites.

2. Experimental

2.1. Apparatus

Fuel cell type temperature-programmed desorption (FC-TPD) experiments were carried out using an apparatus illustrated in Fig. 1. A tube-type YSZ membrane (8 mol% Y_2O_3 , thickness = 1.5 mm, inside diameter = 18 mm, outside diameter = 21 mm, length = 500 mm, effective surface area = 0.0148 m²) was used as an electrolyte. La_{1.8}Al_{0.2}O₃ (abbreviated as LaAlO) prepared by a mist decomposition method was used as an anode catalyst on the inner surface of the tube while La_{0.85}Sr_{0.15}MnO₃ (abbreviated as LSM) prepared by a conventional paste method on the outer side was used as the cathode.

Details of the electrode preparation methods were described elsewhere [3,6,7]. Platinum wire was connected to platinum meshes placed on both electrode surfaces to serve as current collectors. The outlet gas from the anode side was directly connected to a thermal conductivity detector (TCD).

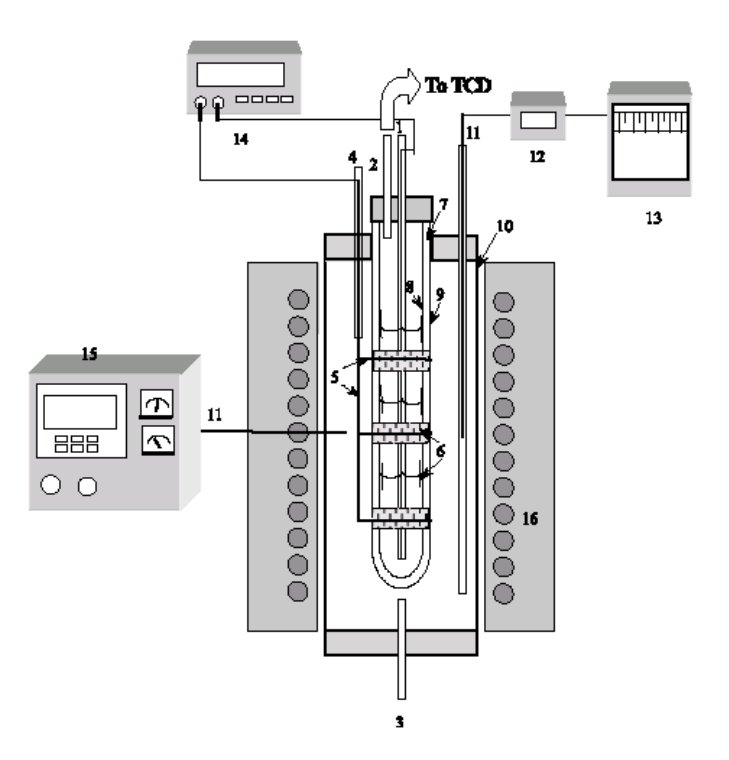


Fig. 1. Schematic diagram of the solid oxide fuel cell type reactor. (1) Anode side feed (air/He). (2) Exit gas from anode side. (3) Cathode side feed (O₂). (4) Exit gas from cathode side. (5) Platinum wire. (6) Platinum mesh. (7) YSZ tube. (8) Anode (LaAlO). (9) Cathode (LSM). (10) Quartz tube. (11) Thermocouple. (12) Temperature indicator. (13) Temperature recorder. (14) Ammeter/voltmeter/potentiostat. (15) Temperature controller. (16) Furnace.

A potentiostat was used to supply an external electrical potential to the system. Oxygen transport from the cathode side to the anode was promoted under the applied positive potential.

2.2. Fuel cell type temperature-programmed desorption (FC-TPD) measurement

Before the FC-TPD measurement, the cell was pretreated under the following condition: the air flow rate in the anode= 1.36×10^{-5} mol s⁻¹, the oxygen flow rate in

the cathode = 1.02×10^{-5} mol s⁻¹ and T=1273 K (the same as the standard maximum temperature of TPD measurements to avoid the phase change or destruction of YSZ due to the removal of lattice oxygen). Three modes of pretreatment, i.e. open circuit pretreatment, closed circuit pretreatment and closed circuit pretreatment with applied potential ($V_{\rm P}$), were considered in this study. After the pretreatment for 7 h, the sample was slowly cooled down to T=600 K at a rate of 0.093 K s⁻¹ under the pretreatment gases. Then, the anode gas was switched to helium carrier gas $(1.36 \times 10^{-5} \text{ mol s}^{-1})$ while the

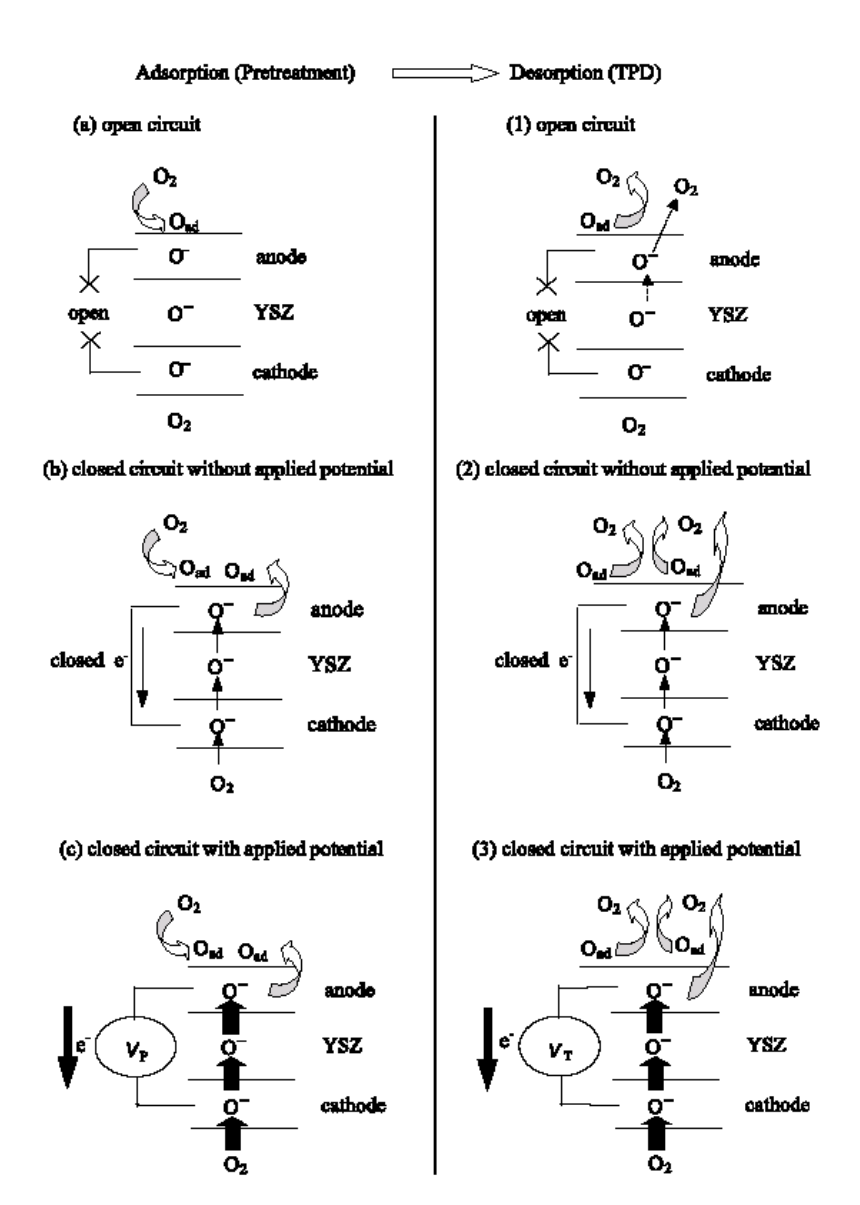


Fig. 2. Proposed scheme for adsorption and desorption of oxygen on the anode of fuel cell system.

Table 1 Summary of FC-TPD experiments

Case no.	Pretreatment condition, V_P	Operating type of FC-TPD, V_T	
1	(a) open circuit	(1) open circuit	see Section 3.2.1
2	(b) closed circuit, 0 V	(1) open circuit	see Section 3.2.1
3	(c) closed circuit, 1 V	(1) open circuit	see Section 3.2.1
4	(c) closed circuit, 2 V	(1) open circuit	see Section 3.2.1
5	(a) open circuit	(2) closed circuit, 0 V	see Section 3.2.2
6	(b) closed circuit, 0 V	(2) closed circuit, 0 V	see Section 3.2.2
7	(c) closed circuit, 2 V	(2) closed circuit, 0 V	see Section 3,2,2
8	(a) open circuit	(3) closed circuit, 1 V	see Section 3.2.3

cathode gas remained unchanged. The applied potential (V_P) was disconnected for the closed circuit pretreatment. The anode exit gas was analyzed using the TCD. After the baseline was stabilized, the FC-TPD measurement was started by increasing the temperature at a desired rate (β =0.05, 0.083, 0.117 and 0.133 K s⁻¹). The rate of temperature increase (β) was determined within the range of good reproducibility of TPD spectra. With these β values, no apparent peak widening which disturbed the analysis was observed. Oxygen spectra were recorded by the TCD. There were three modes of FC-TPD measurement, i.e. open circuit FC-TPD, closed circuit FC-TPD, and closed circuit FC-TPD with applied potential. In the closed circuit mode, both electrodes were connected to allow oxygen permeation

from the cathode to the anode. An external potential $(V_{\rm T})$ can be supplied to the cell by the potentiostat during the closed circuit mode.

3. Results and discussion

3.1. FC-TPD experiment and proposed schemes for oxygen adsorption and desorption

Desorption of oxygen from a fuel cell unit was continuously observed under the constant rate of temperature increase (β) with helium flow at the anode side. Three kinds of TPD operation were conducted after three kinds of pretreatment. Proposed scheme for adsorption and desorption of oxygen on the anode of fuel cell system is summarized in Fig. 2. For open circuit pretreatment, since the circuit is not connected, there is no oxygen permeation from the cathode side to the anode side. Oxygen adsorbed on the anode is from air feed stream at the anode side as shown in Fig. 2-(a). However, a negligible amount of thermal migrations of oxygen ions through the solid electrolyte could occur at the high temperature condition.

When the circuit is closed during the pretreatment, the permeation of oxygen species is also allowed. Therefore, the closed circuit pretreatment provides the combined effect of oxygen adsorption from the surface and the permeation through the electrolyte as shown in Fig. 2-(b). Especially, for the pretreatment under applied potential, it is expected that the amount and quality of the adsorption site should be altered as shown in Fig. 2-(c).

Fig. 2-(1) shows the open circuit FC-TPD where surface oxygen species on the anode desorb without permeation.

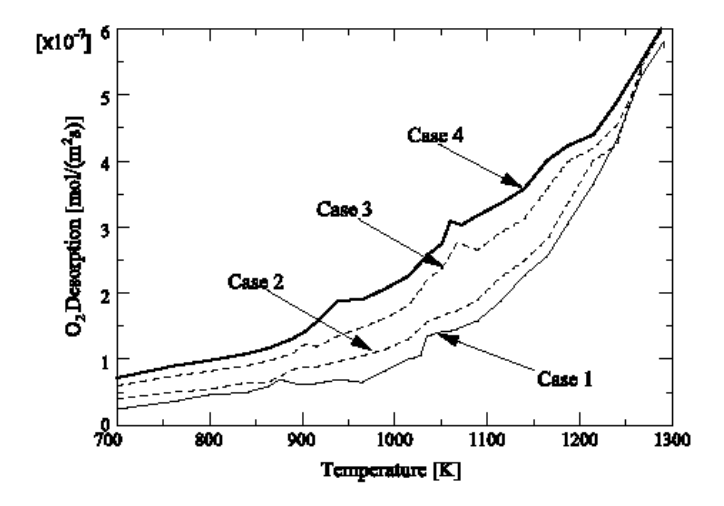


Fig. 3. Effect of pretreatment condition on the open circuit FC-TPD results ($\beta = 0.117 \text{ K s}^{-1}$).

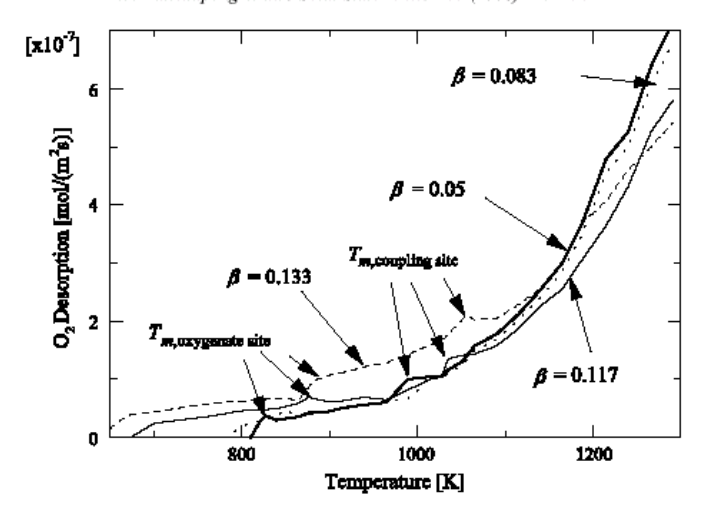


Fig. 4. Effect of rate of temperature increase (β) on the results of the open circuit FC-TPD with the open circuit pretreatment (case 1).

The dotted line with arrow shows a possibility that a small amount of oxygen in YSZ desorbs at high temperature. When the circuit is closed, the permeation of oxygen is also possible in addition to desorption of surface oxygen as shown in Fig. 2-(2). For the closed circuit FC-TPD under applied potential, the rate of oxygen permeation should be promoted with the driving force of applied potential as shown in Fig. 2-(3).

Table 1 lists the FC-TPD experiments (cases 1-8) at various operating modes of FC-TPD ((1)-(3) in Fig. 2) and pretreatment conditions ((a)-(c) in Fig. 2).

3.2. Temperature-programmed desorption results

3.2.1. Open circuit FC-TPD

Open circuit FC-TPD measurements were carried out to investigate the nature of adsorbed oxygen on the anode catalyst of the fuel cell system (LSM/YSZ/LaAlO). Since the circuit was not connected, there was no oxygen permeation from the cathode side to the anode side. Therefore, the observed spectra are arisen from oxygen desorbed from the anode and the electrolyte as shown in Fig. 2-(1). Fig. 3 shows the effect of external applied

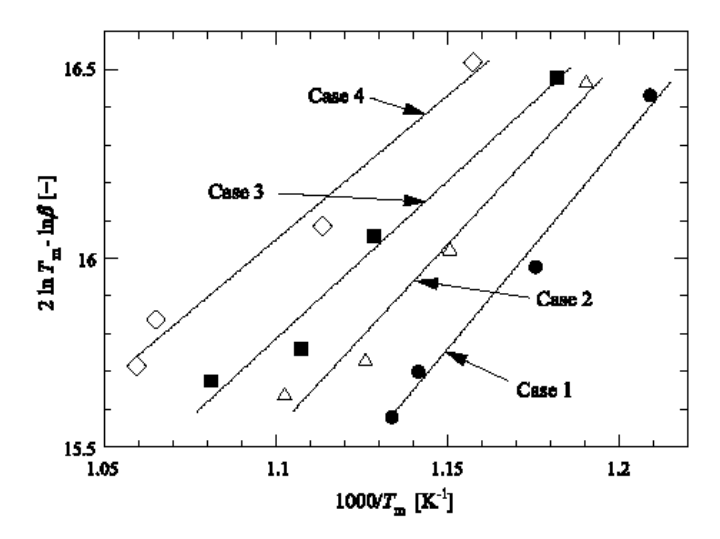


Fig. 5. Plots of $(2\ln T_{\rm m} - \ln \beta)$ against $1/T_{\rm m}$ for oxygenate site in the open circuit FC-TPD mode.

potential during the pretreatment on the FC-TPD spectra. The pretreatment conditions included the open circuit pretreatment, Fig. 2-(a) (case 1), the closed circuit pretreatment, Fig. 2-(b) (case 2) and the closed circuit pretreatment with external applied potential, Fig. 2-(c), $V_P = 1 \text{ V}$ (case 3) and 2 V (case 4). It is noted that an internal potential, which corresponded to electromotive force of concentration cell conditions, existed even if no external potential was applied $(V_P = 0 \text{ V})$ during the pretreatment. These values for the open circuit (case 1) and closed circuit pretreatment (case 2) at 1273 K were as high as 197 and 189 mV, respectively. These internal potentials at 1273 K were not changed during the pretreatment. It was found that the increase of the applied potential during the pretreatment increased the amount of desorbed oxygen especially at temperature lower than 1250 K. This suggests that the applied potential can activate the ability of the anode material (LaAlO) on oxygen adsorption.

In our previous TPD study of the anode powder [5], it was proposed that the oxygen species desorbed at low temperature (below 1000 K) were active for CO and CO₂ formation (oxygenate site) while the oxygen species desorbed at higher temperature (above 1000 K) were active for oxidative coupling of methane to C2-hydrocarbon (coupling site). In Fig. 2 of Ref. [8], TPD of powder LaAlO sample before deposition on YSZ was reported. The result shows two peaks at 930 and 1120 K, corresponding to two peaks shown in Fig. 3. By performing the FC-TPD experiment with different values of temperature increase, the behavior of these two oxygen species can be revealed.

Fig. 4 shows the effect of rate of temperature increase (β) on oxygen desorption in the open circuit mode for case 1 (open circuit FC-TPD with open circuit pretreat-

Table 2
Summary of activation energy of desorption at different levels of applied potential pretreatment condition from the open circuit FC-TPD measurements (cases 1-4)

Case no.	Oxygenate site		Coupling site	
	$A (s^{-1})$	$E_{\rm d}$ (kJ mol ⁻¹)	$A (s^{-1})$	$E_{\mathbf{d}}$ (kJ mol ⁻¹)
1	24.7	90	31.64	111
2	4.86	81	5.62	99
3	0.67	69	1.55	90
4	0.21	63	0.32	78

ment). It was found that the temperatures for maximum amount of desorbed oxygen $(T_{\rm m})$ of oxygenate site and coupling site are shifted to higher temperature with the increasing β . According to Cvetanovic and Amenomiya [20], the activation energy of desorption $(E_{\rm d})$ from TPD data with different β can be estimated by the following equation.

$$2\ln T_{\rm m} - \ln(\beta) = \frac{E_{\rm d}}{R_{\rm g}T_{\rm m}} + \ln \frac{E_{\rm d}}{AR_{\rm g}} \tag{1}$$

With low rate of temperature increase (β), the operation time to a constant temperature increased and the intensity of oxygen at low temperatures became too low to be detected with our TCD. This suggested that a limited amount of oxygen species were desorbed between 700 and 800 K.

Figs. 5 and 6 show the plot of Eq. (1) for the oxygenate site and the coupling site, respectively.

The values of the activation energy of desorption for both sites are summarized in Table 2. It was found that the activation energy of desorption decreases with increasing applied potential during the pretreatment for both

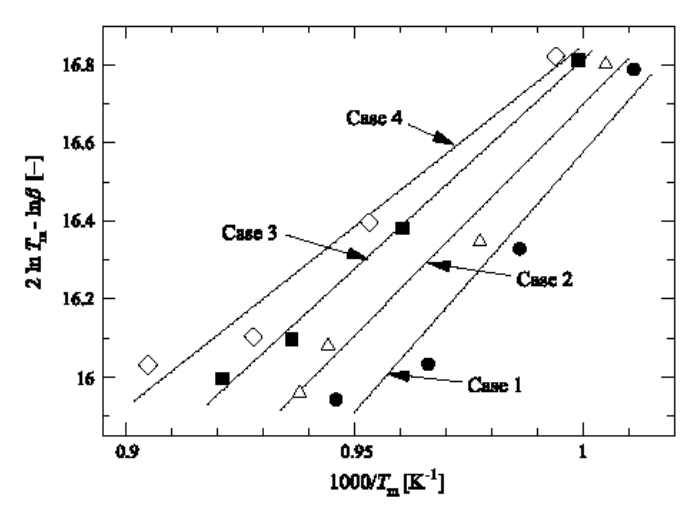


Fig. 6. Plots of $(2\ln T_m - \ln \beta)$ against $1/T_m$ for coupling site in the open circuit FC-TPD mode.

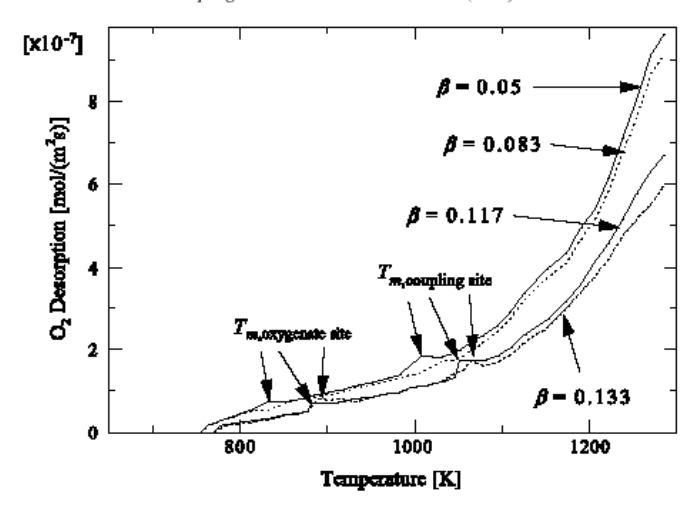


Fig. 7. Effect of rate of temperature increase (β) on the results of the closed circuit FC-TPD with the open circuit pretreatment (case 5).

sites, suggesting the qualitative change of adsorption site with the electrostatic field. Tsiplakides et al. [16] and Neophytides and Vayenas [21] also reported the changes in activation energy of oxygen desorption with applied potential on metal electrodes in the electrochemical system. They also pointed out the importance of these phenomena to understand NEMCA effect. Pacchioni et al. [22] suggested that this decrease in activation energy was largely due to electrostatic effected by considering interaction between the field induced by the ions and the polar metal—oxygen bond from their quantum chemical calculations. Vayenas et al. [23] also suggested the back spillover mechanism on Pt electrode supported on YSZ

from their STM study. These discussions on precious metal surface could be applied to oxide electrode surface in this study to explain the decrease of activation energy of desorption with applied potential during pretreatment. The electrostatic effects arranged the active site to reduce metal—oxygen bonding even in the case of oxide type catalysts. Assuming that the transfer or adsorption of oxygen on these sites was possible during the pretreatment, results in Table 2 (open circuit FC-TPD) suggested that the oxygen species adsorbed on these arranged site kept the weak metal ion—oxygen bonding after the electrostatic field was removed. Further studies are needed to discuss in more details. The activation energy of the

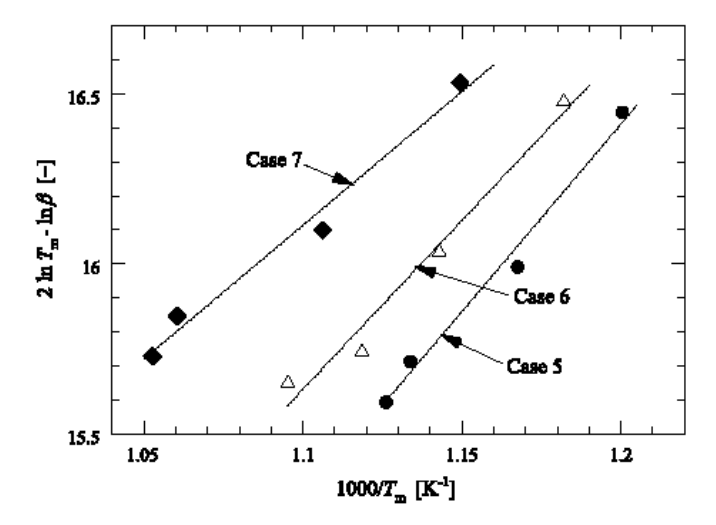


Fig. 8. Plots of $(2 \ln T_{\rm m} - \ln \beta)$ against $1/T_{\rm m}$ for oxygenate site in the closed circuit FC-TPD mode.

steady state oxygen permeation from preliminary experiments is 170 kJ mol⁻¹ which is higher than the activation energy of desorption of adsorbed oxygen (E_d) obtained from this study.

3.2.2. Closed circuit FC-TPD

When the circuit is closed during the FC-TPD experiment, the permeation of oxygen species is also allowed. Therefore, the closed circuit FC-TPD mode provides the combined effect of oxygen desorption from the surface and oxygen permeation through the electrolyte as shown in Fig. 2-(2). The rate of temperature increase (β) was varied to obtain the activation energy. Fig. 7 shows the effect of rate of temperature increase (β) on total oxygen desorption in the closed circuit mode with the open circuit pretreatment (case 5). In spite that $V_T = 0$ V in the cases of 5-7, an internal potential as high as concentration cell existed during TPD operation. The value is estimated as high as 225 mV from steady state permeation experiments. Two peaks similar to those observed in the open circuit mode are found in this case. Oxygen desorption increases with decrease of β . This may be due to the effect of oxygen permeation through cell system. Figs. 8 and 9 show plots of Eq. (1) for the oxygenate site and the coupling site, respectively.

The values of the activation energy for both sites are summarized in Table 3. Similar to the open circuit FC-TPD, the activation energy decreases with increasing applied potential during pretreatment for both sites. This also suggests the qualitative change of adsorption site with the electrostatic field. The activation energies of the oxygenate site with the open circuit and closed circuit operation modes are almost the same. On the other hand, the activation

Table 3
Summary of activation energy at different levels of applied potential pretreatment condition from the closed circuit FC-TPD measurements (cases 5 = 7)

Case no.	Oxygenate site		Coupling site	
	A (s ⁻¹)	$E_{\mathbf{d}}$ (kJ mol ⁻¹)	A (s ⁻¹)	$E_{\mathbf{d}}$ (kJ mol ⁻¹)
5	0.46	92	14.49	140
6	0.09	83	0.48	112
7	4.47×10^{-3}	65	0.03	93

energy of the coupling site from the closed circuit mode is much higher than that from the open circuit mode. The value is rather near that from the steady state permeation $(170 \text{ kJ mol}^{-1})$. As far as YSZ concerns, the oxygen permeation at temperature lower than 1000 K can be neglected. Therefore, the desorption from oxygenate site (T < 1000 K) is not affected by oxygen permeation. However, at higher temperature above 1000 K, the permeation through the YSZ cannot be neglected. Relationship between adsorbed oxygen and permeating oxygen should be studied in further details.

3.2.3. Closed circuit FC-TPD with external applied potential

In our previous work [8], the effects of applied potential on the rates of oxidative coupling of methane in the SOFC reactor were studied. As shown in Fig. 10, the external potential was applied when mixture of air and methane was fed on the anode (air+CH₄/LaAlO/YSZ/LSM/O₂). When the circuit was closed with no applied potential, the rate of CO₂ formation was significantly decreased and the CO formation rate was increased while C₂ formation was almost the same. The

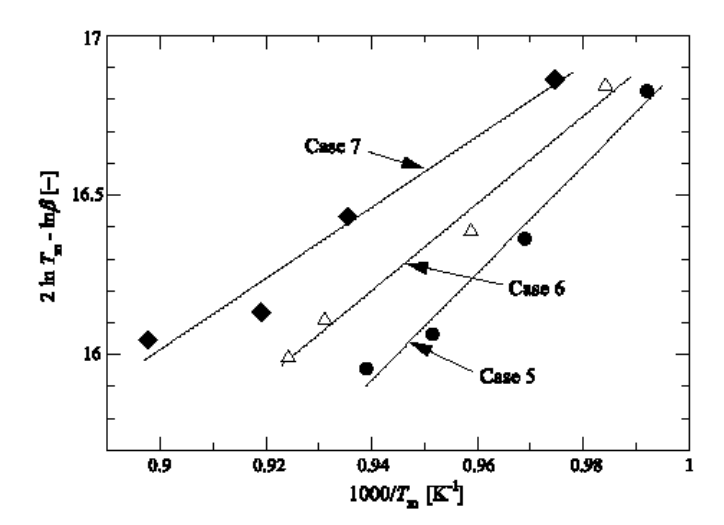


Fig. 9. Plots of $(2 \ln T_m - \ln \beta)$ against $1/T_m$ for coupling site in the closed circuit FC-TPD mode.

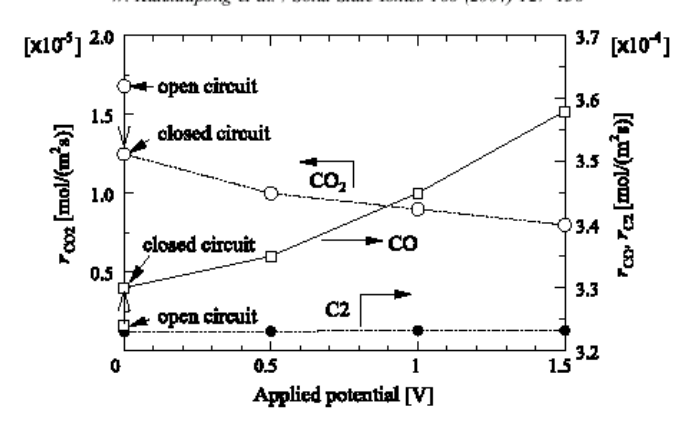


Fig. 10. Effect of applied potential on rates of formation of products (T=1223 K) (pre-mixed feed of oxygen ($2.4 \times 10^{-6} \text{ mol s}^{-1}$) and methane ($5.1 \times 10^{-5} \text{ mol s}^{-1}$) in the anode side and oxygen feed ($6.8 \times 10^{-6} \text{ mol s}^{-1}$) in the cathode side).

similar tendency was observed with applied potential. These effects of applied potential cannot be explained by "Faraday's law". Therefore, we proposed these effects as the NEMCA phenomena [8].

These behaviors can be explained by considering the results from the closed circuit FC-TPD with and without external applied potential (cases 5 and 8, respectively). As shown in Fig. 2-(3), with external applied potential, the qualitative change in adsorption site may be induced as discussed in the previous section at low temperature. Permeation of oxygen is also enhanced at high temperature with applied potential as shown in Fig. 11. Oxygen starts to desorb below 700 K with open circuit mode (case 1), but the temperature shifts to 800 K when the circuit is closed

(case 5). The amount of desorbed oxygen species at 1000 K from the closed circuit mode dominates the open circuit mode. Similar tendency is observed when the external potential (V_T =1 V) was applied (case 8). Assuming that loosely bound oxygen species (the one that desorbs at T=700–800 K) is active for the combustion reaction (CO₂ formation), an increase of interaction between adsorbed oxygen species and the anode by applied potential (species desorbed at 800–1000 K) reduces the activity of oxygen species to form oxygenates and the combustion hardly occurs, resulting in the production of CO. The NEMCA effect shown in Fig. 10 can be correlated to the behavior of active site to interact with oxygen under the electrostatic field

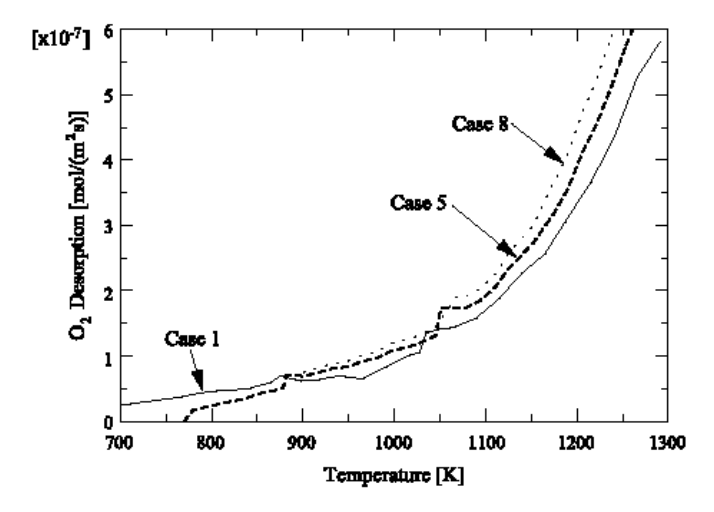


Fig. 11. Effect of applied potential on the FC-TPD results (open circuit pretreatment, $\beta = 0.117 \text{ K s}^{-1}$).

4. Conclusion

The effect of applied potential on the oxygen adsorption and oxygen desorption in the LSM/YSZ/LaAlO SOFC type reactor was studied. The fuel cell type temperature-programmed desorption (FC-TPD) measurements of oxygen were conducted. This technique enables to discuss the oxygen species for the combustion reaction and the coupling reaction separately. By applying external potential, the amount of adsorbed oxygen on the anode catalyst is altered and the activation energy of desorption is decreased. The FC-TPD analysis also correlates the behavior of adsorbed oxygen species to the change in the selectivity of oxidative coupling of methane in SOFC reactor regarded as the NEMCA phenomena.

Nomenclature

```
A pre-exponential factor (s<sup>-1</sup>)
```

 E_d activation energy of desorption (kJ mol⁻¹)

 $R_{\rm g}$ gas constant (J mol⁻¹K⁻¹) T absolute temperature (K)

 $T_{\rm m}$ temperature for the maximum amount of desorbed oxygen (K)

V_P applied external potential during pretreatment (V)

V_T applied external potential during TPD (V)

Greek Letter

 β rate of temperature increase (K s⁻¹)

Acknowledgements

The authors gratefully acknowledged the financial support from The Thailand Research Fund (TRF) and TJTTP-JBIC. A part of this study was also supported by a Grant-in-aid for Scientific Research, from the Ministry of

Education, Culture, Sports, Science and Technology of Japan (MEXT).

References

- [1] B.C.H. Steele, J. Mater. Sci. 36 (2001) 1053.
- [2] O. Yamamoto, Electrochim. Acta 45 (2000) 242.
- [3] T. Tagawa, K.K. Moe, M. Ito, S. Goto, Chem. Eng. Sci. 54 (1999) 1553.
- [4] T. Tagawa, H. Imai, J. Chem. Soc., Faraday Trans. 84 (1) (1988) 923.
- [5] T. Tagawa, K.K. Moe, T. Hiramatsu, S. Goto, Solid State Ion. 106 (1998) 227.
- [6] K.K. Moe, T. Tagawa, S. Goto, J. Ceram. Soc. Jpn. 106 (1998) 242.
- [7] K.K. Moe, T. Tagawa, S. Goto, J. Ceram. Soc. Jpn. 106 (1998) 754.
- [8] T. Tagawa, K. Kuroyanagi, S. Goto, S. Assabumrungrat, P. Praserthdam, Chem. Eng. J. 93 (2003) 3.
- [9] A.S. Carrillo, T. Tagawa, S. Goto, Mater. Res. Bull. 36 (2001) 1017.
- [10] D. Eng, M. Stoukides, Catal. Rev., Sci. Eng. 33 (1991) 375.
- [11] E.N. Voskresenskaya, V.G. Roguleva, A.G. Anshits, Catal. Rev., Sci. Eng. 37 (1995) 101.
- [12] M. Stoukides, Catal. Rev., Sci. Eng. 42 (2000) 1.
- [13] C.G. Vayenas, M.M. Jaksic, S. Bebelis, S.G. Neophytides, in: P. Horsman, B.E. Conway, R.E. White (Eds.), Mod. Aspects Electrochem., vol. 29, Plenum, New York, 1996, p. 57.
- [14] I.S. Metcalfe, Solid State Ion. 152-153 (2002) 669.
- [15] V.D. Belyaev, T.I. Politova, V.A. Sobyanin, Solid State Ion. 136–137 (2000) 721.
- [16] D. Tsiplakides, S. Neophytides, C.G. Vayenas, Solid State Ion. 136–137 (2000) 839.
- [17] P. Vernoux, F. Gaillard, L. Bultel, E. Siebert, M. Primet, J. Catal. 208 (2002) 412.
- [18] P.D. Petrolekas, S. Balomenou, C.G. Vayenas, J. Electrochem. Soc. 145 (1998) 1202.
- [19] R.T. Baker, I.S. Metcalfe, P.H. Middleton, J. Catal. 155 (1995) 21.
- [20] R.J. Cvetanovic, Y. Amenomiya, Application of a Temperature-Programmed Desorption Technique to Catalyst studies, Advance in Catalysis and Related Subjects, vol. 17, Academic Press, New York, 1967.
- [21] S.G. Neophytides, C.G. Vayenas, J. Phys. Chem. 99 (1995) 17063.
- [22] G. Pacchioni, F. Illas, S. Neophytides, C.G. Vayenas, J. Phys. Chem. 100 (1996) 16653.
- [23] C.G. Vayenas, D. Archonta, D. Tsiplakides, J. Electroanal. Chem. 554–555 (2003) 301.

Appendix B
Manuscript "Oxygen transport through LSM/YSZ/LaAlO
system for the use of fuel cell type reactor"



Chemical Engineering Journal 106 (2005) 35-42



www.elsevier.com/locate/cej

Oxygen transport through LSM/YSZ/LaAlO system for use of fuel cell type reactor

Worapon Kiatkittipong^{b,1}, Tomohiko Tagawa^{a,*}, Shigeo Goto^a, Suttichai Assabumrungrat^b, Piyasan Praserthdam^b

^a Department of Chemical Engineering, Nagoya University, Chikusa, Nagoya 464-8603, Japan b Center of Excellence on Catalysis and Catalytic Reaction Engineering, Department of Chemical Engineering, Chulalongkorn University, Bangkok 10330, Thailand

Received 29 September 2004; received in revised form 11 October 2004; accepted 3 November 2004

Abstract

Oxygen transport in an LSM/YSZ/LaAlO solid oxide fuel cell type reactor was studied. The oxygen permeation flux was $8.90 \times 10^{-8} \, \text{mol m}^{-2} \, \text{s}^{-1}$ at $1173 \, \text{K}$ with an activation energy of $170 \, \text{kJ mol}^{-1}$. By applying an external potential, the oxygen permeation flux increased while the activation energy of oxygen permeation decreased. The oxygen permeation fluxes under methane feed in the anode side are 1-2 orders of magnitude higher than those under helium feed. A model of oxygen permeation was presented and the permeation parameters were proposed. In the case of helium feed, the oxygen permeation at the LaAlO anode was the rate-limiting step. However, changing helium to methane as a reactive gas, the resistances for the oxygen permeation in the three parts (LSM/YSZ/LaAlO) were comparable. © 2004 Elsevier B.V. All rights reserved.

Keywords: Solid oxide fuel cell; SOFC reactor; Oxygen permeation; Modeling; Methane

1. Introduction

Solid oxide fuel cell (SOFC) is a promising energy conversion technology for future applications [1,2]. In our previous papers, the SOFC system was applied as a selective oxidation reactor for chemical energy co-generation. Particular focuses were on catalyst preparation method [3-5] and reactor performance test [6-8]. In these studies, the oxidative coupling of methane to ethane and ethylene (C2) was studied. The solid electrolyte was used as an oxygen separator and an oxygen distributor to achieve high C2 selectivity. In these electrocatalytic systems, combined effects of activation of oxygen on an anode and permeation of oxygen through an yttria stabilized zirconia (YSZ) controlled the reactor performance.

1385-8947/\$ - see front matter © 2004 Elsevier B.V. All rights reserved. doi:10.1016/j.cej.2004.11.004

Therefore, the oxygen transport through the electrochemical system should be studied. Several research groups have published their experimental results on the overall oxygen permeation through many oxygen-permeable electrolyte membranes such as YSZ [9], calcia stabilized zirconia (CSZ) [10], mixed ion-electronic conducting materials such as $La_{1-x}Sr_xCo_{1-y}Fe_yO_{3-\delta}$ (LSCF) [11,12] and other perovskite-type ceramics, for example, Bi_{1.5}Y_{0.3}Sm_{0.2}O_{3-δ} (BYS) [13,14], $BaBi_xCo_{0.2}Fe_{0.8-x}O_{3-\delta}$ [15], $BaCo_{0.4}$ $Fe_{0.6-x}Zr_xO_{3-\delta}$ [16].

Several studies focused on the steady-state oxygen permeation in membrane reactors for oxidation reactions, for example, partial oxidation of methane [17] and oxidative coupling of methane [14,18]. However, very limited studies on oxygen permeation in the SOFC reactors have been reported. The conventional YSZ electrolyte has been widely used to provide the electrochemical permeation of oxygen for the oxidative coupling of methane [3-8]. The use of external potential as well as the effect of non-Faradaic electrochemical modification of catalytic activity (NEMCA) are of recent interest.

^{*} Corresponding author. Tel.: +81 52 789 3388; fax: +81 52 789 3388. E-mail address: tagawa@nuce.nagoya-u.ac.jp (T. Tagawa).

Nagoya University Program for Academic Exchange (NUPACE)-Ph.D. student supported by AIEJ.

Nomenclature

 A_j pre-exponential factor of conductivity (S K m⁻¹)

 A_{Per} pre-exponential factor of oxygen permeation (mol m⁻² s⁻¹)

E electromotive force (V)

 E_i activation energy of conductivity (J mol⁻¹)

 \vec{E}_{Per} activation energy of oxygen permeation $(J \text{ mol}^{-1})$

F Faraday's constant, 96487 (C mol⁻¹) J_{O_2} oxygen permeation flux (mol m⁻² s⁻¹)

 $k_{\text{O_2-perm}}$ overall oxygen ions recombination and diffusion coefficient (mol m⁻² s⁻¹)

 $k_{
m O_2 ext{-}Rxn}$ oxygen surface reaction coefficient (mol m $^{-2}$ s $^{-1}$ Pa $^{-1}$)

 $k_{\rm V}$ proportional constant (mol m⁻² s⁻¹ V⁻¹)

L thickness of material (m)

Per, O specific oxygen permeability (mol m⁻¹ s⁻¹)

P_{feed} oxygen partial pressure at feed side (cathode side) (Pa)

 P_{lean} oxygen partial pressure at lean side of materials (Pa)

 $P_{O_2(I)}$ oxygen partial pressure at the gas-membrane interface (Pa)

 $P_{\mathrm{O_2(II)}}$ oxygen partial pressure at membrane-gas interface (Pa)

P_{perm} oxygen partial pressure at permeate side (anode side) (Pa)

 P_{rich} oxygen partial pressure at rich side of materials (Pa)

 $R_{\rm g}$ gas constant, 8.314 (J mol⁻¹ K⁻¹)

T temperature (K)

V_{Per} applied external potential during steady-state permeation (V)

Greek letters

 α permeation rate constants in interface diffusion step (mol m⁻² s⁻¹ Pa^{-1/2})

 β permeation rate constants in bulk diffusion step (mol m⁻¹ s⁻¹ Pa^{-1/4})

 σ conductivities (S m⁻¹)

Subscripts

e electronic i ionic

In the previous paper [8], the fuel cell type temperatureprogrammed desorption (FC-TPD) was studied on the LSM/YSZ/LaAIO system. Increasing the applied potential increased the amount of adsorbed oxygen. The change in the selectivity of active sites gave a new aspect to the NEMCA phenomena in the oxidative coupling of methane in the SOFC reactor. The applied potential also decreased the activation energy of desorption of oxygen at the anode catalyst [19]. In addition, the FC-TPD analysis could correlate the behavior of adsorbed oxygen species to the NEMCA effect.

In this study, the steady-state oxygen permeation using helium or methane as an anode gas was investigated. The effect of applied potential on the oxygen permeation through the LSM/YSZ/LaAlO in the SOFC reactor was studied. In addition, a model of oxygen permeation was proposed.

2. Experimental

2.1. Apparatus

The schematic diagram of the solid oxide fuel cell type reactor is illustrated in Fig. 1. A tube-type YSZ membrane (8 mol% $\rm Y_2O_3$, thickness = 1.5 mm, inside diameter = 18 mm, outside diameter = 21 mm, length = 500 mm, effective surface area = 0.0148 m²) was used as an electrolyte. La_{1.8}Al_{0.2}O₃ (abbreviated as LaAlO) prepared by a mist decomposition method was used as an anode catalyst on the inner surface of the tube while La_{0.85}Sr_{0.15}MnO₃ (abbreviated as LSM) prepared by paste method was used as the cathode on the outer surface [7,8]. Details of the electrode preparation methods were described elsewhere [3,4,7].

Platinum wire was connected to platinum meshes placed on both electrode surfaces to serve as current collectors. The outlet gas from the anode side was directly connected to a gas chromatograph for analysis of gas composition. A potentiostat was used to supply an external electrical potential to the system. Oxygen transport from the cathode side to the anode side was promoted under the applied positive potential.

2.2. Steady-state oxygen permeation

Steady-state oxygen permeation measurements were performed at various temperature levels: i.e., T=1073, 1123, 1173, 1223 and 1273 K. Helium $(1.36 \times 10^{-5} \text{ mol s}^{-1})$ and oxygen $(1.02 \times 10^{-5} \text{ mol s}^{-1})$ were fed to the anode and the cathode, respectively. The oxygen permeation flux was calculated from the flow rate and composition of the anode exit gas. The flow rate and its composition was measured and analyzed by a bubble flow meter and a gas chromatograph with a TCD detector, respectively. Sampling was conducted every 5 min until reaching a steady-state condition (approximately 0.5 h). Another set of steady-state oxygen permeation was carried out by using methane $(6.8 \times 10^{-6} \,\mathrm{mol \, s^{-1}})$ as an anode reactant gas at various temperature levels: i.e. T=1073, 1123, 1173, 1223 and 1273 K. In this case, permeated oxygen has reacted with methane to produce oxygen, containing species such as CO, CO₂, H₂O. Thus, the oxygen permeation flux was estimated by analyzing these oxygen-containing products. The steady-state measurements for both sets of experiments were carried out at various levels of the applied potential.

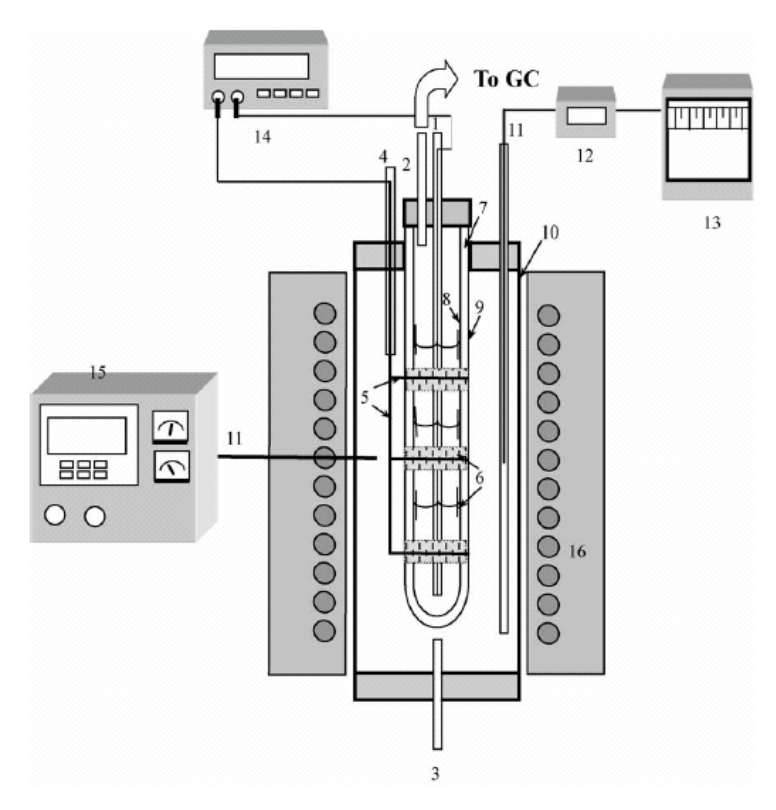


Fig. 1. Schematic diagram of the solid oxide fuel cell type reactor. (1) Anode side feed (He/CH₄), (2) exit gas from anode side, (3) cathode side feed (O₂), (4) exit gas from cathode side, (5) platinum wire, (6) platinum mesh, (7) YSZ tube, (8) anode (LaAlO), (9) cathode (LSM), (10) quartz tube, (11) thermocouple, (12) temperature indicator, (13) temperature recorder, (14) ammeter/voltmeter/potentiostat, (15) temperature controller, (16) furnace.

3. Results and discussion

3.1. Oxygen transport model

3.1.1. Oxygen permeation through thin YSZ membranes modeled by Han et al. [9]

In our previous study on the micro fuel cell system [20], we have referred an oxygen permeation model presented by Han et al. [9]. The proposed permeation process is summarized in Fig. 2. In their study, a thin YSZ membrane prepared by the electrochemical vapor deposition (EVD) method was employed. The oxygen permeation flux can be described by the following equations [9].

At gas-membrane interface of the cathode side:

$$J_{\rm O_2} = \alpha (P_{\rm rich}^{1/2} - P_{\rm O_2(I)}^{1/2}) \eqno(1)$$

In bulk oxide of YSZ:

$$J_{\rm O_2} = \frac{\beta}{L} (P_{\rm O_2(I)}^{1/4} - P_{\rm O_2(II)}^{1/4}) \tag{2}$$

At membrane-gas interface of the anode side:

$$J_{\rm O_2} = \alpha (P_{\rm O_2(II)}^{1/2} - P_{\rm lean}^{1/2}) \eqno(3)$$

The rate parameters α and β at $T=1173~\rm K$ are $9.4\times 10^{-7}~\rm mol\,m^{-2}\,s^{-1}\,Pa^{-1/2}$ and $5.2\times 10^{-11}~\rm mol\,m^{-1}\,s^{-1}\,Pa^{-1/4}$, respectively. The activation energy of α and β are $53.1~\rm kJ\,mol^{-1}\,K^{-1}$ and $72.0~\rm kJ\,mol^{-1}\,K^{-1}$, respectively. As

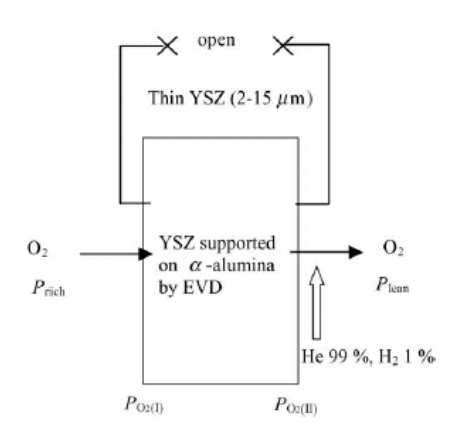


Fig. 2. Oxygen permeation process through thin YSZ membranes prepared by the electrochemical vapor deposition (EVD) method supported on α -alumina reported by Han et al. [9].

shown in Fig. 2, this system was operated under open circuit without the anode and cathode electrodes. One percent of hydrogen in helium was used as a reacting sweep gas. These conditions were not the same as our present system, which was operated under closed circuit with or without applied potential with LSM as the cathode and LaAlO as the anode catalyst.

3.1.2. A model for the oxygen permeation through the LSM/YSZ/LaAlO

In this study, an oxygen permeation model through the LSM/YSZ/LaAlO fuel cell type reaction system with closed circuit and applied potential is proposed. Schematic models of oxygen permeation are shown in Fig. 3. The circuit was closed to allow the electron transfer. Two kinds of carrier gas were used: i.e. helium (Fig. 3(a)) and methane (Fig. 3(b)).

In the case of helium feed without applied potential, Fig. 3(a) shows general reaction paths as follows: (1) electrochemical reduction at the LSM surface to form oxygen ions, (2) incorporation of oxygen ions into the YSZ lattice, (3) recombination and desorption of oxygen ions to form oxygen molecules at the LaAlO anode.

The permeation of oxygen through an electrochemical media depends upon ionic conductivity (σ_i) and electronic conductivity (σ_e) of the media. Assuming surface concentration of oxygen ions is equilibrated with gas phase, they can be estimated from the following equations [21].

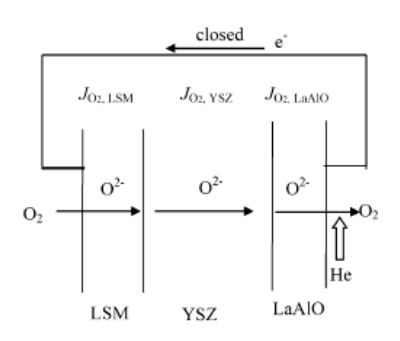
$$J_{O_2} = \frac{\text{Per, O}_2}{L} \ln \left(\frac{P_{\text{rich}}}{P_{\text{lean}}} \right)$$
 (4)

Per,
$$O_2 = \frac{R_g T}{16F^2} \frac{\sigma_i \sigma_e}{\sigma_i + \sigma_e}$$
 (5)

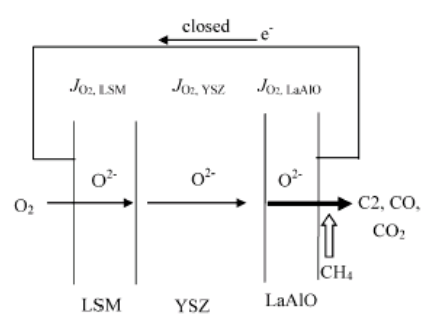
$$\sigma_j = \left(\frac{A_j}{T}\right) \exp\left(\frac{-E_j}{R_{\rm g}T}\right); \quad j = {\rm i,e}$$
 (6)

The ionic conductivities of LSM ($\sigma_{i\text{-LSM}}$) [22], the electronic conductivities of LSM ($\sigma_{e\text{-LSM}}$) [23,24], the ionic conductivities of YSZ ($\sigma_{i\text{-YSZ}}$) [25] and the electronic conductivities of YSZ ($\sigma_{e\text{-YSZ}}$) [26] were cited from the literatures and the values are summarized in Table 1.

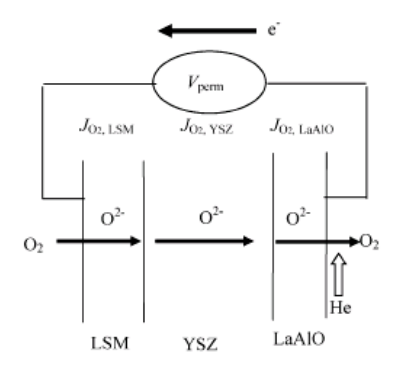
However, these values of LaAlO are not available in the literature. Due to the recombination and desorption of oxygen ions to form oxygen molecules at the LaAlO anode, the overall rate of these processes at LaAlO might be estimated



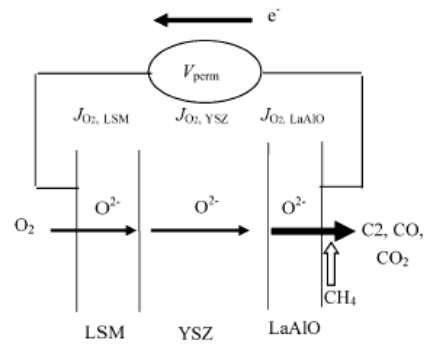
 (a) Helium feed at anode, closed circuit without applied potential



(b) Methane feed at anode, closed circuit without applied potential



 Helium feed at anode, closed circuit with applied potential



 (d) Methane feed at anode, closed circuit with applied potential

Fig. 3. Proposed schemes for oxygen permeation through LSM/YSZ/LaAlO under various conditions.

Table 1 Values of parameters for the calculations of oxygen permeation flux

Parameters	A_f (S K m ⁻¹)	E_j (kJmol ⁻¹)	Reference
$\sigma_{i-LSM} (S m^{-1})$	2.311×10^{11}	284	[22] ^a
$\sigma_{e-LSM} (S m^{-1})$	8.855×10^{7}	9	[23] ^b , [24] ^c
σ_{i-YSZ} (S m ⁻¹)	7.121×10^{7}	88	[25]
$\sigma_{\text{e-YSZ}} (\text{S m}^{-1})$	9.244×10^{5}	87.5	[26]

 $L_{LSM} = 1 \times 10^{-6} \text{ m}, L_{YSZ} = 1.5 \times 10^{-3} \text{ m}, L_{LaAIO} = 5 \times 10^{-6} \text{ m}.$

- ^a At 1173 K, the value was interpolated between La_{0.95}Sr_{0.05}MnO₃ and La_{0.8}Sr_{0.2}MnO₃, and at 1273 K between La_{0.9}Sr_{0.1}MnO₃ and La_{0.8}Sr_{0.2}MnO₃.
 - σ_{e-LSM} was given at 1173 K.
 - ^c The activation energy was shown in the table.

from Eq. (7)

$$J_{\rm O_2} = k_{\rm O_2\text{-perm}} \ln \left(\frac{P_{\rm rich}}{P_{\rm lean}} \right) \tag{7}$$

where P_{rich} and P_{lean} represent partial pressure of oxygen at the rich and lean sides of LaAlO, respectively.

When the permeation is at steady-state, the oxygen permeation flux across different parts of the cell is equal to the observed experimental results.

$$J_{O_2,Exp} = J_{O_2,LSM} = J_{O_2,YSZ} = J_{O_2,LaAlO}$$
 (8)

The values of $k_{\rm O2\text{-}perm}$ of LaAlO at different temperatures were determined by using an all-purpose equation solver, EQUATRAN-G (Omega Simulation, Japan). $P_{\rm rich}$ of LSM is partial pressure of oxygen at the feed side (101.3 kPa) while $P_{\rm lean}$ of LaAlO is partial pressure of oxygen at the permeate side, which are calculated from the experiments. The estimated $k_{\rm O2\text{-}perm}$ value was shown as follows.

$$k_{\text{O_2-perm}} = 0.413 \exp\left(\frac{-170400}{R_g T}\right)$$
 (9)

In the case of methane feed without applied potential, oxygen ions directly reacted with methane at the anode (Fig. 3(b)). It was expected that the oxygen permeation rate could be enhanced. Due to the chemical reaction at the anode catalyst surface, the overall reaction rate could depend on partial pressure of methane and surface oxygen concentration. The oxygen surface reaction coefficient (k_{O_2-Rxn}) was estimated from experimental oxygen permeation flux by the following equation.

$$J_{\rm O_2} = k_{\rm O_2-Rxn} P_{\rm CH_4} \ln \left(\frac{P_{\rm rich}}{P_{\rm lean}} \right)$$
 (10)

No oxygen was observed in gas phase of the permeate side due to reactions with methane. The surface oxygen may not be in the equilibrium with oxygen in gas phase. However, the surface oxygen concentration in methane feed could be assumed similar to the helium case. Therefore, P_{lean} in the helium case was used in Eq. (10)

In the case of closed circuit with applied potential, it was expected that the oxygen transfer could be accelerated with increasing applied potential (in Fig. 3(c and d)). Linear relationship between applied potential and oxygen permeation flux was assumed and the following equation could be proposed.

$$J_{O_2} = J_{O_2,0V} + k_V V_{Per}$$
(11)

The values of $J_{O_2,0V}$ without applied potential can be calculated by Eqs. (4)–(6) and (7) for the helium feed case and by Eqs. (4)–(6) and (10) for the methane feed case, respectively.

3.2. Steady-state oxygen permeation results

3.2.1. Helium feed

Fig. 4 shows the effect of the applied potential on the oxygen flux at various temperatures. Linear relationships between the oxygen permeation flux and the applied potential were observed for all different temperatures. As shown in Fig. 4, the oxygen could be permeated without applied potential due to the system possessed an internal "concentration cell" potential as a driving force. For example, the concentration cell potential is 0.225 V at 1223 K. This value agrees well with OCV value calculated from Nernst equation.

$$E = \frac{R_g T}{4F} \ln \left(\frac{P_{\text{feed}}}{P_{\text{perm}}} \right) \tag{12}$$

Therefore, we can assume surface oxygen concentration at the lean side of LaAlO is in equilibrium with oxygen in gas phase at the permeate side.

The proportional constants (k_V) from Eq. (11) could be determined from the slopes and expressed as Eq. (13).

$$k_{V,He} = 0.102 \exp\left(\frac{-122700}{R_{g}T}\right)$$
 (13)

Fig. 5 shows the plots between $\ln(J_{\rm O_2})$ and 1000/T at different levels of the applied potential. The solid lines represent the results calculated from Eqs. (4)–(7), (11) and (13). The oxygen flux increases with the increasing temperature and applied potential.

The solid lines in Fig. 5, can be approximated by straight lines of Arrhenius' plots by Eq. (14).

$$J_{O_2} = A_{\text{Per}} \exp\left(\frac{-E_{\text{Per}}}{R_{\text{g}}T}\right) \tag{14}$$

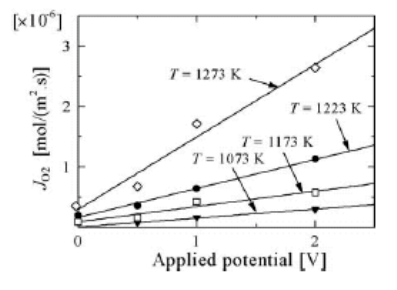


Fig. 4. Effect of applied potential on oxygen flux at various temperatures by steady-state permeation experiments using helium feed at anode side.

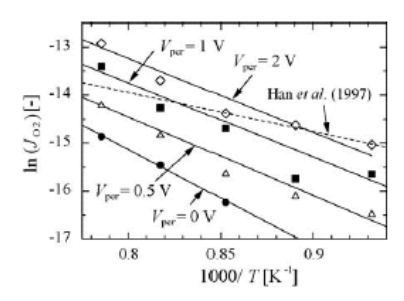


Fig. 5. Arrhenius' plot between $\ln(J_{\rm O_2})$ and 1000/T at different levels of applied potential by steady-state permeation experiments using helium feed at anode side.

The overall activation energy of the oxygen transport through the cell ($E_{\rm Per}$) was calculated from the slopes and the results are shown in Table 2. The activation energy is decreased from 170 kJ/mol in case of closed circuit with no applied potential to 119 kJ/mol with applied potential is 2 V. TPD experiments have shown that the applied potential also decreased the activation energy of the oxygen desorption from 140 kJ/mol to 93 kJ/mol when applied potential 2 V [19]. Comparing these values, the activation energies of oxygen permeation are close to the activation energies of oxygen desorption.

The dashed line in Fig. 5 shows the results calculated from Han's model [9]. The comparison of our model with Han's model will be described later (Section 3.2.4).

3.2.2. Methane feed

Instead of helium, methane was fed to the anode chamber to react with the permeating oxygen. At 1273 K, the electromotive force from the experiment is 1.09 V, which is near to the theoretical value of ethylene formation (1.05 V). Linear relationships between the oxygen permeation flux and the applied potential were observed for all different temperatures as shown in Fig. 6. The proportional constants ($k_{\rm V}$) from Eq. (11) could be determined from the slopes and the expression is shown in Eq. (15).

$$k_{V,CH_4} = 0.875 \exp\left(\frac{-104150}{R_g T}\right)$$
 (15)

Fig. 7 shows the plots between $\ln(J_{\rm O_2})$ and 1000/T at different levels of the applied potential. The oxygen flux with the methane feed was estimated from the equivalent rate of oxygen required for the oxidation reaction. The oxygen surface reaction coefficient $(k_{\rm O_2-Rxn})$ estimated from the experimen-

Table 2
Summary of the values of pre-exponential factors of oxygen permeation and activation energy at different levels of applied potential from steady-state permeation results using helium feed at anode side

V _{Per} (V)	$A_{Per} (\text{mol m}^{-2} \text{s}^{-1})$	E _{Per} (kJ mol ^{−1})	
0	3.499	170	
0.5	1.280	154	
1	0.675	144	
2	0.157	119	

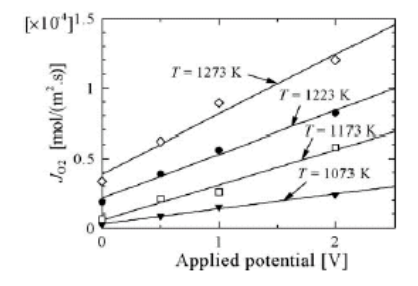


Fig. 6. Effect of applied potential on oxygen flux at various temperatures by steady-state permeation experiments using methane feed at anode side.

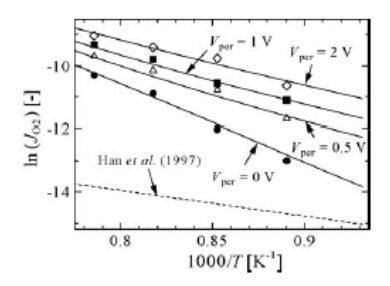


Fig. 7. Arrhenius' plot between $\ln(J_{O_2})$ and 1000/T at different levels of applied potential by steady-state permeation experiments using methane feed at anode side.

tal oxygen permeation flux by using Eq. (8) was shown as follows.

$$k_{\text{O_2-Rxn}} = 8.577 \times 10^{-3} \exp\left(\frac{-195100}{R_g T}\right)$$
 (16)

The solid line with $V_{\rm Per}=0$ V represents the calculated results by Eqs. (4)–(6), (10) and (16). The solid lines for $V_{\rm Per}=0.5$ V, 1 V and 2 V were calculated by Eqs. (4)–(6), (10), (11) and (15), (16).

The solid lines in Fig. 7 can be approximated by straight lines of Arrhenius' plots by Eq. (14). The overall activation energy of the oxygen transport through the cell (E_{Per}) was calculated from the slopes and the results are shown in Table 3. The applied potential increases the oxygen flux and also decreases the activation energy of the oxygen transport.

Compared with the helium feed case, the oxygen flux is significantly improved when methane is fed to the anode side. The oxygen permeation fluxes under the methane feed are 1–2

Table 3 Summary of the values of pre-exponential factors of oxygen permeation and activation energy at different levels of applied potential from steady-state permeation results using methane feed at anode side

$V_{\text{Per}}(V)$	$A_{Per} (\text{mol m}^{-2} \text{s}^{-1})$	$E_{\text{Per}} (k \text{J} \text{mol}^{-1})$
0	3.632×10^4	219
0.5	186.9	157
1	82.84	145
2	15.77	124

orders of magnitude higher than those under the helium feed. It is clear that the reaction of methane with the permeated oxygen at the anode catalyst significantly improves the overall oxygen permeation flux due to the surface oxygen kinetics with methane. The dashed line in Fig. 7 represents the Han's model.

3.2.3. Oxygen partial pressure profiles and permeation mechanism

Fig. 8 shows the oxygen partial pressure profile from the simulation results at 1223 K. In the case of the helium feed (solid line), it is obvious that the major oxygen permeation resistance through the cell or the rate-limiting step of this system is at the LaAlO electrode. Although the thickness of YSZ electrolyte is much more than the electrodes, the resistance of YSZ electrolyte is negligible. With the methane feed case (dashed lines), the resistances of three steps are comparable; consequently, the rate steps at the cathode and the electrolyte need to be taken into account

In the case without methane, oxygen ions release electrons and recombine into oxygen molecules, which are then desorbed into the gas phase. On the other hand, with the methane feed, oxygen ions could directly react with methane to form CO₂, CO and C₂ hydrocarbons.

Mechanisms of the oxygen activation on the LSM and the bulk transport of O^{2-} in YSZ might be the same as the helium feed case as shown in the previous sections. The change in the surface reaction step on the anode from the recombination and desorption of oxygen ion to the reaction of oxygen species with methane would be the main reason for the increase of oxygen flux for the methane feed.

3.2.4. Effect of YSZ thickness

The effect of YSZ thickness on the oxygen permeation flux is simulated and the results are shown in Fig. 9. In the

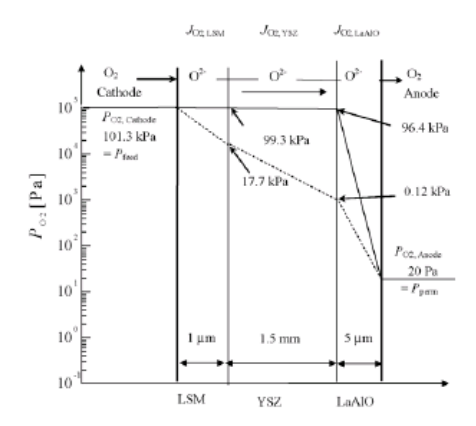


Fig. 8. The mechanism of oxygen permeation and the profile of oxygen partial pressure in LSM/YSY/LaAIO from the simulation results at 1223 K (solid line: helium feed, dashed line: methane feed).

case of helium feed, the oxygen permeation flux is independent on the YSZ thickness as noted in the previous section that LaAlO is the rate-limiting step. However, in the case of methane feed, the resistance of YSZ electrolyte is comparable to that of LaAlO. The rate of oxygen permeation depends on the YSZ electrolyte. The flux increases with decreasing the thickness of YSZ electrolyte membrane. However, for YSZ with thickness below $10~\mu m$, there is no significant improvement on the oxygen flux. The tendency is the same for $T=1223~{\rm K}$ and $1273~{\rm K}$.

3.2.5. Estimation of oxygen permeation from a model proposed by Han et al. [9]

Han et al. [9] proposed Eqs. (1)–(3) for the permeation of oxygen through YSZ membrane but their system was tested under unusual conditions; i.e. very thin YSZ membrane of 2–15 μ m, low oxygen partial pressure in an oxygen source chamber of 5.33 kPa and without external circuit (open circuit). Dashed lines in Figs. 5 and 7 show the oxygen permeation flux calculated from Eqs. (1)–(3) using a YSZ with thickness of 1.5 mm. The estimated oxygen flux is much larger than that of the helium feed (compared with $V_{\rm Per}=0$ in Fig. 5) and far less than that of the methane feed (compared with $V_{\rm Per}=0$ in Fig. 7). This tendency can be understood by considering that the sweep gas of the permeate side contained 1% of hydrogen in their experiments [9].

Hydrogen in the sweep gas caused the promotion of the oxygen permeation by the surface reaction but the partial pressure was too low to complete the enhancement of the oxygen permeation. When hydrogen was mixed in the sweep gas, an electromotive force of about 1 V should be generated between the two electrodes. This may be the reason of the agreement with the plot of $V_{\text{Per}} = 1 \text{ V}$ in Fig. 5.

The differences in the activation energy should be caused by the differences in the surface reaction on the anode material. Further studies are required to find more details.

All these results show that it is essential for the model of the SOFC-type reactor to include the permeation of oxygen through the cathode, the electrolyte and the anode.

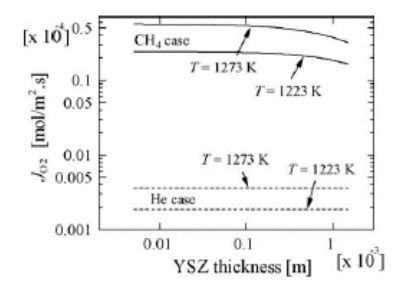


Fig. 9. Effect of YSZ thickness on oxygen permeation in helium and methane case.

4. Conclusion

The oxygen transport through the LSM/YSZ/LaAIO SOFC-type reactor was studied at various operating conditions. The oxygen permeation flux was 8.90×10^{-8} mol m⁻² s⁻¹ at 1173 K with an activation energy of $170\,\mathrm{kJ}$ mol ⁻¹. Increasing the applied potential increased the oxygen permeation fluxes by one order of magnitude and reduced the activation energy of the oxygen permeation. The oxygen permeation fluxes under the methane feed are 1–2 orders of magnitude higher than those under the helium feed. A model of oxygen permeation was proposed. In the helium case, the oxygen permeation at the LaAIO anode was the rate-limiting step for the oxygen permeation. However, by changing helium to reactant gas as methane, the resistances in the three parts (LSM/YSZ/LaAIO) become comparable.

Acknowledgements

The authors gratefully acknowledged the financial support from the Thailand Research Fund (TRF) and TJTTP-JBIC. A part of this study was also supported by a Grant-in-aid for Scientific Research, from the Ministry of Education, Culture, Sports, Science and Technology of Japan (MEXT).

References

- [1] B.C.H. Steele, J. Mater. Sci 36 (2001) 1053-1068.
- [2] O. Yamamoto, Electrochim. Acta 45 (2000) 2423-2435.
- [3] K.K. Moe, T. Tagawa, S. Goto, J. Ceram. Soc. Jpn. 106 (1998) 242–247.
- [4] K.K. Moe, T. Tagawa, S. Goto, J. Ceram. Soc. Jpn. 106 (1998) 754–758.
- [5] A.S. Carrillo, T. Tagawa, S. Goto, Mater. Res. Bull. 36 (2001) 1017–1027.

- [6] T. Tagawa, K.K. Moe, T. Hiramatsu, S. Goto, Solid State Ionics 106 (1998) 227–235.
- [7] T. Tagawa, K.K. Moe, M. Ito, S. Goto, Chem. Eng. Sci. 54 (1999) 1553–1557.
- [8] T. Tagawa, K. Kuroyanagi, S. Goto, S. Assabumrungrat, P. Praserth-dam, Chem. Eng. J. 93 (2003) 3–9.
- [9] J. Han, G. Xomeritakis, Y.S. Lin, Solid State Ionics 93 (1997) 263–272.
- [10] Y. Nigara, J. Mizusaki, M. Ishigame, Solid State Ionics 79 (1995) 208–211.
- [11] Y. Teraoka, Y. Honbe, J. Ishii, H. Furukawa, I. Moriguchi, Solid State Ionics 152–153 (2002) 681–687.
- [12] S. Lee, K.S. Lee, S.K. Woo, J.W. Kim, T. Ishihara, D.K. Kim, Solid State Ionics 158 (2003) 287–296.
- [13] C.E. Platon, W.J. Thomson, Ind. Eng. Chem. Res. 41 (2002) 6637–6641.
- [14] F.T. Akin, Y.S. Lin, Y. Zeng, Ind. Eng. Chem. Res. 40 (2001) 5908–5916.
- [15] Z. Shao, G. Xiong, Y. Cong, W. Yang, J. Membr. Sci. 164 (2000) 167–176.
- [16] J. Tong, W. Yang, B. Zhu, R. Cai, J. Membr. Sci. 203 (2002) 175–189.
- [17] T. Ishihara, Y. Tsuruta, T. Todaka, H. Nishiguchi, Y. Takita, Solid State Ionics 152–153 (2002) 709–714.
- [18] Y. Zeng, Y.S. Lin, J. Catal. 193 (2000) 58-64.
- [19] W. Kiatkittipong, T. Tagawa, S. Goto, S. Assabumrungrat, P. Praserthdam, Solid State Ionics 166 (2004) 127–136.
- [20] S. Goto, T. Tagawa, S. Assabumrungrat, P. Praserthdam, Catal. Today 82 (2003) 223–232.
- [21] V.V. Kharton, A.V. Kovalevsky, A.P. Viskup, F.M. Figueiredo, J.R. Frade, A.A. Yaremchenko, E.N. Naumovich, Solid State Ionics 128 (2000) 117–130.
- [22] I. Yasuda, K. Ogasawara, M. Hishinuma, T. Kawada, M. Dokiya, Solid State Ionics 86–88 (1996) 1197–1201.
- [23] Z. Li, M. Behruzi, L. Fuerst, D. Stovet, in: S.C. Singhal, H. Iwahara (Eds.), SOFC-III, PV 93-4, The Electrochemical Society, Pennington, NJ, 1993, p. 171.
- [24] V.V. Kharton, A.P. Viskup, I.P. Marozau, E.N. Naumocich, Mater. Lett. 57 (2003) 3017–3021.
- [25] S.P.S. Badwal, Solid State Ionics 52 (1992) 23-32.
- [26] C. Xia, S. Zha, W. Yang, R. Peng, D. Peng, G. Meng, Solid State Ionics 133 (2000) 287–297.

Appendix C
Manuscript "Oxidative Coupling of Methane in
LSM/YSZ/LaAlO SOFC Reactor"

Oxidative Coupling of Methane in the LSM/YSZ/LaAIO SOFC Reactor

Worapon KIATKITTIPONG^{1,2*}, Tomohiko TAGAWA¹, Shigeo GOTO¹, Suttichai ASSABUMRUNGRAT² and Piyasan PRASERTHDAM²

¹Department of Chemical Engineering, Nagoya University, Furo-cho, Chikusa-ku, Nagoya-shi, Aichi 464-8603, Japan ²Center of Excellence on Catalysis and Catalytic Reaction Engineering, Department of Chemical Engineering, Chulalongkorn University, Phya Thai Road, Prathumwan, Bangkok 10330, Thailand

Keywords: Solid Oxide Fuel Cell, SOFC Reactor, Oxidative Coupling of Methane, Modeling

Oxidative coupling of methane was studied in a solid oxide fuel cell (SOFC) tube type reactor. $La_{0.85}Sr_{0.15}MnO_3/8\ mol\%\ Y_2O_3-ZrO_2/La_{1.8}Al_{0.2}O_3\ (abbreviated\ as\ LSM/YSZ/LaAlO)\ were\ used\ as\ a\ cathode,\ electrolyte\ and\ anode.$ The C2 selectivity and the methane conversion were 91.7% and 23.7% at 1273 K, respectively. The kinetic rate expression was proposed with two different oxygen species. The internal resistance of cell could be lumped and estimated by maximum power transfer theorem. The effect of external load was investigated both in experiments and calculations. The proposed modeling agreed well with the experimental results.

Introduction

Conversion of methane into other valuable hydrocarbons has significant industrial importance. Among the various schemes for methane conversion, the oxidative coupling of methane (OCM) to ethane and ethylene (C2) is a promising process to upgrade natural gas. Solid oxide fuel cell (SOFC) is one of the most attractive fuel cells (Yamamoto, 2000; Steele, 2001). As a reactor for the OCM reaction, a solid electrolyte was used as an oxygen separator and an oxygen distributor to achieve high C2 selectivity. A recent review (Stoukides, 2000) summarized the state of the art of this technology. It also provided a useful table comparing yields and selectivities of the OCM reaction on various catalysts. Most of the reported studies showed high selectivities but low yields.

In our previous papers, the OCM was studied in an SOFC reactor. Particular focuses were placed on catalyst preparation methods (Moe et al., 1998a, 1998b; Carrillo et al., 2001) and reactor performance tests (Tagawa et al., 1998, 1999, 2003). The oxygen temperature-programmed desorption (O₂-TPD) of the LaAlO powder sample was studied (Tagawa et al., 1999) and it was proposed that oxygen species desorbed at low temperatures (below 1000 K) were active for

CO and CO₂ formation (oxygenate site) while those desorbed at higher temperatures (above 1000 K) were active for the OCM to C2-hydrocarbon (coupling site). The fuel cell type temperature-programmed desorption (FC-TPD) measurements were employed to investigate oxygen species under the fuel cell operation (Kiatkittipong et al., 2004a). Both oxygen species were observed.

Modeling is an important tool for the design of SOFC and prediction of SOFC performances. Most attention has been given to the case where hydrogen or carbon monoxide is used as a fuel (Achenbach, 1994; Bessette et al., 1995; Aguiar et al., 2002; Yamada et al., 2002). Very few investigators studied the modeling of the OCM reaction in SOFC reactors. Guo et al. (1999) proposed a mathematical model based on well mixed flow and plug flow. Although good agreement between their simulation and experimental results were observed, some parameters in the model are unclear.

In this paper, the OCM in an SOFC reactor with a cell of La_{0.85}Sr_{0.15}MnO₃/8 mol% Y₂O₃-ZrO₂/La_{1.8}Al_{0.2}O₃ (abbreviated as LSM/YSZ/LaAlO) was studied. An optimum condition for the anode preparation by the mist pyrolysis method was investigated to achieve high C2 selectivity. The knowledge of oxygen species from FC-TPD (Tagawa et al., 1998; Kiatkittipong et al., 2004a) and the oxygen permeation through the LSM/YSZ/LaAlO (Kiatkittipong et al., 2004b) were taken into account to obtain the kinetic parameters of the reactions on the anode. The effect of external load resistance on the reactor performance was also considered. The model of the overall OCM reaction in the

Received on March 19, 2004. Correspondence concerning this article should be addressed to T. Tagawa (E-mail address: tagawa@nuce.nagoya-u.ac.jp).

Nagoya University Program For Academic Exchange (NUPACE)-Ph.D. student supported by AIEJ.

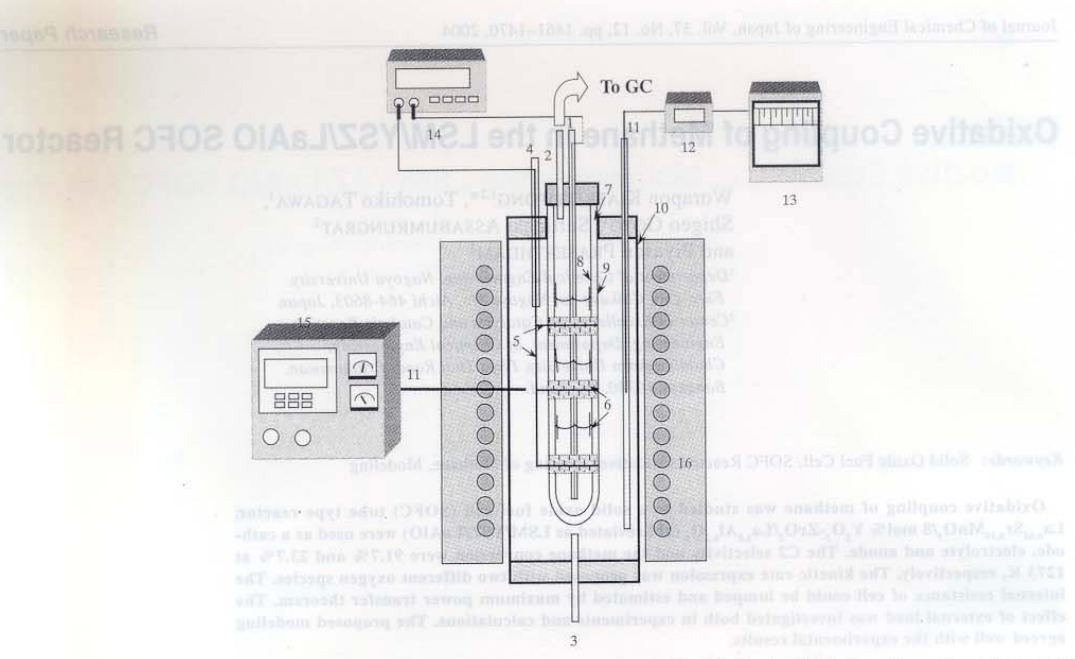


Fig. 1 Schematic diagram of the solid oxide fuel cell type reactor: 1, anode side feed (CH₄); 2, exit gas from the anode side; 3, cathode side feed (O₂/air); 4, exit gas from the cathode side; 5, platinum wire; 6, platinum mesh; 7, YSZ tube; 8, anode (LaAlO); 9, cathode (LSM); 10, Quartz tube; 11, thermocouple; 12, temperature indicator; 13, temperature recorder; 14, current meter/voltmeter/potentiostat; 15, temperature controller; 16, furnace

SOFC reactor was proposed.

1. Experimental

1.1 Apparatus

The schematic diagram of the solid oxide fuel cell type reactor was illustrated in Figure 1. A tube-type YSZ membrane (8 mol% Y₂O₃, thickness = 1.5 mm, inside diameter = 18 mm, outside diameter = 21 mm, length = 500 mm, effective surface area = 0.0148 m²) was used as an electrolyte. La_{1.8}Al_{0.2}O₃ (abbreviated as LaAlO) prepared by a mist decomposition method was used as an anode catalyst on the inner surface of the tube while La_{0.85}Sr_{0.15}MnO₃ (abbreviated as LSM) prepared by a conventional paste method on the outer side was used as the cathode. Platinum wire was connected to the platinum meshes placed on both electrode surfaces to serve as current collectors. A current meter and a voltmeter were used to measure closed circuit current (CCI) and open circuit voltage (OCV), respectively. Voltages at various current values were measured using a potentiostat. The standard operation was as follows.

Methane $(3.4 \times 10^{-6} \text{ mol s}^{-1})$ was fed to the anode without dilution gases. Oxygen or air $(1.02 \times 10^{-5} \text{ mol s}^{-1})$ was fed to the cathode. The operating temperatures were varied: i.e. T = 1073, 1123, 1173, 1223 and 1273 K. The flow rate of the anode exit gas was

measured and its composition was analyzed by a gas chromatograph with a TCD detector every 30 min until reaching a steady state condition.

It should be noted that carbon deposition on the anode is a typical phenomenon which takes place in solid oxide fuel cells with hydrocarbon feed. However, all experimental results in this study were recorded at steady-state conditions and an apparent carbon deposition was not observed. The carbon balance was checked and found to be within 99.8%. In the case of possible carbon deposition, the cell was treated by feeding pure oxygen $(1.02 \times 10^{-5} \text{ mol s}^{-1})$ to the anode side, before running each set of experiments. The temperature was raised to 773 and 1223 K with a holding time of 6 h for each step.

1.2 Electrode preparation

The LSM powder was pounded and mixed with glycerol. It was pasted into thin film on the outside of the YSZ tube and heated at 1223 K for about 3 h in the air (Tagawa *et al.*, 1999, 2003; Kiatkittipong *et al.*, 2004a, 2004b).

The LaAlO anode material was prepared on the inside of the YSZ tube by the mist pyrolysis method as follows (Tagawa *et al.*, 1999, 2003; Kiatkittipong *et al.*, 2004a, 2004b).

Figure 2 shows the setup for the anode preparation. A mixed aqueous solution of lanthanum nitrate $(La(NO_3)_3 \cdot 6H_2O)$ and aluminum nitrate

JOURNAL OF CHEMICAL ENGINEERING OF JAPAN

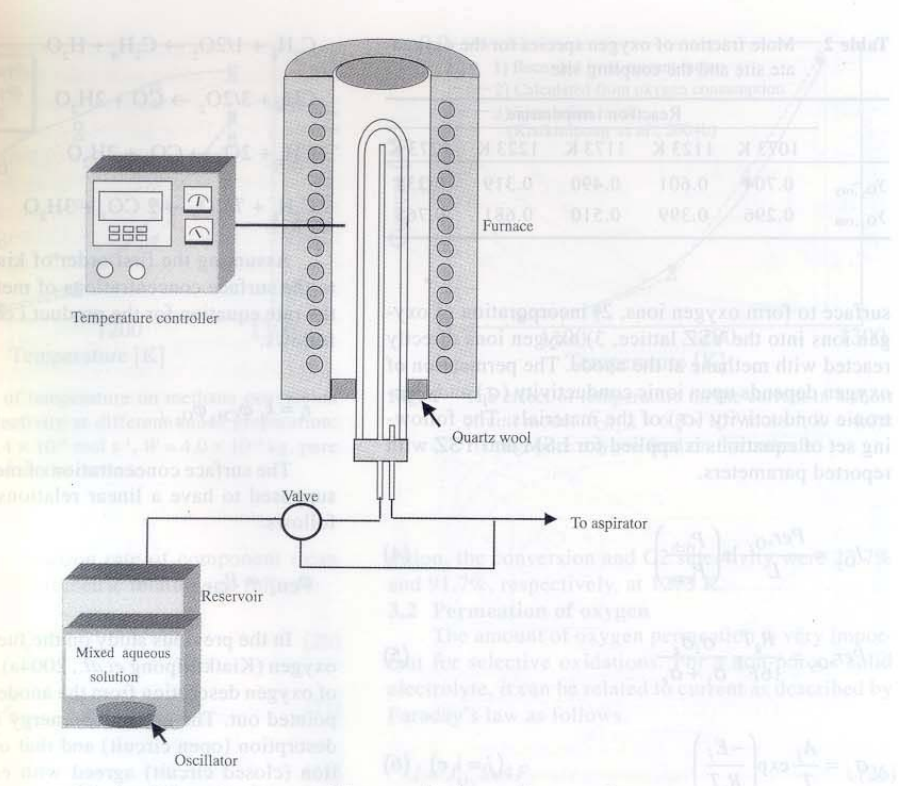


Fig. 2 Schematic diagram of the setup for the anode preparation

 $(Al(NO_3)_3, 9H_2O)$, (La:Al = 9:1) was placed in a reservoir. With a ceramic ultrasonic transducer (1.7 MHz), a mist of solution was generated. The mist was delivered to the YSZ tube with the air flow using an aspirator. The YSZ tube was placed in a furnace and heated. The pyrolysis was generally operated in periodic operations. In this periodic operation, the mist was intermittently sprayed to the YSZ tube and the optimum condition was summarized in Table 1.

2. SOFC Modelling

By assuming a plug flow and isothermal condition, the mass balance equation in the anode side is given as

$$\frac{\mathrm{d}\,\gamma_i}{\mathrm{d}\,x} = \left[r_i + \left(\frac{S}{W}\right)J_i\right] \frac{W}{F_{\mathrm{CH_4,0}}} \tag{1}$$

where the permeation rate of component i except for oxygen is zero $(J_i = 0)$ because the YSZ membrane allows only oxygen to permeate.

At the entrance (x = 0), $\gamma_{CH_4} = 1$, $\gamma_i = 0$ (products)

 Table 1
 Optimum condition for the anode preparation

YSZ temperature	503 K
Concentration of salt solution	1.25 wt%
Spray time	30 s
Interval time	30 s
Total spray time	2 h

The partial pressures in the anode side (AN) and the cathode side (CA) can be determined as

$$P_{i,\text{AN}} = \frac{P_{\text{t,AN}} \gamma_i}{\sum \gamma_i} \tag{2}$$

$$P_{\rm O_2,CA} = \begin{cases} 1.013 \times 10^5 \text{ Pa} & \text{(oxygen feed)} \\ 2.127 \times 10^4 \text{ Pa} & \text{(air feed)} \end{cases}$$
 (3)

The oxygen permeation rate through the LSM/YSZ/LaAlO solid oxide fuel cell type reactor can be estimated from our model (Kiatkittipong *et al.*, 2004b). In the model, general reaction paths are 1) electrochemical reduction of molecular oxygen at the LSM

VOL. 37 NO. 12 2004

Table 2 Mole fraction of oxygen species for the oxygenate site and the coupling site

	Reaction temperature					
	1073 K	1123 K	1173 K	1223 K	1273 K	
y _{O,oxy}	0.704	0.601	0.490	0.319	0.235	
y _{O2} ,cou	0.296	0.399	0.510	0.681	0.765	

surface to form oxygen ions, 2) incorporation of oxygen ions into the YSZ lattice, 3) oxygen ions directly reacted with methane at the anode. The permeation of oxygen depends upon ionic conductivity (σ_i) and electronic conductivity (σ_e) of the materials. The following set of equations is applied for LSM and YSZ with reported parameters.

$$J_{\rm O_2} = \frac{Per_{\rm O_2}}{L} \ln \left(\frac{P_{\rm rich}}{P_{\rm lean}} \right) \tag{4}$$

$$Per_{,O_2} = \frac{R_{\rm g}T}{16F^2} \frac{\sigma_{\rm i}\sigma_{\rm e}}{\sigma_{\rm i} + \sigma_{\rm e}}$$
 (5)

$$\sigma_{j} = \frac{A_{j}}{T} \exp\left(\frac{-E_{j}}{R_{g}T}\right) \qquad (j = i, e) \quad (6)$$

Although, these values of LaAlO are not available in the literature, kinetic parameters were determined in the study. It is suggested in the study that the rate of oxygen permeation with helium flow on the anode was determined by the surface desorption step from the anode. On the other hand, these three rate steps are comparable with the methane feed.

In our previous TPD work on LaAlO powder (Tagawa et al., 1999), it was proposed that the oxygen species desorbed at low temperatures (below 1000 K) were active for CO and CO₂ formation (oxygenate site) while the oxygen species desorbed at higher temperatures (above 1000 K) were active for the OCM to C2-hydrocarbon (coupling site). From the fuel cell type temperature-programmed desorption (FC-TPD) measurements, the fraction of oxygen species for oxygenate site and coupling site were estimated by the results of integration of oxygen FC-TPD operated in a closed circuit mode (as shown in Figure 7 in Kiatkittipong et al., 2004a) and the values are summarized in Table 2.

When methane was fed on the anode and oxygen was permeated from the cathode to the anode side, the following oxidation reactions were proceeded.

$$2CH_4 + 1/2O_2 \to C_2H_6 + H_2O \tag{7}$$

$$C_2H_6 + 1/2O_2 \rightarrow C_2H_4 + H_2O$$
 (8)

$$CH_4 + 3/2O_2 \to CO + 2H_2O$$
 (9)

$$CH_4 + 2O_7 \rightarrow CO_7 + 2H_7O$$
 (10)

$$C_{1}H_{6} + 7/2O_{1} \rightarrow 2 CO_{1} + 3H_{2}O$$
 (11)

Assuming the first order of kinetics with respect to the surface concentrations of methane and oxygen, the rate equation for the product *i* can be expressed as follows.

$$r_i = k_i' \varphi_{\text{CH}_4} \varphi_{\text{O}_2,j} \tag{12}$$

The surface concentration of methane (φ_{CH_4}) was supposed to have a linear relationship with P_{CH_4} as follows.

$$\varphi_{\text{CH}_A} \propto P_{\text{CH}_A}$$
 (13)

In the previous study on the fuel cell type TPD of oxygen (Kiatkittipong $et\ al.$, 2004a), an important role of oxygen desorption from the anode material has been pointed out. The activation energy of surface oxygen desorption (open circuit) and that of oxygen permeation (closed circuit) agreed with each other in both cases of oxygenate oxygen and coupling oxygen. These results suggested the permeation of oxygen strongly depended on the surface oxygen species. Thus linear relationship between surface concentration of oxygen ($\varphi_{0_2,j}$) and oxygen flux ($J_{0_2,j}$) was also supposed as follows.

$$\varphi_{\mathcal{O}_{2},j} \propto J_{\mathcal{O}_{2},j} \tag{14}$$

where j represents either coupling oxygen (cou) or oxygenate oxygen (oxy).

Then, the kinetic rate expressions determined for each of the above reactions are given as follows, respectively.

$$r_1 = k_1 P_{\text{CH}_4} J_{\text{O}_2,\text{cou}} \tag{15}$$

$$r_2 = k_2 P_{\text{C}_2 \text{H}_6} J_{\text{O}_2, \text{cou}} \tag{16}$$

$$r_3 = k_3 P_{\rm CH} J_{\rm Ob, oxy} \tag{17}$$

$$r_4 = k_4 P_{\text{CH}_4} J_{\text{O}_2,\text{oxy}}$$
 (18)

$$r_5 = k_5 P_{\rm C, H_6} J_{\rm O_2, oxy}$$
 (19)

JOURNAL OF CHEMICAL ENGINEERING OF JAPAN

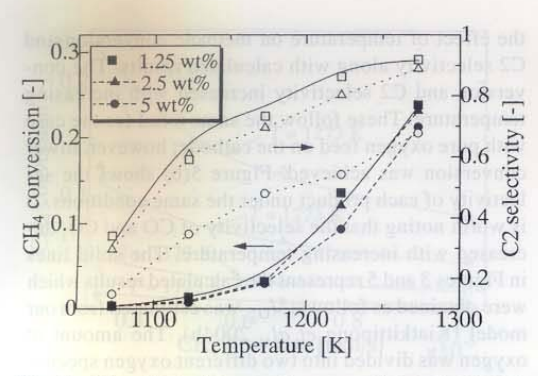


Fig. 3 The effect of temperature on methane conversion and C2 selectivity at different anode preparation: $F_{\text{CH}_1,0} = 3.4 \times 10^{-6} \text{ mol s}^{-1}, W = 4.0 \times 10^{-5} \text{ kg, pure oxygen feed on the cathode}$

Therefore, the reaction rate of component *i* can be expressed by stoichiometric relations as follows:

$$r_{\text{CH}_4} = -2r_1 - r_3 - r_4 \tag{20}$$

$$r_{C_2H_6} = r_1 - r_2 - r_5 \tag{21}$$

$$r_{\rm C_2H_4} = r_{\rm 2}$$
 (22)

$$r_{\rm CO} = r_3 \tag{23}$$

$$r_{\text{CO}_3} = r_4 + r_5$$
 while viewitzeles and both telephone (24)

$$r_{O_2} = -\frac{1}{2}r_1 - \frac{1}{2}r_2 - \frac{3}{2}r_3 - 2r_4 - \frac{7}{2}r_5$$
 (25)

3. Results and Discussion

3.1 Selection of the optimum mist solution concentration for the anode preparation

Figure 3 shows the effect of the mist solution concentration on methane conversion (filled symbols) and C2 selectivity (open symbols). The SOFC reactor was operated in a closed circuit mode without external resistance (short circuit, $R_{\rm L}=0$). The C2 selectivity increased with decreasing concentration of the mist solution or with increasing reaction temperature. The solid lines represent calculated results, which will be described later. At lower concentration of the mist solution, particles with smaller sizes were obtained. The small particle sizes are effective for C2 product formation (Moe *et al.*, 1998a). As the mist solution concentration of 1.25 wt% showed the highest selectivity, it was chosen as the optimum concentration for the following studies. In the optimum anode preparation con-

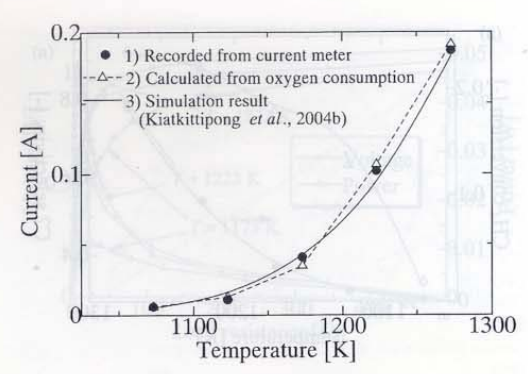


Fig. 4 The effect of temperature on the current in a short circuit mode: $F_{\text{CH}_4,0} = 6.8 \times 10^{-6} \, \text{mol s}^{-1}, W = 4.0 \times 10^{-5} \, \text{kg}$, pure oxygen feed on the cathode

dition, the conversion and C2 selectivity were 23.7% and 91.7%, respectively, at 1273 K.

3.2 Permeation of oxygen

The amount of oxygen permeation is very important for selective oxidations. For a non-porous solid electrolyte, it can be related to current as described by Faraday's law as follows.

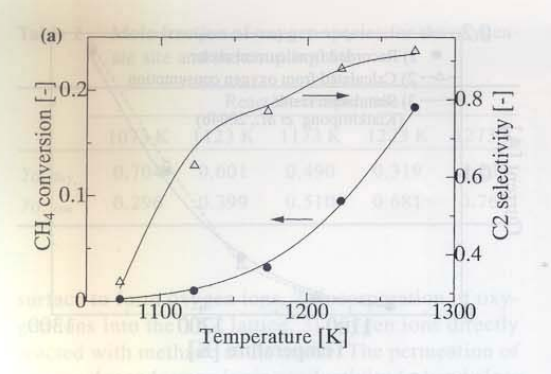
$$I = J_{O_2} Sx 4F \tag{26}$$

Figure 4 shows the effect of temperature on the current. Three kinds of current were plotted as follows: 1) current recorded from the current meter, 2) equivalent current calculated from the oxygen consumption from product distribution and 3) equivalent current estimated from our permeation model (Kiatkittipong et al., 2004b). Due to no oxygen in the gas phase was detected from the anode exit gas, the permeated oxygen was all consumed in the reactions with methane.

As shown in Figure 4, the current values predicted from our model agreed well with those of experimental values from the current meter as well as those from the product distribution. These agreements indicated that the amount of reacted oxygen species ($J_{\rm O_2}$) could be calculated from our permeation model (Kiatkittipong et al., 2004b) and that the electrolyte used in the study was pin-hole free. Then, $J_{\rm O_2}$ was calculated with our permeation model (Kiatkittipong et al., 2004b) for Section 4.3.

3.3 Reactor performance (short circuit, $R_L = 0$)

The SOFC reactor was operated in the closed circuit mode without external resistance (short circuit, $R_{\rm L}=0$). The kinetic rate expressions were determined for each of the above reaction by fitting the experimental data shown in Figure 3.



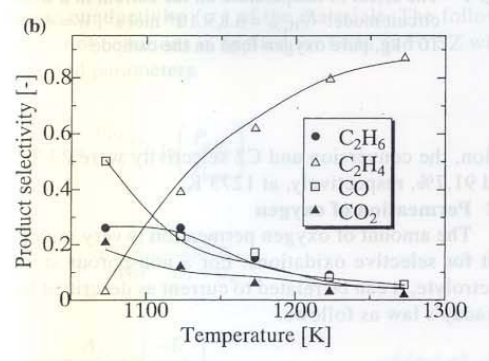


Fig. 5 The effect of temperature (a) on methane conversion and C2 selectivity and (b) on the product selectivity distribution: $F_{\text{CH}_4,0} = 3.4 \times 10^{-6} \text{ mol s}^{-1}$, $W = 4.0 \times 10^{-5} \text{ kg}$, air feed on the cathode

$$k_1 = 3.70 \times 10^7 \exp\left(\frac{-215000}{R_{\rm g}T}\right)$$
 (27)

$$k_2 = 2.96 \times 10^5 \exp\left(\frac{-110000}{R_g T}\right)$$
 (28)

$$k_3 = 4.14 \times 10^3 \exp\left(\frac{-124000}{R_g T}\right)$$
 (29)

$$k_4 = 2.96 \times 10^3 \exp\left(\frac{-131000}{R_g T}\right)$$
 (30)

$$k_5 = 1.78 \times 10^5 \exp\left(\frac{-120000}{R_{\rm g}T}\right)$$
 (31)

Figure 5 shows the reactor performance for the case with air feed on the cathode. Figure 5(a) shows

the effect of temperature on methane conversion and C2 selectivity along with calculated results. The conversion and C2 selectivity increased with increasing temperature. These follow the same trend for the case with pure oxygen feed on the cathode; however, lower conversion was achieved. Figure 5(b) shows the selectivity of each product under the same conditions. It is worth noting that the selectivity of CO and CO₂ decreased with increasing temperature. The solid lines in Figures 3 and 5 represent the calculated results which were obtained as follows: $J_{\rm O_2}$ was estimated from our model (Kiatkittipong et al., 2004b). The amount of oxygen was divided into two different oxygen species; oxygenate and coupling oxygen by using mole fraction of oxygen species shown in Table 2 and the following relations

$$J_{O_2,cou} = y_{O_2,cou} J_{O_2}$$
 (32)

$$J_{O_{\text{conv}}} = v_{O_{\text{conv}}} J_{O} \tag{33}$$

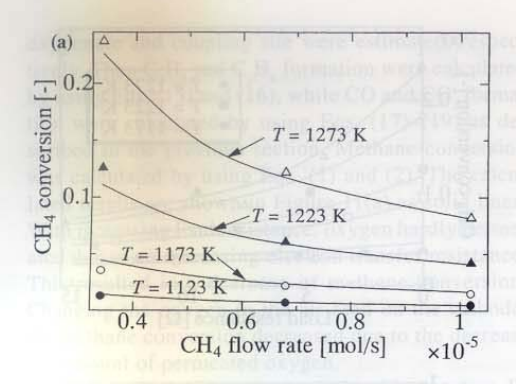
Then the $\rm C_2H_4$ and $\rm C_2H_6$ formations which use the oxygen species for coupling ($\rm O_{2,cou}$) were calculated by using Eqs. (15) and (16). CO and CO $_2$ formation which using the oxygen species for oxygenate ($\rm O_{2,oxy}$) were calculated by using Eqs. (17)–(19). Methane conversion and product selectivity were calculated by using Eqs. (1) and (2). The calculated results (solid lines) agreed well with the experimental results. The maximum C2 yield of 16.8% was obtained at 1273 K in the case of air feed on the cathode side by multiplying the conversion and the selectivity shown in Figure 5(a), where C2 yield of 21.7% was obtained in the case of pure oxygen feed shown in Figure 3.

The effects of the methane flow rate on methane conversion and C2 selectivity are shown in **Figure 6**. The calculated results in Figure 6 followed the same calculation method as used in Figure 5. As shown in Figure 6(a), the methane conversion increased with decreasing methane flow rate, which was in good agreement with the calculated values (solid lines).

As shown in Figure 6(b), the C2 selectivity was almost independent of the methane flow rate. This suggested that oxygenate products and coupling products are formed in a parallel manner. On the other hand, the C_2H_4/C_2H_6 ratio decreased with increasing methane flow rate. Because of shorter residence time, consecutive ethylene production from ethane decreased with increasing methane flow rate. Our developed model can predict the experimental results very well.

It should be noted that Guo et al. (1999) proposed the complex kinetic expressions to explain complicated changes in selectivity while this study proposed the simple kinetics by assuming two kinds of oxygen species with different activity.

JOURNAL OF CHEMICAL ENGINEERING OF JAPAN



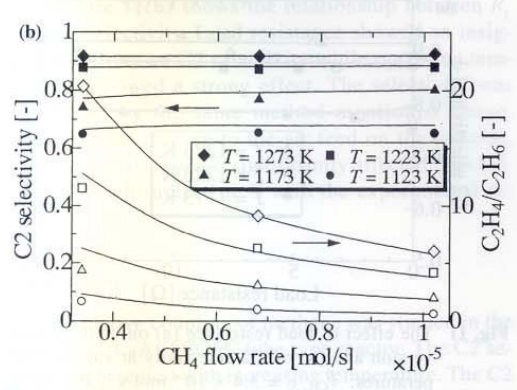


Fig. 6 The effect of the methane flow rate (a) on methane conversion and (b) on C2 selectivity and the C_2H_4/C_2H_6 ratio at various temperatures: $W = 4.0 \times 10^{-5}$ kg, pure oxygen feed on the cathode

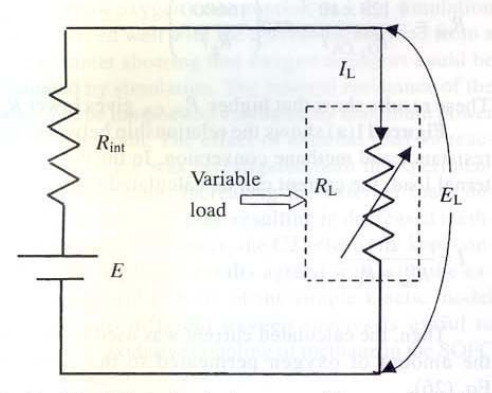
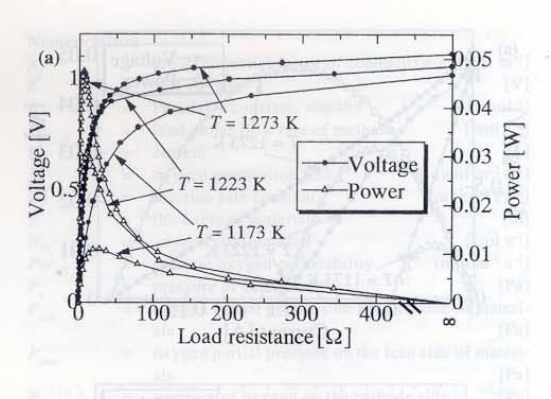


Fig. 7 Simplified circuit diagram to illustrate SOFC involving a variable load resistor

3.4 Chemicals-energy cogeneration with the SOFC reactor (closed circuit with external load, R_1)

The internal resistance of a cell can be determined from the maximum power transfer theorem (Siskind, 1965) as described below. Figure 7 shows a simpli-



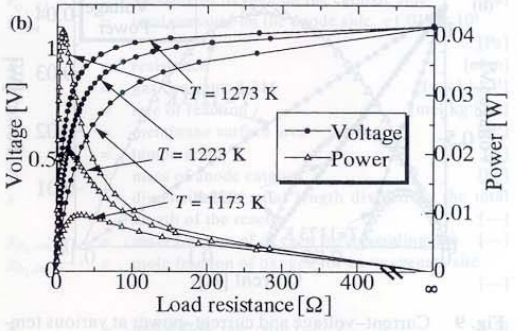
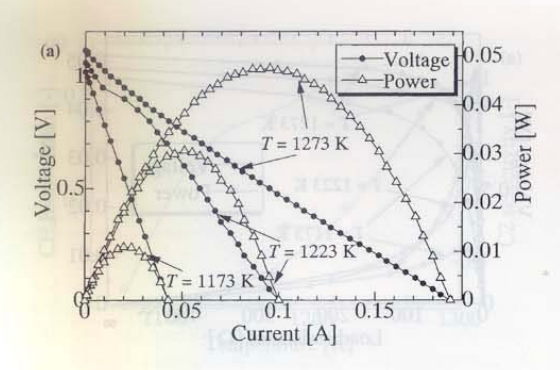


Fig. 8 Load resistance–voltage and load resistance–power at various temperatures in the cases of (a) pure oxygen feed on the cathode and (b) air feed on the cathode: $F_{\text{CH}_1,0} = 6.8 \times 10^{-6} \text{ mol s}^{-1}$, $W = 4.0 \times 10^{-5} \text{ kg}$

fied series circuit model, which consists of a voltage source (SOFC reactor unit) with a variable external load resistor ($R_{\rm L}$). If $R_{\rm L}=\infty$ (open circuit), current $I_{\rm L}=0$, and power at load $P_{\rm L}=0$; also, if $R_{\rm L}=0$ (short circuit), voltage $E_{\rm L}=0$, and $P_{\rm L}=0$. When $R_{\rm L}$ is neither ∞ nor 0, $P_{\rm L}$ is not 0. A maximum power transferred to the load occurs when $R_{\rm L}=R_{\rm int}$. $R_{\rm int}$ is the overall resistance including ohmic, activation and concentration polarization resistances inside the cell unit. Therefore, the $R_{\rm int}$ value varies with operating conditions such as temperature, $P_{\rm O_1,CA}$ and should be experimentally estimated.

Figure 8 shows the load resistance-voltage and load resistance-power plots at various temperatures in the cases of (a) oxygen and (b) air feed on the cathode. The open circuit voltages were in the range of 1.02–1.08 V, which is nearly equal to the theoretical value of the C₂H₄ formation from C₂H₆ (Tagawa et al., 1999). Power increased with increasing temperature. By increasing the operating temperature, the chemical reaction could be enhanced as well as oxygen permeability through the YSZ. It should be noted that when the current-voltage was plotted for both cases as shown in Figure 9, a linear decrease of voltage with current was observed, indicating that the over-potential is mainly governed by the ohmic resistance of the cell.

VOL. 37 NO. 12 2004



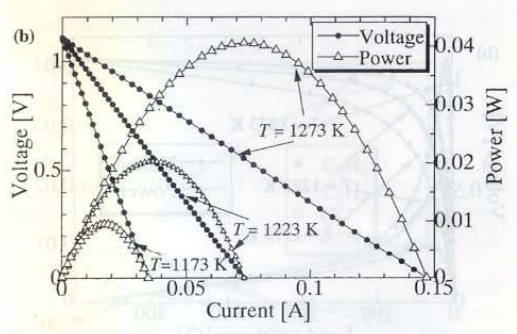


Fig. 9 Current-voltage and current-power at various temperatures in the cases of (a) pure oxygen feed on the cathode and (b) air feed on the cathode: $F_{\text{CH}_4,0}$ = 6.8×10^{-6} mol s⁻¹, $W = 4.0 \times 10^{-5}$ kg

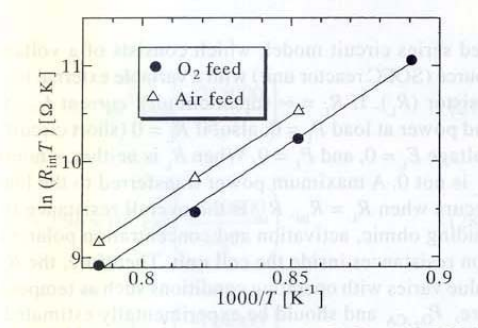
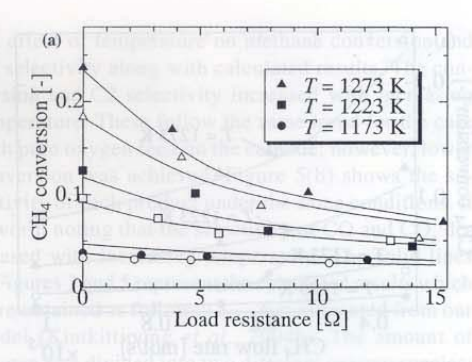


Fig. 10 Arrhenius' plot between $ln(R_{int}T)$ and 1000/T

Comparing Figures 8(a) and (b), changing the oxygen to air feed on the cathode, the power decreased due to the decreasing driving force of oxygen gradient. However, using air instead of oxygen could be competitive from a viewpoint of the oxygen purification cost.

Figure 10 shows the relation of internal cell resistance (R_{int}) and temperature. Following expressions can be obtained;



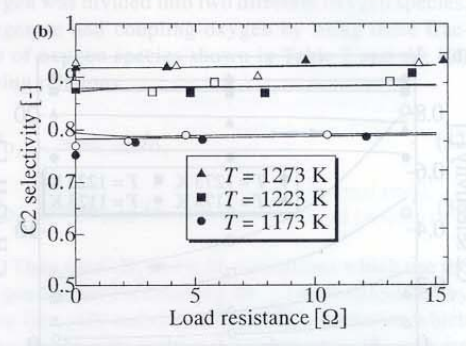


Fig. 11 The effect of load resistance (a) on methane conversion and (b) on C2 selectivity at various temperatures: $F_{\text{CH}_{1},0} = 3.4 \times 10^{-6} \text{ mol s}^{-1}$, $W = 4.0 \times 10^{-5} \text{ kg}$, filled symbol = pure oxygen feed on the cathode, open symbol = air feed on the cathode

$$R_{\rm int} = \frac{1.128 \times 10^{-2}}{P_{\rm O_2, CA}^{0.2} T} \exp\left(\frac{166000}{R_{\rm g}T}\right)$$
 (34)

These results show that higher $P_{\rm O_2,CA}$ gives lower $R_{\rm int}$. Figure 11(a) shows the relationship between load resistance and methane conversion. In the case of external load, the current can be calculated from

$$I = \frac{E}{R_{\rm int} + R_{\rm L}} \tag{35}$$

Then, the calculated current was used to estimate the amount of oxygen permeated to the anode by Eq. (26).

The filled symbol represents pure oxygen feed on the cathode case while the open symbol represents air feed on the cathode case. The solid line represents calculated results. I was estimated from the $R_{\rm L}$ value by Eqs. (34) and (35) using E values shown as a voltage in Figure 8 for oxygen and air feed on the cathode. Using mole fraction of oxygen species shown in Table 2 and Eqs. (32) and (33), the amount of oxygen for

JOURNAL OF CHEMICAL ENGINEERING OF JAPAN

oxygenate and coupling site were estimated, respectively. Then C_2H_4 and C_2H_6 formation were calculated by using Eqs. (15) and (16), while CO and CO₂ formation were calculated by using Eqs. (17)–(19) as described in the previous section. Methane conversion was calculated by using Eqs. (1) and (2). The calculated results are shown in Figure 11(a) as solid lines. With increasing load resistance, oxygen hardly permeated due to an increasing electron transfer resistance. This resulted in a decrease of methane conversion. Changing the oxygen to the air feed on the cathode, the methane conversion decreased due to the decreasing amount of permeated oxygen.

Figure 11(b) shows the relationship between R_L and the selectivity. Load resistance showed an insignificant effect on C2 selectivity while operating temperature showed a strong effect. The selectivity was calculated by the same method mentioned above. Changing the oxygen to the air feed on the cathode, the C2 selectivity was insignificantly affected. The calculated results agreed well with the experimental results.

Conclusion

Oxidative coupling of methane was studied in the LSM/YSZ/LaAlO SOFC tube type reactor. The C2 selectivity increased with increasing temperature. The C2 selectivity and methane conversion were 91.7% and 23.7% at 1273 K with the optimum preparation of anode catalyst. A set of reaction model was proposed with distinguished oxygen species such as oxygenate species and coupling species. The equivalent current calculated from oxygen consumption and the simulation results agreed well with the current values read from a current meter showing that oxygen transport could be estimated by simulation. The internal resistance of the cell could be lumped and estimated by maximum power transfer theorem. The effect of external load on reactor performance was investigated both in experimental and simulation. Increasing the external load, decreased oxygen transport, resulting in decreased methane conversion. However, the C2 selectivity kept constant. The calculated results agreed well with the experimental results. A set of the simple kinetic model by using two different oxygen species is useful to evaluate the oxidative coupling of methane in the SOFC type reactor.

Acknowledgment

The authors gratefully acknowledged the financial support from the Thailand Research Fund (TRF) and TJTTP-JBIC. A part of this study was also supported by a Grant-in-Aid for Scientific Research, from the Ministry of Education, Culture, Sports, Science & Technology of Japan.

Nomencla	ture			
A_i	=	pre-exponential factor of conducti		
É	=	cell voltage	[1	
F	11	Faraday's constant, =96485	[C mol-1]	
$F_{CH=0}$	=	feed molar flow rate of methane	[mol s ⁻¹]	
1	m Pi	current	[A]	
J_0		oxygen permeation flux	[mol m ⁻² s ⁻¹]	
k .	=	reaction rate constant	[m² kg-1 Pa-1]	
L	-	thickness of material	[m]	
$N_{\rm O}$	=	oxygen consumption	[mol s ⁻¹]	
Per,o,	=	specific oxygen permeability	[mol m ⁻¹ s ⁻¹]	
P. 02	nitan	pressure of component i	[Pa]	
Prich	(2) (T)	oxygen partial pressure on the rich side of materials [Pa]		
Plean		oxygen partial pressure on the lean side of mate		
lean		als	[Pa]	
$P_{O,,CA}$	TOLICE	pressure of oxygen on the cathode side [Pa]		
PLAN	=	total pressure on the anode side, = 1.013×10^5		
LAN		Control of the Contro	[Pa]	
R	=	resistance	[ohm]	
R_{g}	=	gas constant, 8.314	[J mol-1 K-1]	
	=	rate of reaction j	[mol kg-1 s-1]	
r _j S	=	membrane surface area	[m ²]	
T	=	temperature	[K]	
W	=	mass of anode catalyst	[kg]	
x	=	dimensionless axial length divid	ed by the total	
		length of the reactor	[-1	
y _{O,cou}	=	mole fraction of oxygen for a coup	oling site [-]	
y _{O.,oxy}	=	mole fraction of oxygen for an oxygenate site		
			[-]	
γ	=	molar flow rate ratio $(=F/F_{CH_{4},0})$	[—]	
φ	=	surface concentration	[mol m ⁻²]	
σ	=	conductivities	[S m ⁻¹]	
<subscrip< td=""><td>t></td><td></td><td></td></subscrip<>	t>			
AN	=	anode side		
CA	=	cathode side		
cou	=	coupling site		
e	=	electronic		
i	=	ionic		
i	=	component i		
int	=	internal		
j	=	reaction j		

Literature Cited

load

feed

oxygenate site

Achenbach, E.; "Three-Dimensional and Time-Dependent Simulation of a Planar Solid Oxide Fuel Cell Stack," J. Power Sources, 49, 333–348 (1994)

Aguiar, P., D. Chadwick and L. Kershenbaum; "Modelling of an Indirect Internal Reforming Solid Oxide Fuel Cell," Chem. Eng. Sci., 57, 1665-1677 (2002)

Bessette, N. F., II, W. J. Wepfer and J. Winnick; "A Mathematical Model of a Solid Oxide Fuel Cell," J. Electrochem. Soc., 142, 3792–3800 (1995)

Carrillo, A. S., T. Tagawa and S. Goto; "Application of Mist Pyrolysis Method to Preparation of Ni/ZrO₂ Anode Catalyst for SOFC Type Reactor," *Mater. Res. Bull.*, 36, 1017–1027 (2001)

Guo, X.-M., K. Hidajat and C.-B. Ching, "Simulation of a Solid Oxide Fuel Cell for Oxidative Coupling of Methane," Catal. Today, 50, 109-116 (1999)

Kiatkittipong, W., T. Tagawa, S. Goto, S. Assabumrungrat and P. Praserthdam; "TPD Study in LSM/YSZ/LaAlO System for the Use of Fuel Cell Type Reactor," *Solid State Ionics*, 166, 127–136 (2004a)

Kiatkittipong, W., T. Tagawa, S. Goto, S. Assabumrungrat and P. Praserthdam; "Oxygen Transport through LSM/YSZ/LaAlO System for Use of Fuel Cell Type Reactor," Proc. of the 10th APCChE, 3P08040, Kitakyushu, Japan (2004b); Chem. Eng. J. (in press)

Moe, K. K., T. Tagawa and S. Goto; "Preparation of Electrode Catalyst for SOFC Reactor by Ultrasonic Mist Pyrolysis of Aqueous Solution," J. Ceram. Soc. Jpn., 106, 242–247 (1998a)

Moe, K. K., T. Tagawa and S. Goto; "Preparation of Electrode Catalyst for SOFC Reactor by Ultrasonic Mist Pyrolysis: Effect of Spray Time," J. Ceram. Soc. Jpn., 106, 754-758 (1998b)

Siskind, C. S.; Electrical Circuits: Direct and Alternating Current, 2nd ed., McGraw-Hill Book, Tokyo, Japan (1965)

Steele, B. C. H.; "Material Science and Engineering: The Enabling Technology for the Commercialisation of Fuel Cell Systems," J. Material. Sci., 36, 1053-1068 (2001)

Stoukides, M.; "Solid-Electrolyte Membrane Reactors: Current

Experience and Future Outlook," Catal. Rev. Sci. Eng., 42, 1-70 (2000)

Tagawa, T., K. K. Moe, T. Hiramatsu and S. Goto; "Design of Electrode for Solid Oxide Fuel Cells Reactor," Solid State Ionics, 106, 227-235 (1998)

Tagawa, T., K. K. Moe, M. Ito and S. Goto; "Fuel Cell Type Reactor for Chemicals-Energy Co-generation," Chem. Eng. Sci., 54, 1553–1557 (1999)

Tagawa, T., K. Kuroyanagi, S. Goto, S. Assabumrungrat and P. Praserthdam; "Selective Oxidation of Methane in an SOFC-Type Reactor: Effect of Applied Potential," Chem. Eng. J., 93, 3-9 (2003)

Yamada, K., N. Takahashi and C. J. Wen; "Design and Evaluation of an Electric Vehicle Using Solid Oxide Fuel Cells," J. Chem. Eng. Japan, 35, 1290–1297 (2002)

Yamamoto, O.; "Solid Oxide Fuel Cells: Fundamental Aspects and Pospects," *Electrochim. Acta*, 45, 2423–2435 (2000)